

# On Symmetry and the Reality of Holomorphic Hartree–Fock Wavefunctions

Bang C. Huynh<sup>1,2, a)</sup> and Alex J. W. Thom<sup>2</sup>

<sup>1)</sup>*School of Chemistry, University of Nottingham, University Park, Nottingham NG7 2RD, United Kingdom*

<sup>2)</sup>*Yusuf Hamied Department of Chemistry, Lensfield Road, Cambridge CB2 1EW, United Kingdom*

(Dated: 3 March 2022)

The coalescence and disappearance of Hartree–Fock (HF) solutions as the molecular structure varies have been a common source of criticism for the breakdown of the HF approximation to the potential energy surfaces. However, recent developments in holomorphic HF theory show that this disappearing behavior is only a manifestation of the way conventional HF equations prevent solutions from being analytically continued, but it is unclear what factors govern the existence and the locations of these disappearances. In this work, we explore some of these factors from the perspective of spatial symmetry by introducing a classification for symmetry constraints on electronic-structure calculations. This forms a framework for us to systematically investigate several analytic holomorphic HF solutions of a model  $[\text{H}_4]^{2+}$  system in STO-3G and demonstrate that, under appropriate conditions, spatial symmetry imposes strict requirements on the reality of certain solutions. The implications for self-consistent-field HF search algorithms are then discussed. Throughout this article, the term *reality* means the quality of a holomorphic HF solution having real molecular orbitals.

## I. INTRODUCTION

It has long been known that the non-linearity of the Hartree–Fock (HF) equations necessitates the existence of multiple self-consistent-field (SCF) solutions.<sup>1–5</sup> Over the last decade, these multiple SCF solutions have recaptured a fair amount of our and some others’ attention, for they are believed to present a feasible alternative pathway to recover electron correlation in ground and excited states.<sup>6–10</sup> However, since chemistry is hardly ever static, it is imperative that the behaviors of these SCF solutions must be followed as the underlying system configuration changes, so that the nature of the potential energy surfaces generated by them can be understood.

In a number of our previous studies, we investigated the behaviors of these solutions upon the variation of molecular geometry or along certain electron-transfer reaction trajectories as part of an attempt to characterize and understand their properties.<sup>9–11</sup> In more than one instance, we observed that the multiple HF solutions that are close to each other in energy can become energetically degenerate at certain points in the configuration space. These points of degeneracy are of particular interest to us. If, at one of these points, the solutions remain physically distinct (*i.e.*, they differ from one another by more than a phase factor), then they are connected by some symmetry operations of the underlying symmetry group of the system. On the other hand, if they become identical at this point, we say that they have *coalesced*.

The simplest and most well-known example for the coalescence of solutions is encountered in the stretching of  $\text{H}_2$  where the lowest doubly-degenerate and spin-symmetry-broken unrestricted Hartree–Fock (UHF) solutions coalesce with the lowest non-degenerate restricted

Hartree–Fock (RHF) solution at H–H bond length of around 1.20 Å.<sup>12,13</sup> From the point of coalescence, if one follows the coalescing solutions in different directions, one can expect to get different behaviors depending on the nature of the solutions. In particular, the lowest doubly-degenerate UHF solutions in  $\text{H}_2$  exist at bond lengths larger than 1.20 Å but fail to be located by conventional methods below 1.20 Å. On the other hand, the lowest non-degenerate RHF solution persists at all bond lengths. We thus say that the UHF solutions have *disappeared* from the conventional SCF landscape past the coalescence point at 1.20 Å as the H–H bond length decreases.

When the conventional theory of HF is reformulated in such a way that the HF equations become holomorphic,<sup>14</sup> it turns out that the disappearing solutions can be analytically continued past the coalescence points, although the molecular-orbital (MO) coefficients will have to become non-real.<sup>13</sup> In the framework of holomorphic HF theory, the points of coalescence therefore mark the configurations at which certain HF solutions switch from being real solutions of both conventional and holomorphic HF equations to being non-real solutions of the latter only. However, the fundamental factors that govern the existence of such coalescence points are not well understood. Without a knowledge of where these points are located in the SCF landscape, one cannot predict when certain SCF HF solutions, perhaps of significant chemical importance, have been missed out by SCF search algorithms that are based only on conventional HF theory. And more importantly, the lack of a satisfactory account for the occurrence of such coalescences renders them to be unfairly considered as shortfalls of the HF theory<sup>15</sup> rather than features that are the consequences of the theory itself. In fact, Fukutome notes in a detailed investigation of the UHF theory for chemical reactions<sup>16</sup> that the disappearance of UHF solutions upon the system becoming asymmetrical constitutes part of a promising theoretical basis to understand the mechanism underlying radical

<sup>a)</sup>Electronic mail: [bang.huynh@nottingham.ac.uk](mailto:bang.huynh@nottingham.ac.uk)

*vs.* ionic character of chemical reactions. Unfortunately, to the best of our knowledge, there has not been much further effort along this line of inquiry since Fukutome’s work.

The  $H_2$  stretching example above is useful because its simplicity enables a straightforward analytic description of the coalescence point.<sup>12</sup> However, it is *too* simple for any useful patterns to be elucidated, since the linear geometry of the diatomic molecule means that the configuration space is only one-dimensional and that the molecular symmetry remains  $\mathcal{D}_{\infty h}$  throughout—the position of the coalescence point therefore appears rather random in connection to the structure of  $H_2$ . Nevertheless, Figure 5 in Ref. 17 reveals that, if one of the two hydrogen nuclei is replaced by a fictitious nucleus  $Z$  with a variable nuclear charge  $Q_Z$  such that the true  $H_2$  molecule corresponds to  $Q_Z = 1.00$  a.u., then, as  $Q_Z$  deviates from this value, the symmetry of the system descends from  $\mathcal{D}_{\infty h}$  to  $\mathcal{C}_{\infty v}$  and some of the RHF solutions that exist at  $Q_Z = 1.00$  a.u. begin to coalesce with each other and disappear.

This simple observation inspires the conjecture that molecular symmetry plays a role in dictating the existence of HF solutions that would otherwise be non-locatable in the conventional SCF HF formalism. In fact, this conjecture is further strengthened by the observations of similar coalescing and disappearing behaviors of multiple RHF and UHF solutions in the vicinity of high-symmetry molecular structures in other systems. The simplest non-trivial example that we consider is the side-way compression and elongation of the hypothetical square two-electron dication  $[H_4]^{2+}$  such that the molecular symmetry interchanges between  $\mathcal{D}_{4h}$  and  $\mathcal{D}_{2h}$ . We show in Figure 1 all low-lying  $M_S = 0$  conventional UHF solutions of  $[H_4]^{2+}$  located numerically in STO-3G using SCF metadynamics<sup>11</sup> in Q-CHEM 5.3,<sup>18</sup> focusing particularly on the coalescence and disappearance of certain solutions in the vicinity of the square geometry.

There exist more complicated examples still. One of them concerns the RHF solutions in the four-electron  $H_4$  as the square four-membered ring opens up into an isosceles trapezium and the point group of the system descends from  $\mathcal{D}_{4h}$  to  $\mathcal{C}_{2v}$  (Figure 2 in Ref. 11). Another more complicated example involves the RHF solutions in ethene as the planar molecule undergoes a torsional twist about the C=C bond and the molecular symmetry lowers from  $\mathcal{D}_{2h}$  to  $\mathcal{D}_2$  (Figure 7a in Ref. 17). And yet another example that is even more complex involves the lowest-lying UHF solutions upon the Jahn–Teller distortion of the octahedral  $[TiF_6]^{3-}$  anions into  $\mathcal{D}_{4h}$  or  $\mathcal{D}_{2h}$  geometries along the  $e_g$  normal vibrational coordinates (Figure 10 in Ref. 10). In all of the above examples, we notice that there are two kinds of solutions: those of the first kind persist at all geometries along the tracking path (*e.g.*, the solutions corresponding to the solid curves in Figure 1), and those of the second kind coalesce with other solutions before ceasing to be locatable by conventional SCF searches as the system descends in molecular symmetry (*e.g.*, the solutions represented by the dashed curves in Figure 1).

The above empirically observed patterns of solution coalescence and disappearance near high-symmetry configurations in a variety of systems with very different structures inspire the investigation into the roles played by molecular symmetry in controlling the reality of solutions to the holomorphic HF equations. A completely general approach requires results from polynomial theories to determine bounds on real solutions of systems of multivariate polynomials.<sup>19,20</sup> Unfortunately, this is a challenging task to accomplish for arbitrary systems where it can be daunting to work out how molecular symmetry affects the structural complexity of the HF equations. This leads us to believe that, as an initial investigation, it is more revealing to seek and study extensively a model system that exhibits such behaviors through an analytic approach. We thus require that this model system is simple enough such that the relationship between molecular symmetry and the structural complexity of the HF equations can be elucidated, and that analytic solutions can be obtained easily and examined thoroughly. However, the model system must be sufficiently complex in order for molecular symmetry to be non-trivial in the sense that the nuclear framework can assume a number of point-group symmetries that are inter-convertible via well-defined pathways.

To this end, we choose the hypothetical dication  $[H_4]^{2+}$  in a minimal basis set STO-3G: there are only two electrons in four atomic-orbital (AO) basis functions, offering a maximum of six degrees of freedom (after accounting for normalization), and the possible high symmetries that can be adopted by the nuclear framework and that are of interest to us are  $\mathcal{T}_d$ ,  $\mathcal{D}_{4h}$ ,  $\mathcal{D}_{2h}$ , and  $\mathcal{D}_2$ , all of which can be easily inter-converted. Furthermore, as pointed out earlier, the numerically located UHF  $M_S = 0$  solutions for  $[H_4]^{2+}$  in STO-3G plotted in Figure 1 show that this system does indeed exhibit the conjectured behaviors around the  $\mathcal{D}_{4h}$  geometry along the sideways compression/elongation pathway. The analytic model we employ for this system can therefore be expected to provide enough richness to cast some light on the roles of symmetry in dictating the observed behaviors while remaining tractable so that the interpretation and analysis of the analytic HF solutions do not become impossibly complicated.

Before delving into the analytic details, we must first explain what it is that we seek to achieve in this article, and why. We mentioned earlier that the empirical observations thus far let us classify HF solutions into two kinds. From our prior experience with wavefunction symmetry analysis using representation theory,<sup>10</sup> we know that the solutions of the second kind are symmetry-broken (we will discuss this in greater depth later) and can thus be used to form multi-determinantal wavefunctions that recover static correlation. It is therefore of great chemical interest to understand the conditions for the existence of these solutions in the real Hilbert space where they can be located quite easily with most contemporary SCF methods. Hence, throughout this article, we

shall be guided by two main questions: (i) What are the qualitative and quantitative differences between the two kinds of solutions observed? and (ii) How does symmetry control the reality of these solutions?

This article is structured as follows. In Section II, we discuss the roles of spin and spatial symmetry constraints on the structure of the Fock matrix and make a fundamental distinction between two types of constraints which we call *intrinsic* and *extrinsic*. We then detail the symmetry constraints applicable to the  $[\text{H}_4]^{2+}$  system that are of main interest to us in Section III before formulating the corresponding algebraic holomorphic HF equations in Section IV. The solutions to these equations are classified and their reality behaviors examined in Section V so as to map out the different real/non-real regimes exhibited by certain solutions and the transition boundaries between them. Section VI then provides an examination of the group-theoretic symmetry of the solutions and relates that to their reality behaviors. The connections between the different imposed constraints are subsequently presented in Section VII in an attempt to explore different local and global SCF landscapes of the  $[\text{H}_4]^{2+}$  system. Finally, we conclude in Section VIII with a few discussional remarks on the implications of our findings and chart out possible directions to generalize the analysis in this work.

## II. SYMMETRY CONSTRAINTS

Every SCF HF procedure that is performed in a basis set of AOs inevitably involves the diagonalization of the Fock matrix expressed in this basis whose form strongly dictates the nature of the SCF solutions obtained. We therefore begin by examining the form of the Fock matrix to gain an understanding of the various kinds of constraints that symmetry can impose on the system.

Let us consider an  $N_e$ -electron single determinant,

$$\Psi_{\text{det}} = |\chi_1 \dots \chi_i \dots \chi_{N_e}| = \hat{\mathcal{A}} \left[ \prod_i^{N_e} \chi_i(\mathbf{x}_i) \right], \quad (1)$$

where  $\chi_i$  denotes the  $i^{\text{th}}$  spin-orbital,  $\mathbf{x}_i$  the spin-spatial coordinates of the  $i^{\text{th}}$  electron, and  $\hat{\mathcal{A}}$  the antisymmetrizer that acts on the electron labels. Let us also define an antilinear conjugation operator  $\hat{\kappa}$  on a determinant as

$$\hat{\kappa}\Psi_{\text{det}} = \hat{\mathcal{A}} \left[ \prod_i^{N_e} \chi_i^*(\mathbf{x}_i) \right], \quad (2)$$

where  $\chi_i^*$  will be defined in Equation 8. We assume that the spin-orbitals  $\chi_i$  optimize either the conventional energy functional,

$$E[\Psi] = \frac{\langle \Psi_{\text{det}} | \hat{\mathcal{H}} | \Psi_{\text{det}} \rangle}{\langle \Psi_{\text{det}} | \Psi_{\text{det}} \rangle}, \quad (3)$$

or the holomorphic energy functional,<sup>13,14</sup>

$$\tilde{E}[\Psi_{\text{det}}] = \frac{\langle \hat{\kappa}\Psi_{\text{det}} | \hat{\mathcal{H}} | \Psi_{\text{det}} \rangle}{\langle \hat{\kappa}\Psi_{\text{det}} | \Psi_{\text{det}} \rangle}. \quad (4)$$

In either case, the spin-orbitals are eigenfunctions of the Fock operator:

$$\hat{f}(\mathbf{x}_m) = \hat{h}(\mathbf{r}_m) + \sum_{j=1}^{N_e} \int d\mathbf{x}_n \bar{\chi}_j^\diamond(\mathbf{x}_n) \frac{1 - \hat{P}_{(mn)}}{|\mathbf{r}_m - \mathbf{r}_n|} \chi_j(\mathbf{x}_n), \quad (5)$$

where  $\hat{h}$  is the one-electron core Hamiltonian operator,  $\bar{\chi}$  the typically complex-conjugated spin-orbital, and  $\hat{P}_{(mn)}$  the permutation operator corresponding to the transposition  $(mn)$  of electron labels. We also use the wildcard operator  $\diamond$  as a generic placeholder which can be either the identity for conventional HF or the conjugation  $*$  for holomorphic HF (to be defined in Equation 8). If we now introduce a covariant<sup>21</sup> spin-spatial direct-product basis,

$$\Sigma = \{\omega_\delta, \omega_\varepsilon, \dots\} \otimes \{\varphi_\mu, \varphi_\nu, \dots\}, \quad (6)$$

with  $\omega$  representing covariant spin basis functions and  $\varphi$  covariant spatial basis functions, such that each spin-orbital can be expanded using the contravariant<sup>21</sup> molecular-orbital coefficients  $G_i^{\delta\mu,\cdot}$  as

$$\chi_i(\mathbf{x}_m) = \omega_{\cdot\delta}(s_m) \varphi_{\cdot\mu}(\mathbf{r}_m) G_i^{\delta\mu,\cdot}, \quad (7a)$$

where  $\delta\mu$  are double indices such that any twice-occurring Greek indices are implicitly contracted over and  $s_m$  and  $\mathbf{r}_m$  are the spin and spatial coordinates of the  $m^{\text{th}}$  electron. We can write this more succinctly as

$$\chi_i = (\boldsymbol{\omega} \otimes \boldsymbol{\varphi})^\top \mathbf{G}_i, \quad (7b)$$

where  $\boldsymbol{\omega}$  and  $\boldsymbol{\varphi}$  are column vectors containing the covariant spin and spatial basis functions respectively, and  $\mathbf{G}_i$  the  $i^{\text{th}}$  column of the contravariant molecular-orbital coefficient matrix  $\mathbf{G}$  of dimensions  $|\Sigma| \times N_e$ . Assuming that the spatial basis functions are all real, we then *define*

$$\chi_i^* \equiv \omega_{\cdot\delta}(\hat{K}\varphi_{\cdot\mu})(G_i^{\delta\mu,\cdot})^* = (\boldsymbol{\omega} \otimes \hat{K}\boldsymbol{\varphi})^\top \mathbf{G}_i^* \quad (8)$$

where  $\hat{K}$  is the typical complex-conjugation operator acting only on the spatial basis functions and the coefficients in  $\mathbf{G}_i$  are complex-conjugated. The action of the  $*$  conjugation on spin-orbitals is therefore not that of an actual complex conjugation. Since the spin functions can be chosen to be orthonormal, it can be shown that this definition of  $\chi_i^*$  ensures that  $\hat{\kappa}$  in Equation 2 is indeed a conjugation operator (see Refs. 22 and 23 for definition). We require in addition that, if the spatial basis functions  $\varphi_\mu$  are real-valued, then  $\hat{K}\varphi_\mu = \varphi_\mu$ . Thus, for real spatial basis functions, which we will consider exclusively from here on,

$$\chi_i^* = (\boldsymbol{\omega} \otimes \boldsymbol{\varphi})^\top \mathbf{G}_i^*. \quad (9)$$

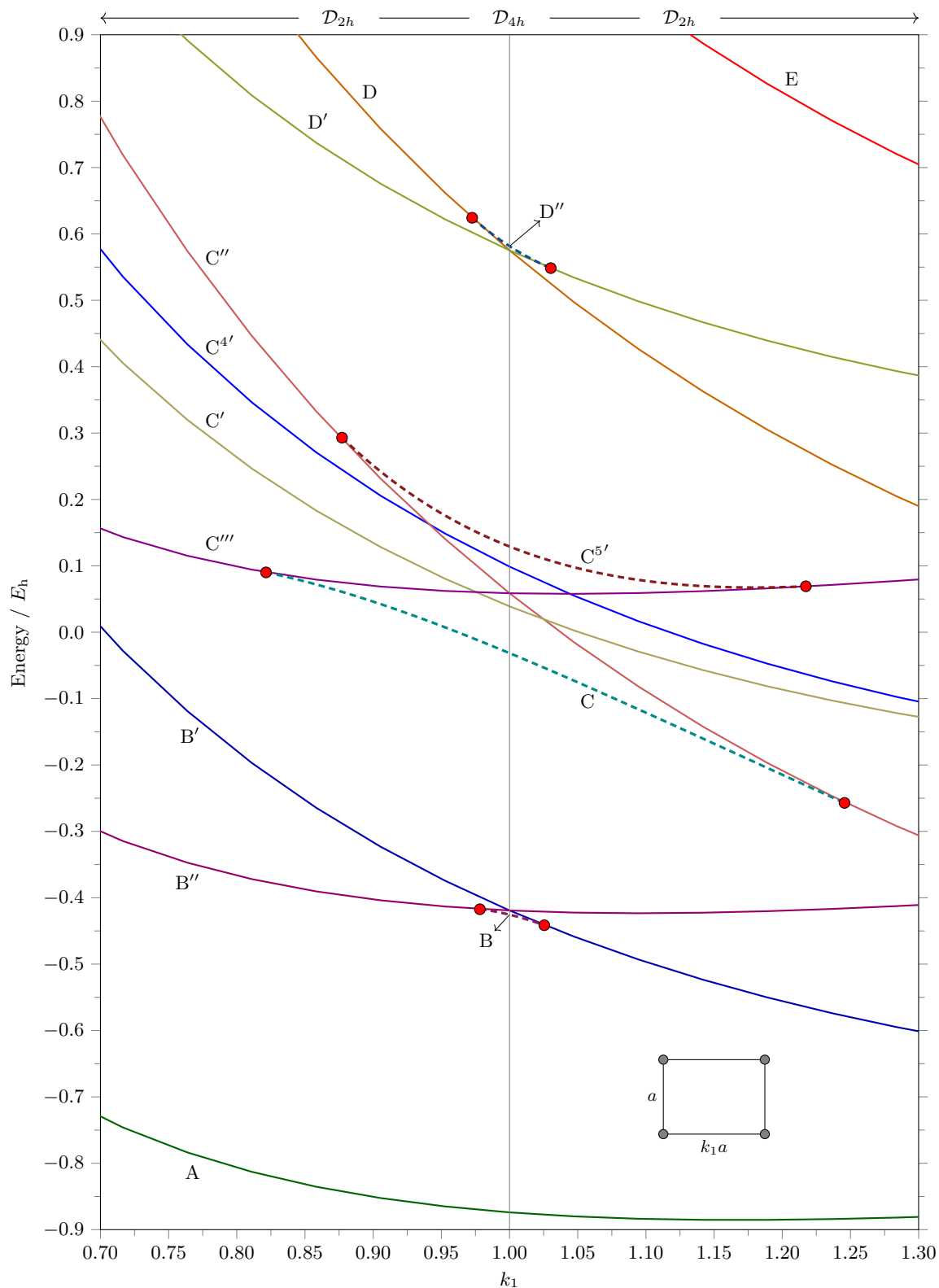


FIG. 1. Low-lying  $M_S = 0$  conventional UHF solutions of  $[\text{H}_4]^{2+}$  (STO-3G) in the vicinity of square geometry for  $a = 1.058350 \text{ \AA}$ . Solutions that persist as the rectangular factor  $k_1$  varies are represented by solid curves. Solutions that coalesce with others and disappear as  $k_1$  deviates from unity are shown with dashed curves. Coalescence points are highlighted with red dots. Solutions are labeled alphabetically in ascending order of their energy at  $\mathcal{D}_{4h}$ . Degenerate or nearly degenerate solutions at  $\mathcal{D}_{4h}$  share the same letter but are distinguished by dashes.



We now write the contravariant one-particle density matrix for  $\Psi_{\text{det}}$  as

$$P^{\delta\mu, \delta'\mu'} = \sum_{i=1}^{N_e} G_i^{\delta\mu, \cdot} (G_i^{\dagger\delta})^{\cdot, \delta'\mu'}$$

$$\Leftrightarrow \mathbf{P} = \mathbf{G}\mathbf{G}^{\dagger\delta},$$

and hence the elements of the Fock matrix  $\mathbf{F}$  as

$$F_{\delta'\mu', \delta\mu} = \langle \omega_{\delta'}(s) \varphi_{\mu'}(\mathbf{r}) | \hat{f}(\mathbf{x}) | \omega_{\delta}(s) \varphi_{\mu}(\mathbf{r}) \rangle$$

$$= H_{\delta'\mu', \delta\mu}^{\text{core}} + \Pi_{\delta'\mu', \varepsilon'\nu', \delta\mu\varepsilon\nu} P^{\varepsilon\nu, \varepsilon'\nu'} \quad (10)$$

$$\Leftrightarrow \mathbf{F} = \mathbf{H}^{\text{core}} + \mathbf{\Pi} \cdot \mathbf{P}, \quad (11)$$

where the one-electron contribution is

$$H_{\delta'\mu', \delta\mu}^{\text{core}} = \Omega_{\delta'\delta} \langle \varphi_{\mu'} | \hat{h} | \varphi_{\mu} \rangle, \quad (12)$$

and the density-independent part of the two-electron contribution is

$$\Pi_{\delta'\mu', \varepsilon'\nu', \delta\mu\varepsilon\nu} = \Omega_{\delta'\delta} \Omega_{\varepsilon'\varepsilon} \langle \varphi_{\mu'} \varphi_{\nu'} | \varphi_{\mu} \varphi_{\nu} \rangle$$

$$- \Omega_{\delta'\varepsilon} \Omega_{\varepsilon'\delta} \langle \varphi_{\mu'} \varphi_{\nu'} | \varphi_{\nu} \varphi_{\mu} \rangle, \quad (13)$$

with  $\langle \cdot \cdot | \cdot \cdot \rangle$  denoting a two-electron repulsion integral in physicists' notation. The binary dot operator in Equation 11 indicates a tensor contraction of the double indices  $\varepsilon\nu$  and  $\varepsilon'\nu'$  as in Equation 10. In both Equations 12 and 13,  $\mathbf{\Omega}$  is the spin-only overlap matrix,

$$\Omega_{\delta\varepsilon} = \langle \omega_{\delta} | \omega_{\varepsilon} \rangle.$$

If we also define  $\mathbf{S}^{\text{AO}}$  as the spatial-AO-only overlap matrix,

$$S_{\mu\nu}^{\text{AO}} = \langle \varphi_{\mu} | \varphi_{\nu} \rangle,$$

then the HF equations in the basis  $\Sigma$  are given by

$$F_{\delta'\mu', \delta\mu} G_i^{\delta\mu, \cdot} = \Omega_{\delta'\delta} S_{\mu'\mu}^{\text{AO}} G_i^{\delta\mu, \cdot} \varepsilon_i, \quad (14)$$

where  $\varepsilon_i$  are the eigenvalues of  $\mathbf{F}$ .

The form of the Fock matrix in Equation 11 shows contributions from three terms, two of which ( $\mathbf{H}^{\text{core}}$  and  $\mathbf{\Pi}$ ) are independent of the MO coefficients and hence of the actual solutions of the HF equations, whereas the remaining one ( $\mathbf{P}$ ) shows a direct dependence on the HF solutions. This allows us to distinguish between two kinds of constraints imposable on the Fock matrix: *intrinsic constraints* are those that arise solely from the properties of the basis functions and affect  $\mathbf{H}^{\text{core}}$  and  $\mathbf{\Pi}$  directly, and *extrinsic constraints* are additional constraints imposed on the MO coefficients that affect  $\mathbf{P}$  but not  $\mathbf{H}^{\text{core}}$  and  $\mathbf{\Pi}$ . We will discuss both types of constraints in turn.

### A. Intrinsic Constraints

Most basis sets used in electronic-structure calculations take the form of a direct-product basis (Equation 6) between an implicit spin basis and a suitable real spatial basis. This decomposability into separate spin and spatial bases enables us to examine intrinsic constraints due to spin and spatial symmetries separately.

## 1. Spin Symmetry

In the familiar two-component orthonormal spinor basis  $\{\alpha, \beta\} \equiv \{|1/2, 1/2\rangle, |1/2, -1/2\rangle\}$ ,  $\mathbf{\Omega}$  must equal the  $2 \times 2$  identity matrix  $\mathbf{I}_2$ . This forces  $\mathbf{H}^{\text{core}}$  to have only two non-zero spin blocks,  $\alpha\alpha$  and  $\beta\beta$ , by Equation 12. Similarly, by Equation 13, the non-zero spin blocks in the first contribution to  $\mathbf{\Pi}$  (the so-called Coulomb term) are  $\alpha\alpha\alpha\alpha$ ,  $\alpha\beta\alpha\beta$ ,  $\beta\alpha\beta\alpha$ , and  $\beta\beta\beta\beta$ , and those in the second contribution to  $\mathbf{\Pi}$  (the so-called exchange term) are  $\alpha\alpha\alpha\alpha$ ,  $\alpha\beta\beta\alpha$ ,  $\beta\alpha\alpha\beta$ , and  $\beta\beta\beta\beta$ , so that  $\mathbf{\Pi}$  can only have up to six non-zero spin blocks. Overall, these constraints cause  $\mathbf{F}$  to be rather sparse, and as soon as a basis set is fixed for a system (in this case,  $\{\alpha, \beta\}$  for the spin basis), the forms of *all* SCF solutions of the HF equations in this basis are indiscriminately governed by the intrinsic constraints.

## 2. Spatial Symmetry

In a completely analogous manner to spin intrinsic constraints, Equations 10, 12, and 13 allow us to recognize that the structures of the one- and two-electron AO integral tensors  $\langle \varphi_{\mu'} | \hat{h} | \varphi_{\mu} \rangle$  and  $\langle \varphi_{\mu'} \varphi_{\nu'} | \varphi_{\mu} \varphi_{\nu} \rangle$  introduce spatial intrinsic constraints to the Fock matrix. However, the sheer number of AO basis functions in each basis set even for very small molecules and the dependence of the electron integrals on the nuclear arrangement of the system make the spatial intrinsic constraints much more complicated than their spin counterparts. This means that the one- and two-electron integral tensors do not possess any general sparse structures for a gross simplification of the Fock matrix.

In spite of that, representation theory provides a way to quantify the degree of intrinsic constraints arising from the spatial basis functions. To this end, we first define the problem more concretely. Given an arrangement of nuclei that is invariant under the operations of a certain point group  $\mathcal{G}$  and a set of AO spatial basis functions  $\{\varphi_{\mu}\}$  localized on these nuclei and transforming according to a (generally reducible) representation  $\Gamma_{\mathcal{G}}$  of  $\mathcal{G}$ , we determine  $n_1(\Gamma_{\mathcal{G}}, \mathcal{G})$ , the number of non-vanishing independent components of the one-electron integral tensor  $\langle \varphi_{\mu} | \hat{o} | \varphi_{\nu} \rangle$  where  $\hat{o}$  is either the identity operator or the one-electron core Hamiltonian  $\hat{h}$ , and  $n_2(\Gamma_{\mathcal{G}}, \mathcal{G})$ , the number of non-vanishing independent components of the two-electron integral tensor  $\langle \varphi_{\mu'} \varphi_{\nu'} | \varphi_{\mu} \varphi_{\nu} \rangle$ . We then define the degree of spatial intrinsic constraints on the one- and two-electron integrals as

$$\eta_i(\Gamma_{\mathcal{G}}, \mathcal{G}) = 1 - \frac{n_i(\Gamma_{\mathcal{G}}, \mathcal{G})}{n_i(\Gamma_{\mathcal{C}_1}, \mathcal{C}_1)}, \quad i = 1, 2. \quad (15)$$

We note that  $n_i(\Gamma_{\mathcal{C}_1}, \mathcal{C}_1) \geq n_i(\Gamma_{\mathcal{G}}, \mathcal{G}) \forall \mathcal{G} \leq \mathbf{O}(3)$ , and hence  $0 \leq \eta_i \leq 1$ . Thus, the closer  $\eta_i$  is to unity, the larger the extent to which the spatial symmetry of the basis functions constrains the values of the electron integrals and hence the structure of the Fock matrix and

the SCF landscape. Detailed expressions for  $n_i(\Gamma_{\mathcal{G}}, \mathcal{G})$  are given in Appendix A.

## B. Extrinsic Constraints

Intrinsic constraints are, however, often still too general to restrict the SCF landscape to the appropriate regions of interest. This is not a problem if one seeks to explore as much of the Hilbert space as possibly allowed by the underlying SCF formalism. However, very often one would choose to focus on certain local regions in the SCF landscape, perhaps after considerations that are motivated by empirical observations, physical reasoning, or computational cost, and extrinsic constraints provide a way to achieve this. For instance, as explained in the next Section, to understand the UHF solutions of  $[\text{H}_4]^{2+}$  in Figure 1 analytically, we need to consider the numerical forms of their MOs and then impose appropriate constraints on the MO coefficients to limit ourselves to the right parts of the SCF landscape in which these solutions reside. Incidentally, this also simplifies the governing equations sufficiently such that analytic forms for these solutions can be obtained. Or more generally, by restricting the structure of the spin blocks of the MO coefficient matrix  $\mathbf{G}$  (Equation 7b) in an arbitrary system, one obtains a hierarchy of HF variants that are simultaneous eigenfunctions of some combination of the spin projection operator  $\hat{S}_z$ , the squared total spin operator  $\hat{S}^2$ , the time reversal operator  $\hat{\Theta}$ , and the complex-conjugation operator  $\hat{K}$ . These have been originally characterized by Fukutome<sup>24</sup> and then later clarified by Stuber and Paldus.<sup>25</sup>

By imposing suitable extrinsic constraints, SCF solutions that exhibit certain desirable symmetries can be targeted, but it is worth noting that these constraints can always be relaxed to allow for more symmetry-broken solutions to be found. For example, let  $\Psi_{\mathcal{H}_0}^{\text{HF}}$  be an SCF solution located within a space  $\mathcal{H}_0$  (such as UHF) that exhibits less restrictive extrinsic constraints than another space  $\mathcal{H}_1$  (such as RHF), then the stability of  $\Psi_{\mathcal{H}_1}^{\text{HF}}$  with respect to spin-orbital transformation in  $\mathcal{H}_0$  has already been explored in great depth for the various Fukutome classes of conventional HF.<sup>26–30</sup> From an epistemological point of view, therefore, there is much to gain from studying the high-symmetry SCF solutions that result from certain extrinsic constraints before venturing out into the more general, less constrained parts of the SCF landscape where symmetry-broken solutions are abundant and special techniques such as non-orthogonal configuration interaction (NOCI)<sup>6,7</sup> or various projection-based methods<sup>31–34</sup> are needed to restore symmetry and obtain sensible quantum numbers, because symmetry-brokenness can often complicate the interpretation of the SCF solutions obtained.<sup>10,35,36</sup>

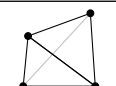

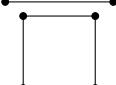
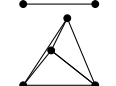
## III. $[\text{H}_4]^{2+}$ MODEL: IMPOSITION OF CONSTRAINTS

In order to formulate the analytic equations for the  $[\text{H}_4]^{2+}$  model, we begin with a description of the constraints applicable to this system in STO-3G. In particular, we discuss the spatial intrinsic constraints that are imposed by the STO-3G basis set in conjunction with the molecular geometry of  $[\text{H}_4]^{2+}$  and comment on how they affect the terms in the HF equations. We then outline the spin and spatial extrinsic constraints that we shall impose to focus on the numerically located UHF solutions shown in Figure 1 and also to explore other related local regions. This allows us to show that these constraints lead to a family of solutions that are identical in form across different specific extrinsic constraints.

### A. Spatial Intrinsic Constraints

Table I shows the number of non-vanishing independent components of the one- and two-electron integrals for  $[\text{H}_4]^{2+}$  in STO-3G with different nuclear arrangements and the corresponding degrees of spatial intrinsic constraints according to Equation 15 and Appendix A. Unsurprisingly, as the molecule becomes more symmetric in the sense that the  $1s$  AO basis functions become related by more symmetry operations, more constraints are imposed on the electron integrals and the degrees of spatial intrinsic constraints increase accordingly. Hence, there are fewer non-zero unique elements in the  $\mathbf{H}_{\text{core}}$  and  $\mathbf{\Pi}$  tensors by virtue of Equations 12 and 13, resulting in more related terms in the basis-dependent HF equations 14. In addition, as the AO basis functions are real, all elements of  $\mathbf{H}_{\text{core}}$  and  $\mathbf{\Pi}$  must also be real and the HF equations 14 in turn become non-linear polynomial equations over the reals where each term is a monomial of overall degree 1 or 3 in the MO coefficients  $\mathbf{G}$ .

TABLE I. Spatial intrinsic constraints for  $[\text{H}_4]^{2+}$  in STO-3G.

Shape	$\mathcal{G}$	$n_1$	$n_2$	$\eta_1$	$\eta_2$
	$\mathcal{D}_2$	4	19	0.600	0.655
	$\mathcal{D}_{2h}$	4	19	0.600	0.655
	$\mathcal{D}_{4h}$	3	13	0.700	0.764
	$\mathcal{T}_d$	2	7	0.800	0.873

The Fundamental Theorem of Algebra<sup>37</sup> inspires the holomorphization of conventional HF theory such that in simple cases where the HF equations can be reparameterized as single univariate polynomial equations,

there must exist a constant number of solutions across all molecular geometries.<sup>14</sup> However, this theorem does not dictate how many of these solutions must be real, nor is it applicable to more complicated problems where multivariate polynomial systems are unavoidable. In fact, if the HF equations are considered as polynomial equations in a certain number of unknowns, then Bézout’s theorem imposes an ultimate upper bound on the number of solutions as the product of the polynomial degrees,<sup>20,38–40</sup> provided that the number of solutions is finite, but it does not say anything about their reality either. This is to be expected since an analysis based solely on the gross algebraic structures of the equations cannot pick up the consequences due to the fine structures within the terms in the polynomials.

To gain any insight into the connection between symmetry and the reality of SCF solutions at all, we must examine the symmetry-induced relations between the monomials in the HF equations. The simplicity of the chosen model  $[\text{H}_4]^{2+}$  system enables us to achieve this on an analytic level with moderate ease. In fact, the values of  $n_1$  and  $n_2$  shown in Table I give the number of one- and two-electron terms in the HF equations after the monomials have been factorized through the common one- and two-electron integrals. We believe that restrictions of this nature play a major role in determining whether solutions must be real or can be non-real and we will demonstrate this more carefully in Section VB. But before this can be done, we must introduce some extrinsic constraints to simplify the equations further, as even the high symmetry of  $\mathcal{T}_d$  still leaves us with too many unknowns and too complicated equation structures to handle analytically for the purposes of this  $[\text{H}_4]^{2+}$  model study.

## B. Spin and Spatial Extrinsic Constraints

To target the UHF solutions shown in Figure 1, we can only impose extrinsic spin constraints that are no more restrictive than UHF. However, we do not wish to have to deal with any  $\hat{s}_z$  symmetry breaking which we feel does not add to our understanding of spatial symmetry constraints in any significant way. We shall therefore stay at the UHF level and focus on the  $M_S = 0$  solutions. Furthermore, we take  $\chi_1$  to have  $m_s = +1/2$  and  $\chi_2$  to have  $m_s = -1/2$  without loss of generality. Following conventions, we shall use  $\alpha$  and  $\beta$  to denote the “spin-up” and “spin-down” components of the electron spin, respectively.

Spatial extrinsic constraints are more involved to describe since they depend on the underlying point group of the molecule and the symmetry pathway under consideration. In particular, any spatial extrinsic constraints we impose must “respect” the point-group symmetry of the molecule in the sense that each constraint follows from an equation of the form

$$\hat{R}\Psi_i^{\text{HF}} = \sum_j \Psi_j^{\text{HF}} D_{ji}(\hat{R}), \quad \text{tr } \mathbf{D}(\hat{R}) = \chi^{\Gamma_{\mathcal{G}}^{\text{ir}}}(\hat{R}) \quad (16)$$

for a particular  $\hat{R} \in \mathcal{G}$  where the sum runs over all linearly independent HF determinants that are degenerate and equivalent to  $\Psi_i^{\text{HF}}$  by symmetry,  $\Gamma_{\mathcal{G}}^{\text{ir}}$  is an *irreducible* representation in the underlying point group  $\mathcal{G}$  of the molecule, and  $\chi^{\Gamma_{\mathcal{G}}^{\text{ir}}}$  its character—the distinction between  $\chi$  as a character and  $\chi$  as a spin-orbital should be clear from the context. In other words, each spatial extrinsic constraint represents a required conserved symmetry element  $\hat{R}$  in  $\mathcal{G}$  (see Ref. 10 for the definition of *symmetry conservation*).

In Figure 2, we show the two symmetry pathways that we will consider throughout this investigation. Each pathway represents a particular direction in which the symmetry of the system can be varied and has been constructed to consist of general low-symmetry segments connecting several high-symmetry special points. In addition, the low-symmetry group must be a common subgroup of all the high-symmetry groups so that only the elements of the low-symmetry point group persist throughout the entire pathway and can thus be used to form spatial extrinsic constraints that are well defined at every geometry on the pathway. Each pathway is characterized by two parameters: a symmetry factor  $k_i$  that controls the variation in symmetry of the system along the pathway, and a scale length  $a$  that controls the characteristic distance between neighboring hydrogen atoms. Pathway A is also the pathway along which the numerical UHF solutions in Figure 1 are tracked and shall therefore be the main focus of our discussion. We will elaborate later in Section VIIB that, via pathway B, different *extrinsic* constraints along pathway A can be connected. The relationship between the two pathways and the high-symmetry points is illustrated in Figure 3a.

We introduce a new notation to facilitate the systematic description of extrinsic constraints. If  $\psi$  is a generic wavefunction, then  $\psi\{\hat{s}, \mu_s\}_i[\hat{R}, \chi^{\Gamma_{\mathcal{G}}^{\text{ir}}}(\hat{R})]_j$  denotes that  $\psi$  is constrained to be an eigenfunction of a generic spin operator  $\hat{s}$  with eigenvalue  $\mu_s$ , and also to conserve symmetry under the spatial operation  $\hat{R}$  with character  $\chi^{\Gamma_{\mathcal{G}}^{\text{ir}}}(\hat{R})$  as in Equation 16. More than one set of curly (square) brackets can be used to denote multiple spin (spatial) extrinsic constraints, in which case they are distinguished by subscripts such as  $i$  and  $j$ .

Occasionally, it is desirable to remove one or more constrained conserved symmetries in order to explore larger regions of the SCF landscape in the vicinity of the conserved-symmetry constraints. However, removing a constraint entirely can sometimes cause the problem to become too general and too intractable analytically. Therefore, an alternative would be to *relax* the constraint in a controlled manner so as to keep the problem manageable while still being able to enlarge the SCF regions of interest. One way this can be done is to allow  $\mu_s$  to be expectation values of  $\hat{s}$  that deviate from its exact eigenvalues, or to let  $\text{tr } \mathbf{D}(\hat{R})$  in Equation 16 take on values other than exact characters of irreducible representations. We then replace  $\{\hat{s}, \mu_s\}$  and  $[\hat{R}, \chi^{\Gamma_{\mathcal{G}}^{\text{ir}}}(\hat{R})]$

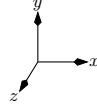
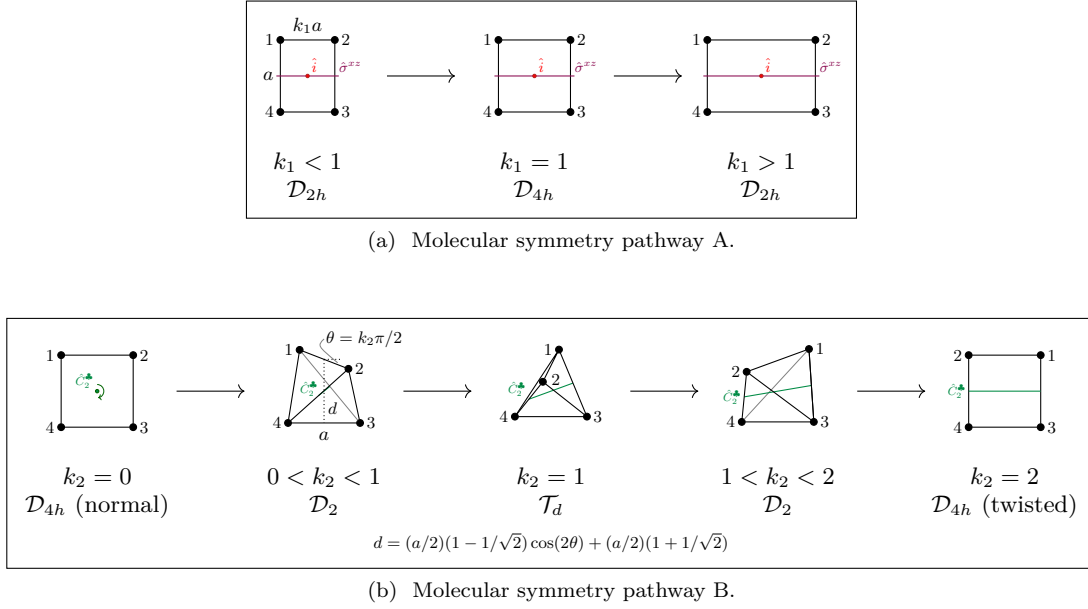


FIG. 2. Molecular symmetry pathways considered in this study. Each pathway is parametrised by  $k_i \in [0, \infty)$ ,  $i = 1, 2$  such that  $k_i = 1$  corresponds to the highest-symmetry geometry along that pathway. Pathway A is non-periodic, while pathway B is periodic with period 4. The extrinsic constraining elements introduced in Table II are also shown here.

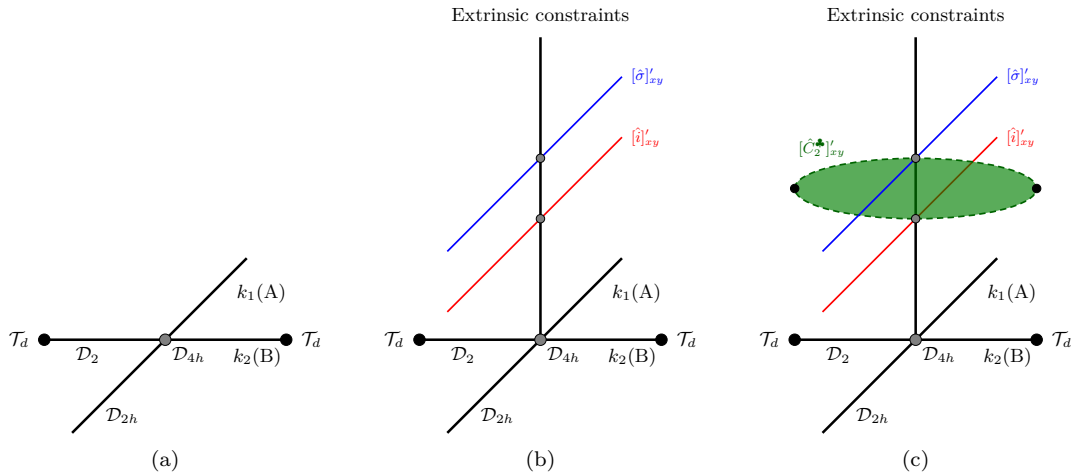


FIG. 3. Relationship between the molecular symmetry pathways and extrinsic constraints considered in this study. In (a), we depict the two-dimensional subspace defined by pathway A (parameterized by  $k_1$ ) and pathway B (parameterized by  $k_2$ ) and mark out the high-symmetry points. In (b), we introduce a third axis to represent the extrinsic constraints imposed on the SCF solutions, together with the red and blue solid lines representing pathway A subject to the extrinsic constraining spaces  $[\hat{i}]'_{xy}$  and  $[\hat{\sigma}]'_{xy}$ , respectively. Finally, in (c), we add the green dashed loop representing the periodic pathway B subject to the extrinsic constraining space  $[\hat{C}_2^z]_{xy}'$  chosen to connect the constraining spaces of pathway A. In all plots, the high-symmetry points along the molecular symmetry pathways are marked out with black dots ( $\mathcal{T}_d$ ) or grey dots ( $\mathcal{D}_{4h}$ ).

with  $\{\hat{s}\}'$  and  $[\hat{R}]'$  respectively to signify that the SCF regions are still being constrained by  $\hat{s}$  and  $\hat{R}$ , but we drop the eigenvalues or character values as they are no longer fixed or meaningful. In addition, we use dashes to signify the general symmetry breaking with respect to  $\hat{s}$  or  $\hat{R}$ .

Using the above notations, we show in Table II the SCF extrinsic constraints that we will consider for the symmetry pathways A and B in this article. The spin extrinsic constraints are strict to ensure that only  $M_S = 0$  UHF solutions are obtained, while the spatial extrinsic constraints are loose in the sense that, for each spatial symmetry operation  $\hat{R}$  considered ( $\hat{R} = \hat{i}, \hat{\sigma}^{xz}, \hat{C}_2^*$ ), we define a closed domain of two real parameters  $(x, y) \in \mathcal{D} = [-1, +1] \times [-1, +1]$  such that each parameter constrains the coefficients of one of the two MOs. A visualization of how these extrinsic constraints are related to the symmetry pathways A and B is provided in Figures 3b and 3c.

In each of the SCF constraining spaces  $[\hat{R}]$  considered, the four corners of  $\mathcal{D}$  are special as they correspond to extrinsic constraints that conserve  $\hat{R}$ -symmetry. We will pay particular attention to the solutions that are subject to these constraints since they correspond to true SCF stationary points as will be explained in Section VII C. We thus give these constraints special shorthand notations as shown in Table III to facilitate the following discussions. While the solutions obtained under these constraints must conserve all the symmetries imposed by the constraints, they are free to break other symmetries without any *a priori* restrictions.

## IV. $[\text{H}_4]^{2+}$ MODEL: ALGEBRAIC EQUATIONS

### A. Holomorphic Normalization Re-parameterization

In all cases of extrinsic constraints in Table II, it can be shown that the holomorphic normalization of the spin-orbitals  $\chi_1$  and  $\chi_2$ ,  $\langle \chi_i^* | \chi_j \rangle = \delta_{ij}$ , translates to

$$2[(G_1^{\alpha 1, \cdot})^2 + (G_1^{\alpha 2, \cdot})^2]S_1^- + 4G_1^{\alpha 1, \cdot}G_1^{\alpha 2, \cdot}S_2^- = 1, \quad (17a)$$

$$2[(G_2^{\beta 1, \cdot})^2 + (G_2^{\beta 2, \cdot})^2]S_1^+ + 4G_2^{\beta 1, \cdot}G_2^{\beta 2, \cdot}S_2^+ = 1, \quad (17b)$$

where  $S_1^\pm$  and  $S_2^\pm$  are functions of the spatial-AO-only overlap integrals  $\langle \varphi_\mu^* | \varphi_\nu \rangle$ . Since the AOs in STO-3G are real, we do not need to worry about the distinction between the conventional and holomorphic formalisms for the AO integrals and can therefore simply write  $\langle \varphi_\mu | \varphi_\nu \rangle$  for  $\langle \varphi_\mu^* | \varphi_\nu \rangle$ . The exact functional forms of the coefficients  $S_1^\pm$  and  $S_2^\pm$  depend on the precise extrinsic and intrinsic constraints being imposed and are detailed in Section S-I of the Supplementary Material, but they shall not affect the genericity of the analysis to follow. In fact, the holomorphic normalisation constraints in Equation 17 facilitate the re-parametrisation of the MO coefficients in

terms of two angular parameters  $\theta_\alpha$  and  $\theta_\beta$  as

$$G_1^{\alpha 1, \cdot} = \sqrt{\frac{\eta^-}{2}} \left( -\frac{\cos \theta_\alpha}{\sqrt{1-\gamma^-}} + \frac{\sin \theta_\alpha}{\sqrt{1+\gamma^-}} \right), \quad (18a)$$

$$G_1^{\alpha 2, \cdot} = \sqrt{\frac{\eta^-}{2}} \left( +\frac{\cos \theta_\alpha}{\sqrt{1-\gamma^-}} + \frac{\sin \theta_\alpha}{\sqrt{1+\gamma^-}} \right), \quad (18b)$$

$$G_2^{\beta 1, \cdot} = \sqrt{\frac{\eta^+}{2}} \left( -\frac{\cos \theta_\beta}{\sqrt{1-\gamma^+}} + \frac{\sin \theta_\beta}{\sqrt{1+\gamma^+}} \right), \quad (18c)$$

$$G_2^{\beta 2, \cdot} = \sqrt{\frac{\eta^+}{2}} \left( +\frac{\cos \theta_\beta}{\sqrt{1-\gamma^+}} + \frac{\sin \theta_\beta}{\sqrt{1+\gamma^+}} \right), \quad (18d)$$

where

$$\gamma^\pm = \frac{S_2^\pm}{S_1^\pm} \quad \text{and} \quad \eta^\pm = \frac{1}{2S_1^\pm} \quad (19)$$

are AO-overlap-dependent coefficients. The combination of the extrinsic constraints in Table II (four coefficient relations in each case) and the natural constraints provided by the normalization of the MOs (two more coefficient relations) reduces the original eight degrees of freedom to only two which are parameterized by  $\theta_\alpha$  and  $\theta_\beta$ . The problem becomes more tractable since we can now variationally optimize the holomorphic energy expression analytically with relative ease.

### B. Variation of the Holomorphic Energy

It turns out that, for all of the extrinsic constraints listed in Table II and the associated intrinsic constraints defined by the geometry of the molecule, the one- and two-electron holomorphic energies (signified by tildes) can be written generically as

$$\begin{aligned} \tilde{E}_1 = & [(G_1^{\alpha 1, \cdot})^2 + (G_1^{\alpha 2, \cdot})^2] A_1^- \\ & + [(G_2^{\beta 1, \cdot})^2 + (G_2^{\beta 2, \cdot})^2] A_1^+ \\ & + 2G_1^{\alpha 1, \cdot}G_1^{\alpha 2, \cdot} A_2^- \\ & + 2G_2^{\beta 1, \cdot}G_2^{\beta 2, \cdot} A_2^+, \end{aligned} \quad (20a)$$

$$\begin{aligned} \tilde{E}_2 = & [(G_1^{\alpha 1, \cdot})^2(G_2^{\beta 1, \cdot})^2 + (G_1^{\alpha 2, \cdot})^2(G_2^{\beta 1, \cdot})^2] A_3 \\ & + 2[(G_1^{\alpha 1, \cdot})^2 + (G_1^{\alpha 2, \cdot})^2]G_2^{\beta 1, \cdot}G_2^{\beta 2, \cdot} A_4^+ \\ & + 2G_1^{\alpha 1, \cdot}G_1^{\alpha 2, \cdot}[(G_2^{\beta 1, \cdot})^2 + (G_2^{\beta 2, \cdot})^2] A_4^- \\ & + [(G_1^{\alpha 1, \cdot})^2(G_2^{\beta 2, \cdot})^2 + (G_1^{\alpha 2, \cdot})^2(G_2^{\beta 1, \cdot})^2] A_5 \\ & + 4G_1^{\alpha 1, \cdot}G_1^{\alpha 2, \cdot}G_2^{\beta 1, \cdot}G_2^{\beta 2, \cdot} A_6, \end{aligned} \quad (20b)$$

where the coefficients  $A_1^\pm$  and  $A_2^\pm$  are functions of the one-electron integrals  $\langle \varphi_{\mu'} | \hat{h} | \varphi_\mu \rangle$ , and the coefficients  $A_3$ ,  $A_4^\pm$ ,  $A_5$ , and  $A_6$  are functions of the two-electron integrals  $\langle \varphi_{\mu'} \varphi_{\nu'} | \varphi_\mu \varphi_\nu \rangle$ . The exact functional forms of these coefficients depend on the precise constraints at hand as shown in Section S-I of the Supplementary Material and do not affect the following generic analysis, but via these



TABLE II. SCF extrinsic constraining spaces along pathways A and B. Each constraining space is parameterized by two real parameters  $(x, y)$  defining a domain  $\mathcal{D} = [-1, +1] \times [-1, +1]$ . The constraining elements are shown in color under the *Visualization* column. The variations of these constraining elements along their respective pathways are also shown in Figure 2. For pathway B,  $\hat{C}_2^\bullet$  denotes the two-fold rotation whose axis coincides with the common perpendicular bisector of the bonds  $H^1-H^3$  and  $H^2-H^4$ , which becomes  $\hat{C}_2^z$  at  $\mathcal{D}_{4h}$  (normal) and  $\hat{C}_2^x$  at  $\mathcal{D}_{4h}$  (twisted).

Path.	SCF extrinsic constraining space	Coefficient relations	Visualization
A	$\Psi\{\hat{s}_z, 0\}[\hat{i}]'_{xy}$ $=  \chi_1\{\hat{s}_z, +1/2\}[\hat{i}]'_x \chi_2\{\hat{s}_z, -1/2\}[\hat{i}]'_y $	$xG_1^{\alpha 1\cdot} = G_1^{\alpha 3\cdot}, yG_2^{\beta 1\cdot} = G_2^{\beta 3\cdot}$ $xG_1^{\alpha 2\cdot} = G_1^{\alpha 4\cdot}, yG_2^{\beta 2\cdot} = G_2^{\beta 4\cdot}$	
	$\Psi\{\hat{s}_z, 0\}[\hat{\sigma}^{xz}]'_{xy}$ $=  \chi_1\{\hat{s}_z, +1/2\}[\hat{\sigma}^{xz}]'_x \chi_2\{\hat{s}_z, -1/2\}[\hat{\sigma}^{xz}]'_y $	$xG_1^{\alpha 1\cdot} = G_1^{\alpha 4\cdot}, yG_2^{\beta 1\cdot} = G_2^{\beta 4\cdot}$ $xG_1^{\alpha 2\cdot} = G_1^{\alpha 3\cdot}, yG_2^{\beta 2\cdot} = G_2^{\beta 3\cdot}$	
B	$\Psi\{\hat{s}_z, 0\}[\hat{C}_2^\bullet]'_{xy}$ $=  \chi_1\{\hat{s}_z, +1/2\}[\hat{C}_2^\bullet]'_x \chi_2\{\hat{s}_z, -1/2\}[\hat{C}_2^\bullet]'_y $	$xG_1^{\alpha 1\cdot} = G_1^{\alpha 3\cdot}, yG_2^{\beta 1\cdot} = G_2^{\beta 3\cdot}$ $xG_1^{\alpha 2\cdot} = G_1^{\alpha 4\cdot}, yG_2^{\beta 2\cdot} = G_2^{\beta 4\cdot}$	

TABLE III. Shorthand notations for special  $\hat{R}$ -symmetry-conserved extrinsic constraints.

Constraint	$(x, y)$			
	$(+1, +1)$	$(-1, +1)$	$(+1, -1)$	$(-1, -1)$
A $\Psi\{\hat{s}_z, 0\}[\hat{i}]'_{xy}$	$ \alpha^g \beta^g $	$ \alpha^u \beta^g $	$ \alpha^g \beta^u $	$ \alpha^u \beta^u $
$\Psi\{\hat{s}_z, 0\}[\hat{\sigma}^{xz}]'_{xy}$	$ \alpha' \beta' $	$ \alpha'' \beta' $	$ \alpha' \beta'' $	$ \alpha'' \beta'' $
B $\Psi\{\hat{s}_z, 0\}[\hat{C}_2^\bullet]'_{xy}$	$ \alpha^+ \beta^+ $	$ \alpha^- \beta^+ $	$ \alpha^+ \beta^- $	$ \alpha^- \beta^- $

coefficients, the electron integrals govern the nature of the solutions obtained.

By substituting the parameterization of the MO coefficients in Equation 18 into the energy expressions in Equation 20, and then optimizing with respect to the angular parameters  $\theta_\alpha$  and  $\theta_\beta$ , we obtain a particularly simple system of trigonometric equations which we denote  $P(\theta; \mathbf{B}) = 0$ :

$$B_1^- \sin 2\theta_\alpha + B_2^- \sin 2\theta_\alpha \cos^2 \theta_\beta + B_2^+ \sin 2\theta_\alpha \sin^2 \theta_\beta + B_3 \cos 2\theta_\alpha \sin 2\theta_\beta = 0, \quad (21a)$$

$$B_1^+ \sin 2\theta_\beta + B_2^- \sin 2\theta_\beta \cos^2 \theta_\alpha + B_2^+ \sin 2\theta_\beta \sin^2 \theta_\alpha + B_3 \cos 2\theta_\beta \sin 2\theta_\alpha = 0, \quad (21b)$$

where  $(\theta_\alpha, \theta_\beta) \in \mathbb{C}^2$ , and the  $B$  coefficients are *definitive* functions of the  $\gamma$ ,  $\eta$ , and  $A$  coefficients:

$$B_1^\pm = \frac{2\eta^\pm}{1 - (\gamma^\pm)^2} (-\gamma^\pm A_1^\pm + A_2^\pm), \quad (22a)$$

$$B_2^{\pm\pm} = \frac{\eta^- \eta^+ [-\gamma^+ (A_3 + A_5) + 2(\mp \gamma^+ A_4^- + A_4^+)]}{[1 - (\gamma^+)^2](1 \pm \gamma^-)} \pm 2A_6, \quad (22b)$$

$$B_2^{\pm\pm} = \frac{\eta^- \eta^+ [-\gamma^- (A_3 + A_5) + 2(\mp \gamma^- A_4^+ + A_4^-)]}{[1 - (\gamma^-)^2](1 \pm \gamma^+)} \pm 2A_6, \quad (22c)$$

$$B_3 = \frac{\eta^- \eta^+}{\sqrt{1 - (\gamma^-)^2} \sqrt{1 - (\gamma^+)^2}} (A_3 - A_5). \quad (22d)$$

By converting  $P(\theta; \mathbf{B}) = 0$  to an exponential form using Euler's formula and substituting  $z_1 = e^{2i\theta_\alpha}$  and

$z_2 = e^{2i\theta_\beta}$ , we obtain an equivalent polynomial form  $\bar{P}(\mathbf{z}; \mathbf{B}) = 0$ :

$$(z_1^2 - 1)[4B_1^- z_2 + B_2^- (z_2 + 1)^2 - B_2^+ (z_2 - 1)^2] + 2B_3 (z_1^2 + 1)(z_2^2 - 1) = 0, \quad (23a)$$

$$(z_2^2 - 1)[4B_1^+ z_1 + B_2^+ (z_1 + 1)^2 - B_2^- (z_1 - 1)^2] + 2B_3 (z_1^2 - 1)(z_2^2 + 1) = 0. \quad (23b)$$

The system  $\bar{P}(\mathbf{z}; \mathbf{B}) = 0$  contains the governing equations for the SCF solutions in the constraining spaces listed in Table II. In what follows, we will solve  $\bar{P}(\mathbf{z}; \mathbf{B}) = 0$  for  $z_1$  and  $z_2$  analytically to obtain closed-form expressions for the angular parameters  $\theta_\alpha$  and  $\theta_\beta$ .

## V. $[H_4]^{2+}$ MODEL: ANALYTIC SOLUTIONS

### A. General Forms of Solutions

Since each equation in  $\bar{P}(\mathbf{z}; \mathbf{B}) = 0$  has  $z_1^2 z_2^2$  as its highest-order term, Bézout's theorem<sup>20,39</sup> requires that, if the system  $\bar{P}(\mathbf{z}; \mathbf{B}) = 0$  has a finite number of solutions, then it can have *at most* 16 solutions. However, if we now let  $\bar{Q}(\mathbf{z}; \mathbf{B}) = 0$  be the corresponding auxiliary system

$$(2B_3 + B_2^- - B_2^+) z_1^2 z_2^2 = 0,$$

$$(2B_3 + B_2^+ - B_2^-) z_1^2 z_2^2 = 0,$$

which is constructed from the highest-degree terms of the equations in  $\bar{P}(\mathbf{z}; \mathbf{B}) = 0$ , then, by Theorem 3.1 of Ref. 38, that  $\bar{Q}(\mathbf{z}; \mathbf{B}) = 0$  has non-trivial solutions (*e.g.*,  $z_1 \in \mathbb{C}, z_2 = 0$ ) implies that the system  $\bar{P}(\mathbf{z}; \mathbf{B}) = 0$  *must* have fewer than 16 solutions. The upper bound due to Bézout's theorem is therefore not tight.

In fact, the system  $\bar{P}(\mathbf{z}; \mathbf{B}) = 0$  turns out to admit eight solutions as obtained using the symbolic solvers in Mathematica 12.1.<sup>41</sup> And although each solution  $(z_1, z_2)$

of  $\bar{P}(\mathbf{z}; \mathbf{B}) = 0$  yields infinitely many algebraically different solutions for  $P(\boldsymbol{\theta}; \mathbf{B}) = 0$  of the form  $(\theta_\alpha + m\pi, \theta_\beta + n\pi)$  for  $m, n \in \mathbb{Z}$ , they all correspond to MOs that differ from one another by a factor of  $\pm 1$  (see Equation 18), and therefore give only a single physically distinct SCF determinant. It thus suffices to examine only the principal solution  $([\theta_\alpha], [\theta_\beta])$  arising from each  $(z_1, z_2)$  pair. The analytic forms for these solutions are given in Table IV.

*a. Persistently Real Solutions.*  $\bar{P}(\mathbf{z}; \mathbf{B}) = 0$  admits four obvious solutions (labeled 1a–d in Table IV) which give rise to  $\theta_\alpha$  and  $\theta_\beta$  that are real and independent of the  $B$  coefficients, so long as the functional forms of  $P(\boldsymbol{\theta}; \mathbf{B}) = 0$  and  $\bar{P}(\mathbf{z}; \mathbf{B}) = 0$ , which are determined by the various intrinsic and extrinsic constraints under consideration (Tables I and II), remain unchanged. In other words, when the molecular symmetry of  $[\text{H}_4]^{2+}$  has been fixed and appropriate requirements for symmetry conservation have been imposed on the MOs, solutions 1a–d will always exist in the real domain of the coefficients, regardless of the H–H bond lengths, and must therefore always be locatable by conventional SCF HF methods. In fact, they are controlled entirely by the AO-overlap integrals via the  $\gamma$  and  $\eta$  coefficients in Equation 18 while the core-Hamiltonian and the two-electron AO integrals have no effects on them.

*b. Transiently Real Solutions.*  $\bar{P}(\mathbf{z}; \mathbf{B}) = 0$  admits four more solutions (labeled 2a, 2a', 2b, and 2b' in Table IV) which give rise to generally complex  $\theta_\alpha$  and  $\theta_\beta$ . From the general form  $[\theta_\sigma] = -i \text{Ln}(u_\sigma \pm iv_\sigma)$  for the principal values of the angular parameters, if we write

$$u_\sigma \pm iv_\sigma = r_\sigma e^{i\varphi_\sigma}, \quad r_\sigma \in \mathbb{R}_+^*, \quad \varphi_\sigma \in (-\pi, \pi], \quad (24)$$

then

$$[\theta_\sigma] = \varphi_\sigma - i \ln r_\sigma, \quad (25)$$

which implies that  $\theta_\sigma$  is real if and only if the quantity

$$\begin{aligned} \rho_\sigma &\equiv \Im[\theta_\sigma] = -\ln r_\sigma \\ &= -\ln \sqrt{(\Re u_\sigma \mp \Im v_\sigma)^2 + (\Im u_\sigma \pm \Re v_\sigma)^2} \end{aligned} \quad (26)$$

vanishes. Here,  $\sigma \in \{\alpha, \beta\}$  and  $u_\sigma, v_\sigma$  refer to the appropriate variants of  $u^{\pm\pm}$  and  $v^{\pm\pm}$  that correspond to the solution of interest as given in Table IV. The relation between  $\theta_\alpha$  and  $\theta_\beta$  imposed by  $P(\boldsymbol{\theta}; \mathbf{B}) = 0$  in Equation 21 requires that if  $\theta_\alpha$  is real, then so is  $\theta_\beta$ , and *vice versa*, which enables us to define  $\rho \equiv \rho_\alpha$  as a reality indicator for solutions 2a and 2b.

It turns out that all of the numerically located  $M_S = 0$  conventional UHF solutions shown in Figure 1 conserve  $\hat{i}$ -symmetry along molecular symmetry pathway A. As such, they can all be captured by the analytic solutions obtained under the special  $\hat{i}$ -symmetry-conserved extrinsic constraints  $|\alpha^g \beta^g|$ ,  $|\alpha^u \beta^g|$ , and  $|\alpha^u \beta^u|$ . Table V maps the analytic solutions to the numerical solutions using the labels in Figure 1. We therefore focus on the analytic solutions for these three extrinsic constraints in

the following discussion. The holomorphic energies of these solutions together with their reality indicators are plotted in Figure 4, the corresponding variations of their spin-orbitals are shown in Table VII, and the accompanying animations in the included video (see Section S-II in the Supplementary Material).

## B. Consequences of Symmetry Constraints

### 1. Strong Reality Requirements

The dependence of the reality indicator  $\rho$  on the  $B$  coefficients, and hence the electron integrals, via  $u_\sigma$  and  $v_\sigma$  (Equation 26) prompts the questions of whether there exist conditions on these coefficients such that  $\rho$  is forced to vanish identically, and how these conditions are related to the various constraints imposed by symmetry on the system. General answers to these questions are challenging to obtain without a more in-depth analysis of the algebraic complexity of the HF equations which we do not intend to carry out in the current study. Instead, we merely wish to demonstrate the existence of several such conditions that arise from the interplay between the intrinsic and extrinsic constraints exhibited by the model  $[\text{H}_4]^{2+}$  system so as to provide some insight into the attributes of the transiently real solutions.

In Table VI, we list the electron-integral coefficients  $S$  and  $A$  that are forced to vanish identically by particular combinations of spatial intrinsic constraints ( $\mathcal{D}_{4h}$ ) and spin and spatial extrinsic constraints ( $|\alpha^u \beta^g|$  and  $|\alpha^u \beta^u|$ ) along pathway A (*cf.* the explicit functional forms for these coefficients in Section S-I of the Supplementary Material). Consequently, by Equations 19 and 22, several related  $\gamma$  and  $B$  coefficients must vanish, as also listed in Table VI. This simplifies  $u_\sigma$  and  $v_\sigma$  via the various expressions for the  $D$  and  $\Delta$  coefficients in Table IV and eventually annihilates  $\rho$  for both solutions 2a and 2b, thus mandating these generally complex solutions to be real. In fact, the indicator plots for the extrinsic constraints  $|\alpha^u \beta^g|$  and  $|\alpha^u \beta^u|$  in Figure 4 show clearly the vanishing of  $\rho$  at  $\mathcal{D}_{4h}$ . This explains the ability to numerically locate the transiently real solutions B, C, C<sup>5'</sup>, and D'' in the vicinity of  $\mathcal{D}_{4h}$  using conventional HF, but not further away. This also reveals that there are four more solutions—namely, the transiently real solutions of  $|\alpha^g \beta^g|$ —that cannot be found numerically using conventional HF for the particular length scale  $a = 1.058350 \text{ \AA}$  even at  $\mathcal{D}_{4h}$  since the combined extrinsic constraint of  $|\alpha^g \beta^g|$  and intrinsic constraint of  $\mathcal{D}_{4h}$  are not sufficient to force them to be real.

The required vanishing of  $\rho$  at  $\mathcal{D}_{4h}$  for  $|\alpha^u \beta^g|$  and  $|\alpha^u \beta^u|$  depends only on the combinations of intrinsic and extrinsic symmetry constraints but not at all on the actual value of the scale length  $a$ . We thus consider such reality requirements to be *strong*. This is illustrated in Figure 5 where the reality indicator  $\rho$  for solutions 2a and 2b is plotted over both geometrical parameters  $a$  and  $k_1$ .

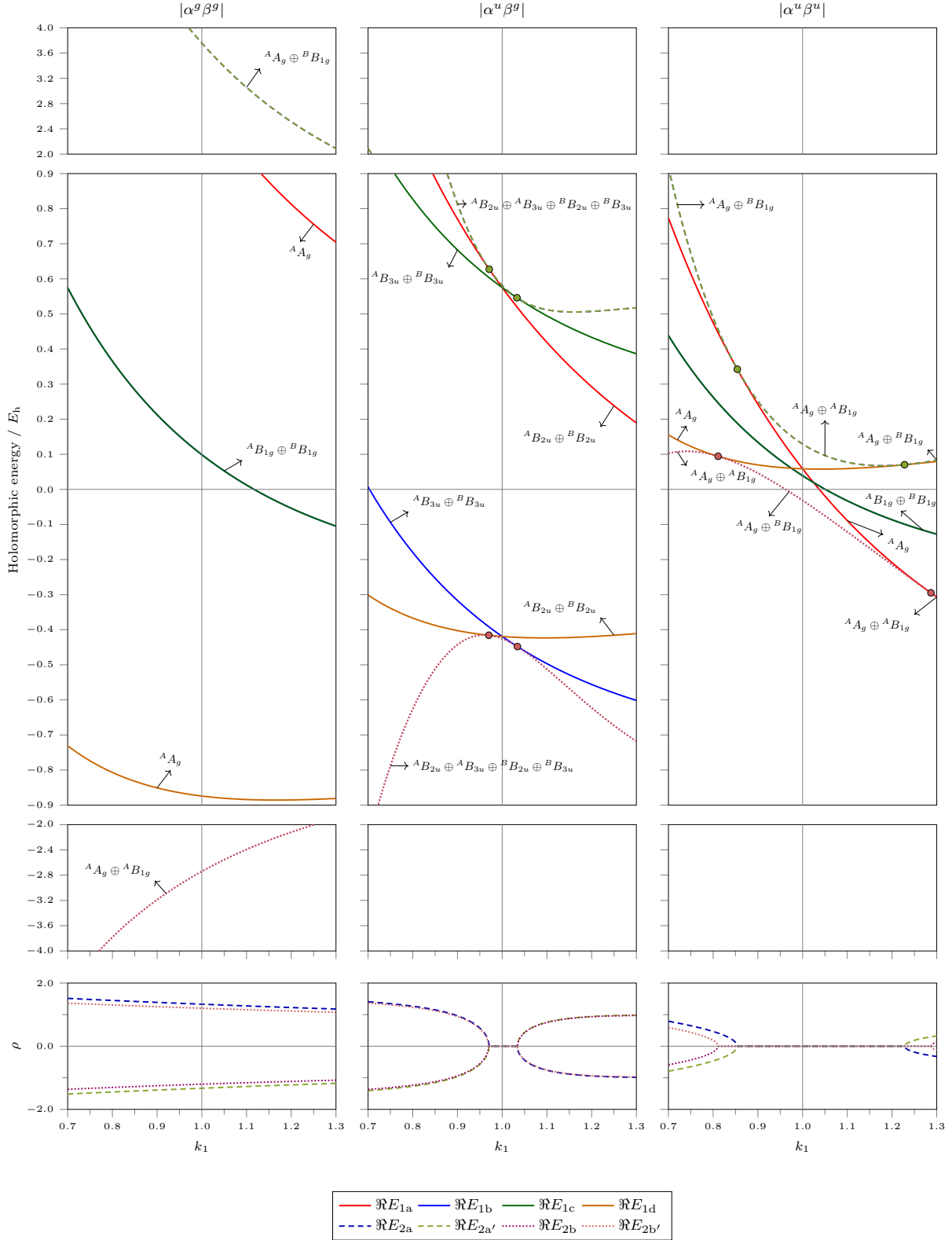


FIG. 4. Holomorphic energy, symmetry, and reality indicator of the analytic solutions for  $[\text{H}_4]^{2+}$  in STO-3G for the special  $\hat{i}$ -symmetry-conserved extrinsic constraints in the vicinity of  $\mathcal{D}_{4h}$  along molecular symmetry pathway A at  $a = 1.058350 \text{ \AA}$ . The holomorphic energy is real in all cases. The exact locations where solutions 2a and 2b undergo real–non-real transition are indicated by colored dots on the energy curves. The irreducible corepresentations in  $\mathcal{T} \otimes \mathcal{D}_{2h}$  are denoted by  ${}^\gamma \Gamma$  where  $\gamma$  is an irreducible corepresentation in  $\mathcal{T}$  and  $\Gamma$  an irreducible representation in  $\mathcal{D}_{2h}$ .

TABLE IV. Analytic SCF solutions of  $[H_4]^{2+}$  in STO-3G under the extrinsic constraints considered in Table II.  $[\theta_\alpha]$  and  $[\theta_\beta]$  denote the principal solutions of the  $P(\boldsymbol{\theta}; \mathbf{B}) = 0$  system and  $\text{Ln } z$  denotes the principal natural logarithm of a complex number  $z$ , *i.e.*, if  $z = re^{i\varphi}$ , then  $\text{Ln } z = \ln r + i\varphi$  for  $r \in \mathbb{R}_+^*$  and  $\varphi \in (-\pi, \pi]$ . For solutions 2a and 2b, only two out of the four possible  $(z_1, z_2)$  combinations are true solutions of  $\bar{P}(\mathbf{z}; \mathbf{B}) = 0$  while the other two are extraneous—the exact combinations that solve  $\bar{P}(\mathbf{z}; \mathbf{B}) = 0$  depend on the precise values of the  $B$  coefficients. When non-real, the angular parameters for the primed and unprimed variants of 2a and 2b are complex-conjugates of each other.

Solution	$z_1$	$z_2$	$[\theta_\alpha]$	$[\theta_\beta]$
1a	+1	+1	0	0
1b	+1	-1	0	$\pi/2$
1c	-1	+1	$\pi/2$	0
1d	-1	-1	$\pi/2$	$\pi/2$
2a	$(u^{--} + iv^{-+})^2$	$(u^{+-} \pm iv^{++})^2$	$-i \text{Ln}(u^{--} + iv^{-+})$	$-i \text{Ln}(u^{+-} \pm iv^{++})$
2a'	$(u^{--} - iv^{-+})^2$		$-i \text{Ln}(u^{--} - iv^{-+})$	
2b	$(u^{-+} + iv^{--})^2$	$(u^{++} \pm iv^{+-})^2$	$-i \text{Ln}(u^{-+} + iv^{--})$	$-i \text{Ln}(u^{++} \pm iv^{+-})$
2b'	$(u^{-+} - iv^{--})^2$		$-i \text{Ln}(u^{-+} - iv^{--})$	

$$u^{-\mp} = \frac{\sqrt{D_1^{-+} \mp D_2^- \sqrt{\Delta}}}{\sqrt{D_1^{--} + D_1^{-+}}} \quad v^{-\pm} = \frac{\sqrt{D_1^{--} \pm D_2^- \sqrt{\Delta}}}{\sqrt{D_1^{--} + D_1^{-+}}}$$

$$u^{+\mp} = \frac{\sqrt{D_1^{++} \mp D_2^+ \sqrt{\Delta}}}{\sqrt{D_1^{+-} + D_1^{++}}} \quad v^{+\pm} = \frac{\sqrt{D_1^{+-} \pm D_2^+ \sqrt{\Delta}}}{\sqrt{D_1^{+-} + D_1^{++}}}$$

$$D_1^{\pm} = 4B_3^4 \pm 2(B_1^- + B_2^{-})(B_1^- + B_2^{-})(B_1^+ + B_2^{+\pm})(B_2^{\pm-} - B_2^{++})$$

$$+ B_3^2 \left[ (2B_1^- + B_2^{-} + B_2^{+})^2 \pm (B_2^{-} - B_2^{+})(2B_1^+ - B_2^{\mp} + 3B_2^{\pm}) \right]$$

$$D_1^{\pm} = 4B_3^4 \pm 2(B_1^+ + B_2^{+})(B_1^+ + B_2^{+})(B_1^- + B_2^{\pm})(B_2^{\pm-} - B_2^{-})$$

$$+ B_3^2 \left[ (2B_1^+ + B_2^{+} + B_2^{+})^2 \pm (B_2^{+} - B_2^{-})(2B_1^- - B_2^{\mp} + 3B_2^{\pm}) \right]$$

$$D_2^{\pm} = B_3(2B_1^{\pm} + B_2^{\pm-} + B_2^{++})$$

$$\Delta = 4B_3^4 + 4(B_1^- + B_2^{-})(B_1^- + B_2^{-})(B_1^+ + B_2^{+})(B_1^+ + B_2^{+})$$

$$+ B_3^2 \left[ (2B_1^- + B_2^{-} + B_2^{+})^2 + (2B_1^+ + B_2^{+} + B_2^{+})^2 - 2(B_2^{-} - B_2^{+})(B_2^{\pm-} - B_2^{++}) \right]$$

TABLE V. Identification of analytic solutions with numerical UHF solutions along molecular pathway A at  $a = 1.058350 \text{ \AA}$ . Repeated labels indicate solutions related by spatial symmetry.

Sol.	$ \alpha^g \beta^g $	$ \alpha^u \beta^g $	$ \alpha^u \beta^u $
1a	E	D	C''
1b	C <sup>4'</sup>	B'	C'
1c	C <sup>4'</sup>	D'	C'
1d	A	B''	C'''
2a	-	D''	C <sup>5'</sup>
2a'	-	D''	C <sup>5'</sup>
2b	-	B	C
2b'	-	B	C

TABLE VI. Vanishing electron-integral coefficients along pathway A.

Extrinsic constraints	$\mathcal{D}_{2h}$ ( $k_1 \neq 1$ )	$\mathcal{D}_{4h}$ ( $k_1 = 1$ )
$ \alpha^g \beta^g $	-	-
$ \alpha^u \beta^g $	-	$S_2^-$ $A_2^-$ $A_4^-$ $A_6$ $\gamma^-$ $B_1^-$ $B_2^\pm$
$ \alpha^u \beta^u $	-	$S_2^\pm$ $A_2^\pm$ $A_4^\pm$ $\gamma^\pm$ $B_1^\pm$

These plots show that the aforementioned required reality for  $|\alpha^u \beta^g|$  and  $|\alpha^u \beta^u|$  at  $\mathcal{D}_{4h}$  holds for all values of  $a$ .

## 2. Weak Reality Requirements

Figure 5 also reveals the existence of “seas” of real solutions (white regimes) surrounding “islands” of non-real holomorphic solutions (colored regimes). In other words, these features show that, even at configurations where the electron-integral coefficients are not forced to vanish identically by symmetry as indicated in Table VI, the reality indicator  $\rho$  can still vanish and the corresponding transiently real solutions are still required to be real-valued. This turns out to be a consequence of the fine balances between the electron-integral coefficients. An algebraic consideration as detailed in Section S-III of the Supplementary Material shows that, under the constraints listed in Table II, a more general condition for  $\rho$  to vanish is

$$\frac{D_1^{-+} - D_2^- \sqrt{\Delta}}{D_1^{-+} + D_1^{++}} \geq 0 \quad \text{and} \quad \frac{D_1^{--} + D_2^- \sqrt{\Delta}}{D_1^{--} + D_1^{++}} \geq 0 \quad (27a)$$

for solutions 2a, and

$$\frac{D_1^{-+} + D_2^- \sqrt{\Delta}}{D_1^{+-} + D_1^{++}} \geq 0 \quad \text{and} \quad \frac{D_1^{--} - D_2^- \sqrt{\Delta}}{D_1^{+-} + D_1^{++}} \geq 0 \quad (27b)$$

for solutions 2b. These inequalities implicitly define the regions of reality over the parameter space of interest, and they are now dependent on the scale length  $a$  via the electron-integral coefficients, even though their forms are still fixed by the imposed constraints. For this reason, we consider the resulting reality requirements to be *weak*.

## 3. Coalescence Boundaries

When the conditions in Inequalities 27 cease to hold, the corresponding transiently real solutions become non-real. If the  $D$  and  $\Delta$  coefficients vary smoothly, then the onset of this transition occurs when

$$D_1^{-+} - D_2^- \sqrt{\Delta} = 0 \quad \text{or} \quad D_1^{--} + D_2^- \sqrt{\Delta} = 0 \quad (28a)$$

for solutions 2a, and

$$D_1^{-+} + D_2^- \sqrt{\Delta} = 0 \quad \text{or} \quad D_1^{--} - D_2^- \sqrt{\Delta} = 0 \quad (28b)$$

for solutions 2b. These equations give implicit descriptions of the locations of the *coalescence boundaries* across which real conventional HF solutions that we classify in this article as transiently real are commonly known to coalesce and disappear as they become holomorphically non-real.

When the forms of the transiently real solutions 2a and 2b (Table IV) are subject to the conditions in Equation 28, the primed and unprimed variants become identical to each other and also to one of the persistently real solutions. The coalescence boundaries in all cases exhibit a triple degeneracy (ignoring any additional degeneracies due to time-reversal symmetry) where each pair of corresponding transiently real solutions are required to coalesce with each other and with one of the persistently real solutions as they transition between the real and non-real regimes. Such coalescence points are also marked out in Figure 4 and can be seen to form one-dimensional boundaries over the  $a$ - $k_1$  plane in Figure 5.

## VI. $[\text{H}_4]^{2+}$ MODEL: SOLUTION SYMMETRY

### A. Complex-Conjugation Symmetry

#### 1. Real Regimes

The solutions of  $\bar{P}(z; \mathbf{B}) = 0$  exhibit special behaviors under complex conjugation due to the forms they adopt. Trivially, the persistently real solutions 1a–1d are invariant under the action of  $\hat{\kappa}$  (defined in Equation 2), so that their conventional and holomorphic energies coincide and



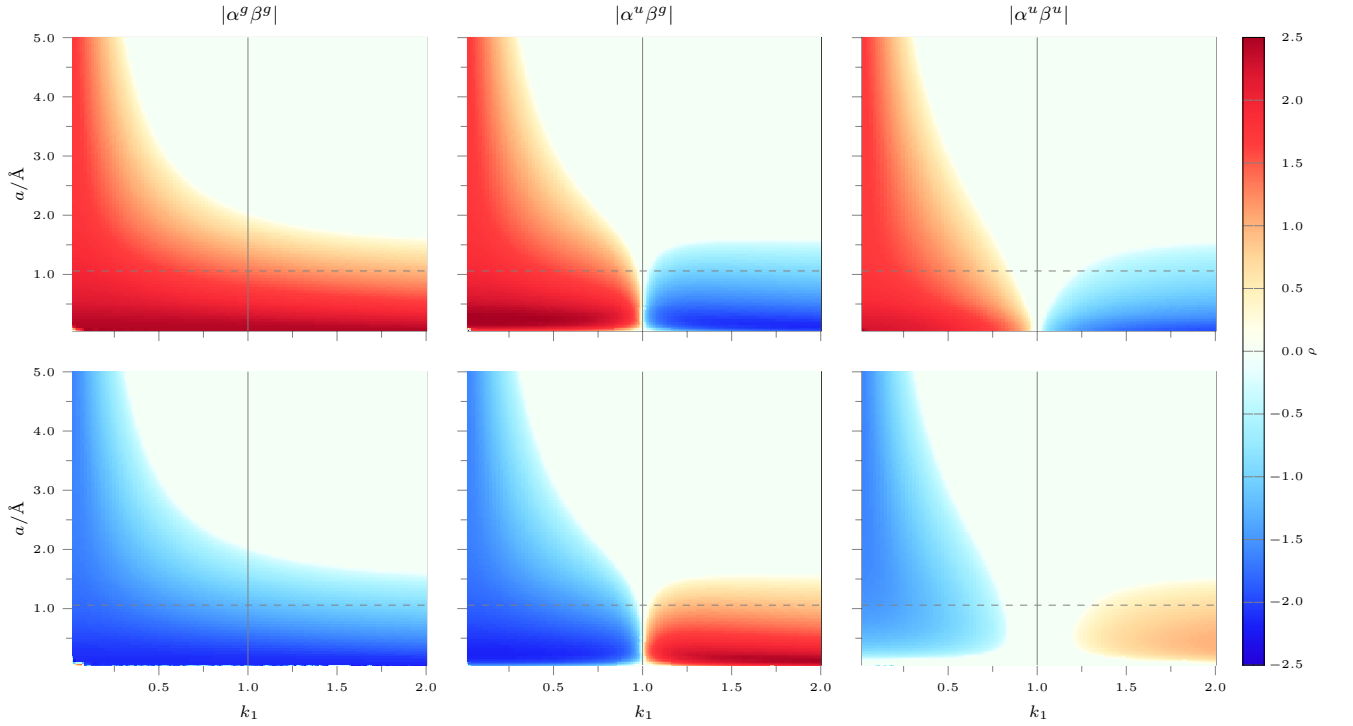


FIG. 5. Reality indicator of solutions 2a and 2b along pathway A at different scale lengths  $a$  for the special  $\hat{i}$ -symmetry-conserved extrinsic constraints. In each case, the reality indicator for solutions 2a is shown in the top panel while that for solutions 2b in the bottom panel. The vertical line at  $k_1 = 1$  indicates  $\mathcal{D}_{4h}$  symmetry, and the dashed horizontal line indicates  $a = 1.058350 \text{ \AA}$ . The real regimes are white whereas the non-real regimes are colored.

must both be real:

$$\begin{aligned}
 E[\Psi^{\text{HF}}] &= \frac{\langle \Psi^{\text{HF}} | \hat{\mathcal{H}} | \Psi^{\text{HF}} \rangle}{\langle \Psi^{\text{HF}} | \Psi^{\text{HF}} \rangle} = \frac{\langle \hat{\kappa} \Psi^{\text{HF}} | \hat{\mathcal{H}} | \hat{\kappa} \Psi^{\text{HF}} \rangle^*}{\langle \hat{\kappa} \Psi^{\text{HF}} | \hat{\kappa} \Psi^{\text{HF}} \rangle^*} \\
 &= \frac{\langle \Psi^{\text{HF}} | \hat{\mathcal{H}} | \Psi^{\text{HF}} \rangle^*}{\langle \Psi^{\text{HF}} | \Psi^{\text{HF}} \rangle^*} = E^*[\Psi^{\text{HF}}], \quad (29a)
 \end{aligned}$$

$$\begin{aligned}
 \tilde{E}[\Psi^{\text{HF}}] &= \frac{\langle \hat{\kappa} \Psi^{\text{HF}} | \hat{\mathcal{H}} | \Psi^{\text{HF}} \rangle}{\langle \hat{\kappa} \Psi^{\text{HF}} | \Psi^{\text{HF}} \rangle} = \frac{\langle \Psi^{\text{HF}} | \hat{\mathcal{H}} | \Psi^{\text{HF}} \rangle}{\langle \Psi^{\text{HF}} | \Psi^{\text{HF}} \rangle} = E[\Psi^{\text{HF}}], \quad (29b)
 \end{aligned}$$

where we have used the antiunitarity of  $\hat{\kappa}$  and its commutativity with  $\hat{\mathcal{H}}$  for the second equality in the first line.

The transiently real solutions, however, behave less straightforwardly. Let us take  $\Psi^{\text{HF}}$  to be any one of them. In the regimes where the reality indicator  $\rho$  vanishes for this solution, its angular parameters  $\theta_\sigma$  are real, its spin-orbitals  $\chi_i$  must be real-valued, and  $\Psi^{\text{HF}}$  itself must once again be invariant under  $\hat{\kappa}$ . The conditions of Equation 29 thus apply and the same conclusion can be drawn for the energies of this solution in these regimes of reality.

## 2. Non-Real Regimes

*a. Energy Reality.* Outside of the real regimes,  $\rho$  is non-zero,  $\theta_\sigma$  is complex, and generally there is not much to say about the behavior of  $\Psi^{\text{HF}}$  under  $\hat{\kappa}$ . However, it turns out that the real part of  $[\theta_\sigma]$  is *not* arbitrary, and this dictates how  $\hat{\kappa}$  affects  $\Psi^{\text{HF}}$ . From Equations 24 and 25, we obtain

$$\Re[\theta_\sigma] = \varphi_\sigma = \text{Arg}(u_\sigma \pm iv_\sigma) \quad (30)$$

where  $\text{Arg}$  is the principal argument function. As explained in Section S-III of the Supplementary Material, under the conditions in this work,  $u_\sigma$  and  $v_\sigma$  are either purely real or purely imaginary, and hence, for  $\rho$  to be non-zero, one of them must be real and the other one imaginary. Consequently,  $u_\sigma \pm iv_\sigma$  must also be either purely real or purely imaginary, so  $\varphi_\sigma$  can only take values of 0 or  $\pm\pi/2$ , and by virtue of Equation 18, we deduce that

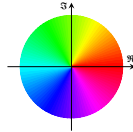
$$\begin{cases} (G_i^{\sigma 1, \cdot})^* = -G_i^{\sigma 2, \cdot} & \text{if } [\theta_\sigma] = i\rho_\sigma, \\ (G_i^{\sigma 1, \cdot})^* = +G_i^{\sigma 2, \cdot} & \text{if } [\theta_\sigma] = \pm\frac{\pi}{2} + i\rho_\sigma. \end{cases}$$

Because of these relations, the effect of  $\hat{\kappa}$  on  $\Psi^{\text{HF}}$  as given by Equations 2 and 8 is thus

$$\hat{\kappa} \Psi^{\text{HF}} = \pm \hat{R} \Psi^{\text{HF}} \quad (31)$$

TABLE VII. Spin-orbitals of special  $\hat{i}$ -symmetry-conserved solutions at three representative points along molecular pathway A. Each circle represents the coefficient of a  $1s$  AO: the circle's area is proportional to the magnitude of the coefficient, and the angular position of the dot on the circumference, as well as the hue of the fill color, indicates its phase. Circles corresponding to real coefficients have thicker boundaries. Shown beneath the spin-orbitals are the reality indicator  $\rho$  and the symmetry classifications in  $\mathcal{T} \otimes \mathcal{D}_{2h}$ . The irreducible corepresentations in  $\mathcal{T} \otimes \mathcal{D}_{2h}$  are denoted by  ${}^\gamma\Gamma$  where  $\gamma$  is an irreducible corepresentation in  $\mathcal{T}$  and  $\Gamma$  an irreducible representation in  $\mathcal{D}_{2h}$ . Only one set of symmetry symbols is given for brevity if the solution symmetry is the same at all three  $k_1$  values. See also the accompanied animations (Section S-II of the Supplementary Material) that show the variations of these spin-orbitals along pathway A.

Sol.	$ \alpha^g\beta^g $			$ \alpha^u\beta^g $			$ \alpha^u\beta^u $		
	$k_1 = 0.70$	$k_1 = 1.00$	$k_1 = 1.30$	$k_1 = 0.70$	$k_1 = 1.00$	$k_1 = 1.30$	$k_1 = 0.70$	$k_1 = 1.00$	$k_1 = 1.30$
1a		 ${}^A A_g$			 ${}^A B_{2u} \oplus {}^B B_{2u}$			 ${}^A A_g$	
1b		 ${}^A B_{1g} \oplus {}^B B_{1g}$			 ${}^A B_{3u} \oplus {}^B B_{3u}$			 ${}^A B_{1g} \oplus {}^B B_{1g}$	
1c		 ${}^A B_{1g} \oplus {}^B B_{1g}$			 ${}^A B_{3u} \oplus {}^B B_{3u}$			 ${}^A B_{1g} \oplus {}^B B_{1g}$	
1d		 ${}^A A_g$			 ${}^A B_{2u} \oplus {}^B B_{2u}$			 ${}^A A_g$	
2a	 $\rho = +1.514$	 $\rho = +1.331$ ${}^A A_g \oplus {}^B B_{1g}$	 $\rho = +1.177$	 $\rho = +1.409$	 $\rho = +0.000$ ${}^A B_{2u} \oplus {}^A B_{3u} \oplus {}^B B_{2u} \oplus {}^B B_{3u}$	 $\rho = -0.984$	 $\rho = +0.791$ ${}^A A_g \oplus {}^B B_{1g}$	 $\rho = +0.000$ ${}^A A_g \oplus {}^A B_{1g}$	 $\rho = -0.326$ ${}^A A_g \oplus {}^B B_{1g}$
2a'	 $\rho = -1.514$	 $\rho = -1.331$ ${}^A A_g \oplus {}^B B_{1g}$	 $\rho = -1.177$	 $\rho = -1.409$	 $\rho = +0.000$ ${}^A B_{2u} \oplus {}^A B_{3u} \oplus {}^B B_{2u} \oplus {}^B B_{3u}$	 $\rho = +0.984$	 $\rho = -0.791$ ${}^A A_g \oplus {}^B B_{1g}$	 $\rho = +0.000$ ${}^A A_g \oplus {}^A B_{1g}$	 $\rho = +0.326$ ${}^A A_g \oplus {}^B B_{1g}$
2b	 $\rho = -1.364$	 $\rho = -1.202$ ${}^A A_g \oplus {}^A B_{1g}$	 $\rho = -1.075$	 $\rho = -1.368$	 $\rho = +0.000$ ${}^A B_{2u} \oplus {}^A B_{3u} \oplus {}^B B_{2u} \oplus {}^B B_{3u}$	 $\rho = +0.972$	 $\rho = -0.589$ ${}^A A_g \oplus {}^A B_{1g}$	 $\rho = +0.000$ ${}^A A_g \oplus {}^B B_{1g}$	 $\rho = +0.131$ ${}^A A_g \oplus {}^A B_{1g}$
2b'	 $\rho = +1.364$	 $\rho = +1.202$ ${}^A A_g \oplus {}^A B_{1g}$	 $\rho = +1.075$	 $\rho = +1.368$	 $\rho = +0.000$ ${}^A B_{2u} \oplus {}^A B_{3u} \oplus {}^B B_{2u} \oplus {}^B B_{3u}$	 $\rho = -0.972$	 $\rho = +0.589$ ${}^A A_g \oplus {}^A B_{1g}$	 $\rho = +0.000$ ${}^A A_g \oplus {}^B B_{1g}$	 $\rho = -0.131$ ${}^A A_g \oplus {}^A B_{1g}$



where  $\hat{R}$  interchanges the MO coefficients on  $H^1$  with those on  $H^2$  and those on  $H^3$  with those on  $H^4$  for every spin-orbital  $\chi_i$  (see Table II). The operator  $\hat{R}$  is therefore a unitary spatial-symmetry operation of the system. As  $\hat{k}$  is involutory, *i.e.*,  $\hat{k}^2 = \text{id}$ ,<sup>42</sup> it follows that  $\hat{R}$  must be too. For all of the constraints in this work, we can identify  $\hat{R}$  with the  $\hat{C}_2^y$  rotation whose axis forms the com-

mon perpendicular bisector of the  $H^1-H^2$  and  $H^3-H^4$  bonds. This relation can be better appreciated by inspecting the forms of the spin-orbitals for the transiently real solutions with  $\rho \neq 0$  in Table VII. We then deduce

that the conventional energy is still real:

$$\begin{aligned} E[\Psi^{\text{HF}}] &= \frac{\langle \Psi^{\text{HF}} | \hat{\mathcal{H}} | \Psi^{\text{HF}} \rangle}{\langle \Psi^{\text{HF}} | \Psi^{\text{HF}} \rangle} = \frac{\langle \hat{\kappa} \Psi^{\text{HF}} | \hat{\mathcal{H}} | \hat{\kappa} \Psi^{\text{HF}} \rangle^*}{\langle \hat{\kappa} \Psi^{\text{HF}} | \hat{\kappa} \Psi^{\text{HF}} \rangle^*} \\ &= \frac{\langle \hat{R} \Psi^{\text{HF}} | \hat{\mathcal{H}} | \hat{R} \Psi^{\text{HF}} \rangle^*}{\langle \hat{R} \Psi^{\text{HF}} | \hat{R} \Psi^{\text{HF}} \rangle^*} = \frac{\langle \Psi^{\text{HF}} | \hat{\mathcal{H}} | \Psi^{\text{HF}} \rangle^*}{\langle \Psi^{\text{HF}} | \Psi^{\text{HF}} \rangle^*} \\ &= E^*[\Psi^{\text{HF}}], \end{aligned} \quad (32a)$$

but the holomorphic energy is no longer identical to the conventional energy:

$$\begin{aligned} \tilde{E}[\Psi^{\text{HF}}] &= \frac{\langle \hat{\kappa} \Psi^{\text{HF}} | \hat{\mathcal{H}} | \Psi^{\text{HF}} \rangle}{\langle \hat{\kappa} \Psi^{\text{HF}} | \Psi^{\text{HF}} \rangle} = \frac{\langle \hat{R} \Psi^{\text{HF}} | \hat{\mathcal{H}} | \Psi^{\text{HF}} \rangle}{\langle \hat{R} \Psi^{\text{HF}} | \Psi^{\text{HF}} \rangle} \\ &\neq E[\Psi^{\text{HF}}]. \end{aligned} \quad (32b)$$

In addition, making use of the involutority and unitarity of  $\hat{R}$ , we obtain

$$\begin{aligned} \tilde{E}[\Psi^{\text{HF}}] &= \frac{\langle \hat{\kappa} \Psi^{\text{HF}} | \hat{\mathcal{H}} | \Psi^{\text{HF}} \rangle}{\langle \hat{\kappa} \Psi^{\text{HF}} | \Psi^{\text{HF}} \rangle} = \frac{\langle \Psi^{\text{HF}} | \hat{\mathcal{H}} | \hat{\kappa} \Psi^{\text{HF}} \rangle^*}{\langle \Psi^{\text{HF}} | \hat{\kappa} \Psi^{\text{HF}} \rangle^*} \\ &= \frac{\langle \Psi^{\text{HF}} | \hat{\mathcal{H}} | \hat{R} \Psi^{\text{HF}} \rangle^*}{\langle \Psi^{\text{HF}} | \hat{R} \Psi^{\text{HF}} \rangle^*} = \frac{\langle \hat{R} \Psi^{\text{HF}} | \hat{\mathcal{H}} | \Psi^{\text{HF}} \rangle^*}{\langle \hat{R} \Psi^{\text{HF}} | \Psi^{\text{HF}} \rangle^*} \\ &= \tilde{E}^*[\Psi^{\text{HF}}], \end{aligned} \quad (32c)$$

which shows that the holomorphic energy must also be real, despite the non-real coefficients. Therefore, there is no need to show the imaginary parts of the holomorphic energy for the transiently real solutions in Figure 4.

The required reality exhibited by the energy functionals in non-real-coefficient regimes is due specifically to Equation 31 which relates the action of an antiunitary operator  $\hat{\kappa}$  to that of an involutory unitary spatial-symmetry operator  $\hat{R}$ . In fact, more generally, for any determinant  $\Psi^{\text{HF}}$  with complex MO coefficients, if we insist that the energies be real, then

$$\begin{aligned} E[\Psi^{\text{HF}}] &= E^*[\Psi^{\text{HF}}] \\ \Rightarrow \frac{\langle \Psi^{\text{HF}} | \hat{\mathcal{H}} | \Psi^{\text{HF}} \rangle}{\langle \Psi^{\text{HF}} | \Psi^{\text{HF}} \rangle} &= \frac{\langle \hat{\kappa} \Psi^{\text{HF}} | \hat{\mathcal{H}} | \hat{\kappa} \Psi^{\text{HF}} \rangle}{\langle \hat{\kappa} \Psi^{\text{HF}} | \hat{\kappa} \Psi^{\text{HF}} \rangle} \end{aligned}$$

and

$$\begin{aligned} \tilde{E}[\Psi^{\text{HF}}] &= \tilde{E}^*[\Psi^{\text{HF}}] \\ \Rightarrow \frac{\langle \hat{\kappa} \Psi^{\text{HF}} | \hat{\mathcal{H}} | \Psi^{\text{HF}} \rangle}{\langle \hat{\kappa} \Psi^{\text{HF}} | \Psi^{\text{HF}} \rangle} &= \frac{\langle \Psi^{\text{HF}} | \hat{\mathcal{H}} | \hat{\kappa} \Psi^{\text{HF}} \rangle}{\langle \Psi^{\text{HF}} | \hat{\kappa} \Psi^{\text{HF}} \rangle}, \end{aligned}$$

both of which imply that the action of  $\hat{\kappa}$  on  $\Psi^{\text{HF}}$  must be identifiable with an involutory unitary symmetry operation  $\hat{U}$ ,

$$\hat{\kappa} \Psi^{\text{HF}} = \pm \hat{U} \Psi^{\text{HF}}, \quad (33)$$

where  $\hat{U}$  need not be a spatial symmetry operation, as long as  $\hat{U}$  acts on the same wavefunction space as  $\hat{\kappa}$  and  $\hat{\mathcal{H}}$  do and  $\hat{U}$  commutes with  $\hat{\mathcal{H}}$ .

*b. Transiently Real Pairs.* The reality of  $\tilde{E}[\Psi^{\text{HF}}]$  means that, if  $\tilde{E}[\Psi^{\text{HF}}]$  is a stationary point in the SCF landscape with a particular set of extrinsic constraints, then so is  $\tilde{E}[\hat{\kappa} \Psi^{\text{HF}}] = \tilde{E}^*[\Psi^{\text{HF}}] = \tilde{E}[\Psi^{\text{HF}}]$ . Thus, in non-real regimes, if  $\Psi^{\text{HF}}$  is one of the transiently real solutions, then  $\hat{\kappa} \Psi^{\text{HF}}$  must be a *different* transiently real solution, which means that the transiently real solutions must occur in complex-conjugate pairs when they are non-real. This is not at all surprising given the algebraic form of  $P(\boldsymbol{\theta}; \mathbf{B}) = 0$  in Equation 21 in which all of the  $B$  coefficients are real. In fact, from Table IV and from the fact that  $u_\sigma$  and  $v_\sigma$  are either purely real or purely imaginary, it can be shown that  $\rho = -\rho'$ , where  $\rho$  and  $\rho'$  are the reality indicators, which are also the imaginary parts, of the unprimed and primed 2a and 2b solutions, respectively.

Due to the identification of  $\hat{\kappa}$  with  $\hat{C}_2^y$  in Equation 31, the primed and unprimed solutions are also related by the  $\hat{C}_2^y$  spatial symmetry in the non-real regimes. But unlike the antilinear  $\hat{\kappa}$ ,  $\hat{C}_2^y$  is linear and we expect its action on  $\Psi^{\text{HF}}$  to be independent of whether  $\Psi^{\text{HF}}$  is real or non-real. The  $\hat{C}_2^y$ -relation between the primed and unprimed solutions therefore persists through all regimes. Consider for example the forms of the 2a and 2a' solutions in the  $|\alpha^u \beta^g|$  constraint shown in Table VII. The  $\hat{C}_2^y$ -relation between 2a and 2a' can be seen at all three values of  $k_1$  plotted, regardless of whether these solutions are real or not. The  $\hat{\kappa}$ -relation between them, however, is absent at  $k_1 = 1.00$  where these two solutions are real.

## B. Time-Reversal Symmetry

Generally, on the domain  $\mathcal{D}$  within each *spatial* extrinsic constraining space (Table II), if  $x \neq y$ , the spatial parts of  $\chi_1$  and  $\chi_2$  must always be linearly independent. In other words, if  $\hat{q}$  is a one-particle spin rotation through an angle of  $\pi$  about the  $y$ -axis such that

$$\hat{q}(\alpha \ \beta) = (\alpha \ \beta) \begin{pmatrix} 0 & -1 \\ 1 & 0 \end{pmatrix},$$

then  $\hat{q}\chi_1$  and  $\chi_2$  are linearly independent, as are  $\chi_1$  and  $\hat{q}\chi_2$ . Hence, for any of the solutions  $\Psi^{\text{HF}}$  obtained under an extrinsic constraint with  $x \neq y$  such as  $|\alpha^u \beta^g|$ , if we define the total spin rotation

$$\hat{Q} \equiv \hat{q}_1 \hat{q}_2 \quad (34)$$

where  $\hat{q}_i$  acts on the  $i^{\text{th}}$  particle, then  $\Psi^{\text{HF}}$  and  $\hat{Q}\Psi^{\text{HF}}$  must be linearly independent. On the other hand, when  $x = y$ , such as in the  $|\alpha^g \beta^g|$  and  $|\alpha^u \beta^u|$  cases, the linear independence between  $\Psi^{\text{HF}}$  and  $\hat{Q}\Psi^{\text{HF}}$  is no longer always guaranteed. We will distinguish between two kinds of solutions: in the first kind, the spatial parts of  $\chi_1$  and  $\chi_2$  are identical up to a phase factor such that  $\hat{q}\chi_1 = \pm\chi_2$  and hence  $\hat{Q}\Psi^{\text{HF}} = \pm\Psi^{\text{HF}}$ ; and in the second kind,  $\hat{q}\chi_1 \neq \pm\chi_2$  so that  $\hat{Q}\Psi^{\text{HF}}$  and  $\Psi^{\text{HF}}$  are linearly independent. For brevity, we shall refer to solutions of the

first kind as *RHF-like solutions* and those of the second kind *non-RHF solutions*. Note that, despite these names, all of the solutions discussed in this work are still UHF in nature due to the spin extrinsic constraint under which they were obtained (see Section III B).

Let us now consider the antiunitary time-reversal operator<sup>42</sup> for  $[\text{H}_4]^{2+}$ :

$$\hat{\Theta} = \hat{Q}\hat{\kappa} = \hat{\kappa}\hat{Q}, \quad (35)$$

where  $\hat{\kappa}$  is given by Equations 2 and 8. Appendix B gives the character table and irreducible corepresentations<sup>42–45</sup> for the time-reversal group  $\mathcal{T}$  generated by  $\hat{\Theta}$ . For the persistently real solutions and the transiently real solutions in the real regimes,  $\hat{\kappa}$  is simply the identity, and therefore the effect of time reversal on these solutions boils down to their behaviors under  $\hat{Q}$  as discussed in the previous paragraph. Specifically, for RHF-like solutions,

$$\hat{Q}\Psi^{\text{HF}} = \pm\Psi^{\text{HF}} \Rightarrow \hat{\Theta}\Psi^{\text{HF}} = \pm\Psi^{\text{HF}},$$

so that  $\Psi^{\text{HF}}$  conserves time-reversal symmetry in the sense that it spans a one-dimensional irreducible corepresentation in  $\mathcal{T}$ . Conversely, for non-RHF solutions,  $\Psi^{\text{HF}}$  and  $\hat{\Theta}\Psi^{\text{HF}}$  are linearly independent and together they span a two-dimensional reducible corepresentation in  $\mathcal{T}$ ; we thus say that  $\Psi^{\text{HF}}$  is now time-reversal symmetry-broken.

More specifically, we note that, whenever the two spin-orbitals  $\chi_1$  and  $\chi_2$  are subject to the same spatial extrinsic constraint such that  $x = y$ , then solutions 1b and 1c become time-reversal partners of each other and must therefore be degenerate. This can be easily verified by inspecting their analytic forms in Table IV, or by inspecting the  $|\alpha^g\beta^g|$  and  $|\alpha^u\beta^u|$  panels in Figure 4 in which the energy curves for solutions 1b and 1c fall exactly on top of each other at all geometries. In addition, the fact that 1b and 1c are time-reversal partners but must remain distinct solutions of  $\bar{P}(\mathbf{z}; \mathbf{B}) = 0$  implies that  $\hat{q}\chi_1 \neq \pm\chi_2$  (as  $\hat{\kappa} = \text{id}$  for persistently real solutions), and so 1b and 1c must be non-RHF solutions and together span a two-dimensional reducible corepresentation in  $\mathcal{T}$ . On the other hand, 1a and 1d are not only distinct but also unrelated by time-reversal symmetry which implies that each of them is its own time-reversal partner and thus conserves time-reversal symmetry. This makes 1a and 1d two qualitatively different RHF-like solutions.

However, when the spatial extrinsic constraints on  $\chi_1$  and  $\chi_2$  differ and  $x \neq y$ , such as for  $|\alpha^u\beta^g|$ , then all four solutions 1a–1d must be non-RHF whose time-reversal partners live in the space in which  $x$  and  $y$  are swapped. The domain  $\mathcal{D}$  in each constraining space  $[\hat{R}]'_{xy}$  thus contains time-reversal partners that are symmetric about the diagonal  $x = y$ . The spin-orbital forms in Table VII can be consulted for concrete examples that illustrate the above description.

Outside the real regimes,  $\hat{\kappa}$  is no longer the identity, and the action of  $\hat{\Theta}$  depends on the composite behaviors

TABLE VIII. Time-reversal symmetry of the UHF solutions for  $[\text{H}_4]^{2+}$  in this work.

coefficients	real	non-real
RHF-like	$\hat{q}\chi_1 = \pm\chi_2,$ $\hat{\Theta}\Psi^{\text{HF}} = \pm\Psi^{\text{HF}}$	$\chi_i^* = -\chi_i$ $\Leftrightarrow \hat{\Theta}\Psi^{\text{HF}} = \pm\Psi^{\text{HF}}$
non-RHF	$\hat{q}\chi_1 \neq \pm\chi_2,$ $\hat{\Theta}\Psi^{\text{HF}} \neq \pm\Psi^{\text{HF}}$	$\hat{q}\chi_1 = \pm\chi_2^*$ $\Leftrightarrow \hat{\Theta}\Psi^{\text{HF}} = \pm\Psi^{\text{HF}}$

of  $\hat{\kappa}$  and  $\hat{Q}$  on  $\Psi^{\text{HF}}$ . In particular, for RHF-like solutions, there are two possibilities: (i) in the special case where  $\chi_i^* = -\chi_i$ , *i.e.*, the spin-orbitals have purely imaginary coefficients, then  $\Psi^{\text{HF}}$  and  $\hat{\Theta}\Psi^{\text{HF}}$  differ only by a phase factor and  $\Psi^{\text{HF}}$  still conserves time-reversal symmetry; (ii) more generally, if  $\chi_i^* \neq -\chi_i$ , then  $\Psi^{\text{HF}}$  and  $\hat{\Theta}\Psi^{\text{HF}}$  are necessarily linearly independent and  $\Psi^{\text{HF}}$  now breaks time-reversal symmetry. For non-RHF solutions, there are also two cases: (i) in the special case where  $\hat{q}\chi_1 = \pm\chi_2^*$ , *i.e.*, the spatial parts of  $\chi_1$  and  $\chi_2$  are complex-conjugates of each other, then  $\Psi^{\text{HF}}$  and  $\hat{\Theta}\Psi^{\text{HF}}$  are linearly dependent, and so  $\Psi^{\text{HF}}$  conserves time-reversal symmetry; (ii) in general, there is no constraint between  $\chi_1$  and  $\chi_2$ , so  $\Psi^{\text{HF}}$  is time-reversal symmetry-broken. These various behaviors under time reversal are summarized in Table VIII.

As a particular solution  $\Psi^{\text{HF}}$  varies smoothly along any molecular symmetry pathway, its spin-orbitals must also vary smoothly due to holomorphicity.<sup>13</sup> This thus has implications concerning the time-reversal symmetry of  $\Psi^{\text{HF}}$  along this pathway. Consider an RHF-like transiently real solution  $\Psi^{\text{HF}}$ , such as the 2a and 2a' solutions of  $|\alpha^u\beta^u|$ . In the real regimes, clearly  $\chi_i^* = +\chi_i$  and  $\hat{\Theta}\Psi^{\text{HF}} = \pm\Psi^{\text{HF}}$ , so that  $\Psi^{\text{HF}}$  conserves time-reversal symmetry. As  $\Psi^{\text{HF}}$  enters the non-real regimes, however, it cannot be that  $\chi_i^* = -\chi_i$  abruptly since a smoothly varying normalized spin-orbital as constrained by Equation 17 cannot switch suddenly from being entirely real to being entirely imaginary. Hence,  $\hat{\Theta}\Psi^{\text{HF}}$  cannot equal  $\pm\Psi^{\text{HF}}$  and  $\Psi^{\text{HF}}$  now breaks time-reversal symmetry. This switch in time-reversal behavior across the real/non-real boundary is thus essential for RHF-like solutions and, more generally, for the RHF spin extrinsic constraint. An example of this can be seen in the 2a and 2a' solutions of  $|\alpha^u\beta^u|$  which independently span the corepresentation  $A$  of  $\mathcal{T}$  in the real regime but then switch to spanning  $A \oplus B$  together in the non-real regimes (Table VII).

If  $\Psi^{\text{HF}}$  is a non-RHF transiently real solution instead, then in general,  $\Psi^{\text{HF}}$  breaks time-reversal symmetry throughout. This is certainly always true in the real regimes. However, if the relation  $\hat{q}\chi_1 = \pm\chi_2^*$  holds in the non-real regimes, then  $\Psi^{\text{HF}}$  and  $\hat{\Theta}\Psi^{\text{HF}}$  describe the same state and  $\Psi^{\text{HF}}$  thus conserves time-reversal symmetry (see Table VIII). As such, this switch in time-

reversal behavior across the real/non-real boundary does not necessarily occur unless other symmetries of the spin-orbitals permit the above relation, such as those observed in the 2b and 2b' solutions under the  $|\alpha^u\beta^u|$  extrinsic constraint (see Table VII). On the other hand, in the extrinsic constraint  $|\alpha^u\beta^g|$ , or more generally, in any extrinsic constraint  $[\hat{R}]'_{xy}$  with  $x \neq y$  (see Table II), the relation  $\hat{q}\chi_1 = \pm\chi_2^*$  is forbidden by the constraining symmetry element  $\hat{R}$ , and no conservation of time-reversal symmetry can be observed in the non-real regimes for non-RHF solutions.

Before moving on, we remark that the discussion so far reveals that the effects of time reversal on holomorphic solutions can be counter-intuitive, particularly because of the antilinearity of the time-reversal operator. Two key features stand out. Firstly, while the spatial symmetry of a solution remains unchanged throughout the molecular pathway (except at coalescence points; see Section VIC below), the same cannot be said for time-reversal symmetry. This is because the antilinearity of the time-reversal operator captures and reflects any transition between the real and non-real regimes of a solution. As a consequence, the normal association of time-reversal symmetry conservation/breaking to restricted/unrestricted spin constraints breaks down outside of real regimes: the antilinearity of the time-reversal operator  $\hat{\Theta}$  sets it apart from the closely-related, but linear, operator  $\hat{Q}$  (defined in Equation 34) that simply effects spin-flipping.

### C. Symmetry and Solution Connectivity

We mention in Section VB3 that, on coalescence boundaries, the two solutions in a transiently real pair become identical to one of the persistently real solutions. The two transiently real solutions therefore lose their linear independence and must span an identical (co)representation space to that of the persistently real solution. As they move away from the coalescence boundary, they become linearly independent and their (co)representation space must increase in dimensionality, but in so doing, it must include the (co)representation space of the persistently real solution, as proven in Appendix C. Consequently, along *any* pathway connecting some coalescence boundaries, the (co)representation space spanned by the transiently real solutions must contain those spanned by the persistently real solutions with which they come into coalescence.

The above property is best illustrated by the  $|\alpha^u\beta^g|$  and  $|\alpha^u\beta^u|$  solutions: the transiently real solutions connect various persistently real solutions (see the energy curves in Figure 4), and the symmetry symbols of the transiently real solutions always include those of the persistently real solutions they connect (see also Table VII). For example, the transiently real 2a and 2a' solutions under  $|\alpha^u\beta^g|$  (middle panel in Figure 4) have  ${}^A B_{2u} \oplus {}^A B_{3u} \oplus {}^B B_{2u} \oplus {}^B B_{3u}$  symmetry, which includes the  ${}^A B_{2u} \oplus {}^B B_{2u}$  symmetry and the  ${}^A B_{3u} \oplus {}^B B_{3u}$  of the

persistently real 1a and 1c solutions, respectively. Here, the symmetry terms of the 2a and 2a' solutions are a disjoint union of those of the 1a and 1c solutions. However, this need not be always the case. Consider the  $|\alpha^u\beta^u|$  transiently real 2a and 2a' solutions and the persistently real 1a and 1d solutions (right panel in Figure 4). The symmetry of 2a and 2a' is  ${}^A A_g \oplus {}^{A/B} B_{1g}$ , while the 1a and 1d solutions both have  ${}^A A_g$  symmetry. The switch in the time-reversal symmetry associated with the  $B_{1g}$  spatial component of the 2a and 2a' solutions (discussed in Section VIB) and the necessary lack thereof in the 1a and 1d solutions mean that the  ${}^{A/B} B_{1g}$  component of the transiently real solutions cannot arise from the two persistently real solutions they connect. Nevertheless, this does not violate the property raised in the preceding paragraph since the  ${}^A A_g$  symmetry of the two persistently real solutions is certainly included in the symmetry of the connecting transiently real solutions.

If the persistently real solutions being connected span different (co)representations, then the transiently real solutions that connect them are guaranteed to span reducible (co)representations and therefore be symmetry-broken. The spin-orbital forms for the transiently real solutions in Table VII show that, in the real regimes, the symmetry breaking occurs via the magnitudes of the MO coefficients, whereas in the non-real regimes, the symmetry breaking is due to the coefficient phases instead. The origin of this behavior can be traced back to the identification of  $\hat{\kappa}$  with  $\hat{C}_2^g$  in Equation 31. More significantly, the forced symmetry breaking of the transiently real solutions implies that, as investigated in our earlier work,<sup>10</sup> these solutions carry some description of electron correlation and can be symmetry-restored to yield multi-determinantal wavefunctions that have the right symmetry and that also incorporate more electron correlation. The solution structure detailed in Table IV thus means that the constraints in Table II necessitate the existence of the symmetry-broken transiently real solutions, even though without appropriate reality requirements, they are non-real and cannot be found by conventional HF methods.

## VII. $[\text{H}_4]^{2+}$ MODEL: CONSTRAINT CONNECTIONS

The extrinsic constraints considered so far ( $|\alpha^g\beta^g|$ ,  $|\alpha^u\beta^g|$ , and  $|\alpha^u\beta^u|$ ) have been deliberately chosen to target the numerically locatable UHF solutions along molecular symmetry pathway A (Figure 1). However, it is of theoretical interest to explore other local regions and global structures of the SCF landscape by varying the extrinsic and intrinsic constraints, respectively. This helps identify hidden connections between solutions that have so far been described in separate extrinsically constrained spaces.

In this Section, we first discuss solutions obtained under a set of extrinsic constraints induced by  $\hat{\sigma}^{xz}$ , a different symmetry element that also persists along pathway



A. This is to further demonstrate the effects of extrinsic constraints on the forms and reality of SCF solutions. We then show the one-to-one correspondence between solutions with  $\hat{i}$  extrinsic constraints and those with  $\hat{\sigma}^{xz}$  extrinsic constraints via molecular pathway B, incidentally exploring their strong reality requirements in the vicinity of the high-symmetry  $\mathcal{T}_d$  geometry. Finally, we explore the symmetry-breaking regions that inter-connect the special extrinsic constraints that have been the focus of the discussion to gain some insight into how relaxing the extrinsic constraints imposed on the molecular orbitals affects solution reality.

### A. Special $\hat{\sigma}^{xz}$ -Symmetry-Conserved Extrinsic Constraints

We show in Figure 6 the energy, symmetry, and reality regimes of the solutions obtained under the special  $\hat{\sigma}^{xz}$ -symmetry-conserved extrinsic constraints (see Table III for their definitions). In addition, the forms of their spin-orbitals along pathway A are given in the included animations (Section S-II of the Supplementary Material). It can be verified that the persistently real solutions in all cases have already been found with the  $\hat{i}$ -symmetry-conserved extrinsic constraints. The transiently real solutions, however, are all not previously encountered. In fact, the symmetry of these solutions (Figure 6a) shows that they are neither purely  $g$  nor  $u$  under  $\hat{i}$  and thus must be excluded from the  $\hat{i}$ -symmetry-conserved regions of the SCF landscape.

Figure 6b reveals that there is now no longer any strong reality requirement at  $\mathcal{D}_{4h}$  in any of the special  $\hat{\sigma}^{xz}$ -symmetry-conserved extrinsic constraints. Weak reality requirements, however, are still in effect and these only allow the transiently real solutions to become real at  $\mathcal{D}_{4h}$  for scale length  $a$  of at least approximately 1.45 Å. This explains why none of these solutions can be found numerically in the vicinity of  $\mathcal{D}_{4h}$  at  $a = 1.058\,350$  Å, as clearly lacking in Figure 1.

Comparing the energy curves and reality indicators of the  $\hat{i}$ -symmetry-conserved in Figure 4 to those of the  $\hat{\sigma}^{xz}$ -symmetry-conserved solutions in Figure 6a, we notice that, due to the lack of strong reality requirements in the latter, none of the transiently real solutions appear to coalesce with more than one persistently real solution along pathway A. Nevertheless, their corepresentations in  $\mathcal{T} \otimes \mathcal{D}_{2h}$  suggest otherwise. For example, the 2a and 2a' solutions of  $|\alpha''\beta''|$  span  ${}^A B_{1g} \oplus {}^A B_{2u} \oplus {}^B B_{1g} \oplus {}^B B_{2u}$  but only coalesce with the 1a solution that spans  ${}^A B_{2u} \oplus {}^B B_{2u}$  along pathway A. We thus suspect that there exist other pathways along which the unobserved coalescence between 2a and 2a' with another persistently real solution that spans  ${}^A B_{1g} \oplus {}^B B_{1g}$  (1b or 1c) occurs.

### B. Connecting $[\hat{i}]'_{xy}$ and $[\hat{\sigma}^{xz}]'_{xy}$ via Pathway B

The similarity in the patterns of the energy curves between the  $\hat{i}$ -symmetry-conserved solutions and the  $\hat{\sigma}^{xz}$ -symmetry-conserved solutions (Figures 4 and 6a) and the identity in their analytic forms (Table IV) both suggest that there is a one-to-one correspondence between these two sets of solutions. In fact, it can be seen from Table II that, for a particular  $(x, y)$ , if  $H^1$  and  $H^2$  are swapped, then the  $\hat{i}$  constraints become  $\hat{\sigma}^{xz}$  and *vice versa*. This thus suggests that the solutions obtained under the two constraints can be connected by a pathway along which the  $H^1$ — $H^2$  bond is rotated about its mutual perpendicular bisector with the  $H^3$ — $H^4$  bond. This is almost pathway B that we introduced earlier (Figure 2b), except that along pathway B, the perpendicular distance between the two bonds is also varied such that when the symmetry factor  $k_2$  equals 1 or 3, the system attains a tetrahedral symmetry. Incidentally, this enables us to access another high symmetry configuration and examine any strong reality requirements that result. The energy variation and reality indicators along pathway B under the special  $\hat{C}_2^\bullet$ -symmetry-conserved extrinsic constraints are plotted in Figure 7. The spin-orbital forms of these solutions and their symmetry can be seen in the included animations (see Section S-II of the Supplementary Material). By comparing these plots with Figures 4, 5, and 6, we see that the  $\hat{C}_2^\bullet$  constraints have been chosen specifically to connect the  $\hat{i}$ -symmetry-conserved solutions at  $\mathcal{D}_{4h}$  ( $k_2 = 0$ ) to the  $\hat{\sigma}^{xz}$ -symmetry-conserved solutions at  $\mathcal{D}_{4h}$  ( $k_2 = 2$ ).

We first observe, on the basis of the reality regimes in Figure 7b, that the  $|\alpha^-\beta^+|$  and  $|\alpha^-\beta^-|$  extrinsic constraints afford strong reality requirements at  $\mathcal{T}_d$  ( $k_2 = 1$  or 3), a property that can be verified analytically by considering vanishing electron-integral coefficients in a similar way to those shown in Table VI. This once again demonstrates the forced reality of the transiently real solutions at a high-symmetry point ( $\mathcal{T}_d$  in this case) which quickly coalesce with other persistently real solutions and become non-real as the molecular symmetry is descended. But more importantly, due to the connectivity of  $\hat{i}$  and  $\hat{\sigma}^{xz}$  constraints via pathway B, the transiently real solutions under the special  $\hat{\sigma}^{xz}$  constraints  $|\alpha''\beta''|$  and  $|\alpha''\beta''|$  that exhibit no strong reality requirements at  $\mathcal{D}_{4h}$  ( $k_2 = 2$ ; see also Figure 6b) can *always* be located in the strongly required real regimes at  $\mathcal{T}_d$  for *any* scale length  $a$  and then tracked to the desired geometry. Unfortunately, no such guarantee can be made for the  $|\alpha^+\beta^+|$  extrinsic constraint which does not exhibit any strong reality requirements along pathway B.

The connectivity provided by pathway B also helps make sense of the corepresentation spaces spanned by the transiently real solutions of  $|\alpha''\beta''|$ . For example, as mentioned at the very end of Section VII A, the coalescence between the 2a/2a' solutions and the 1a solution along pathway A only accounts for two of the four symmetry

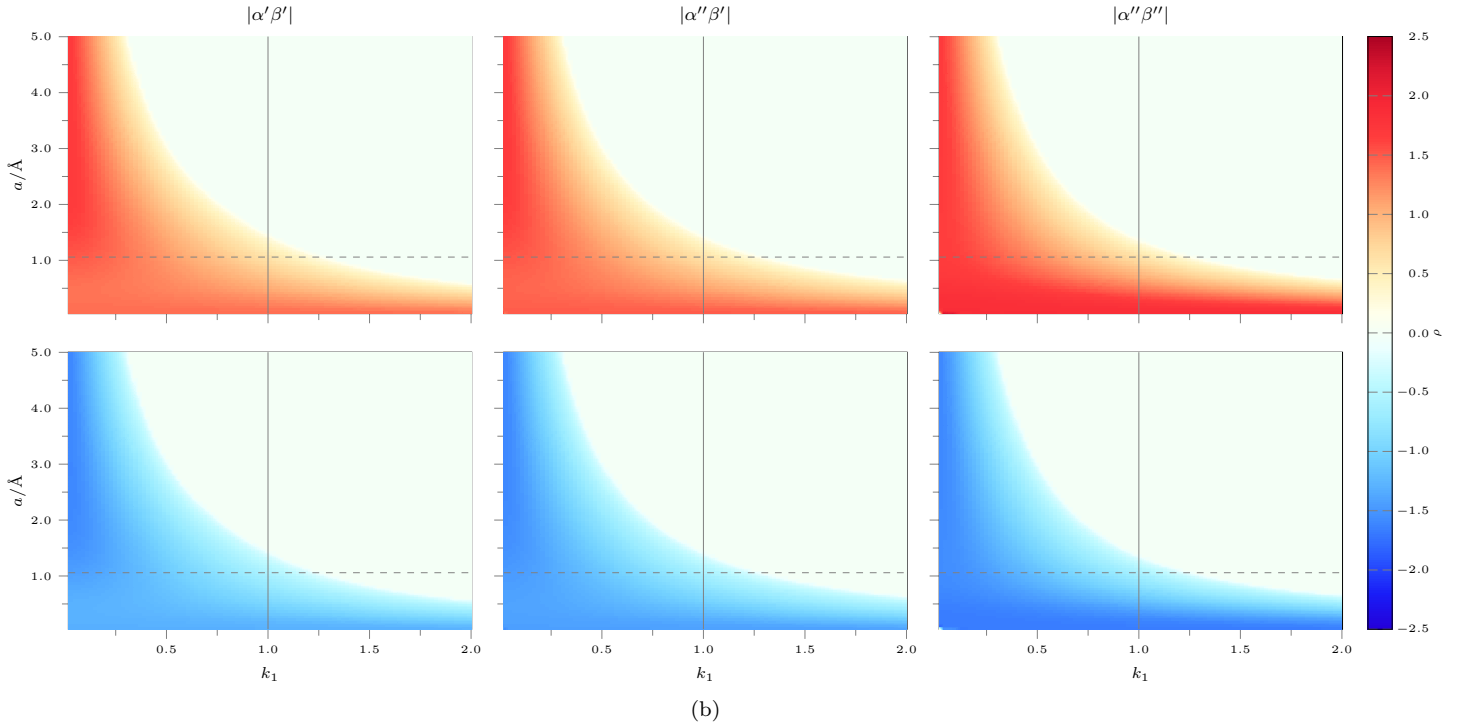
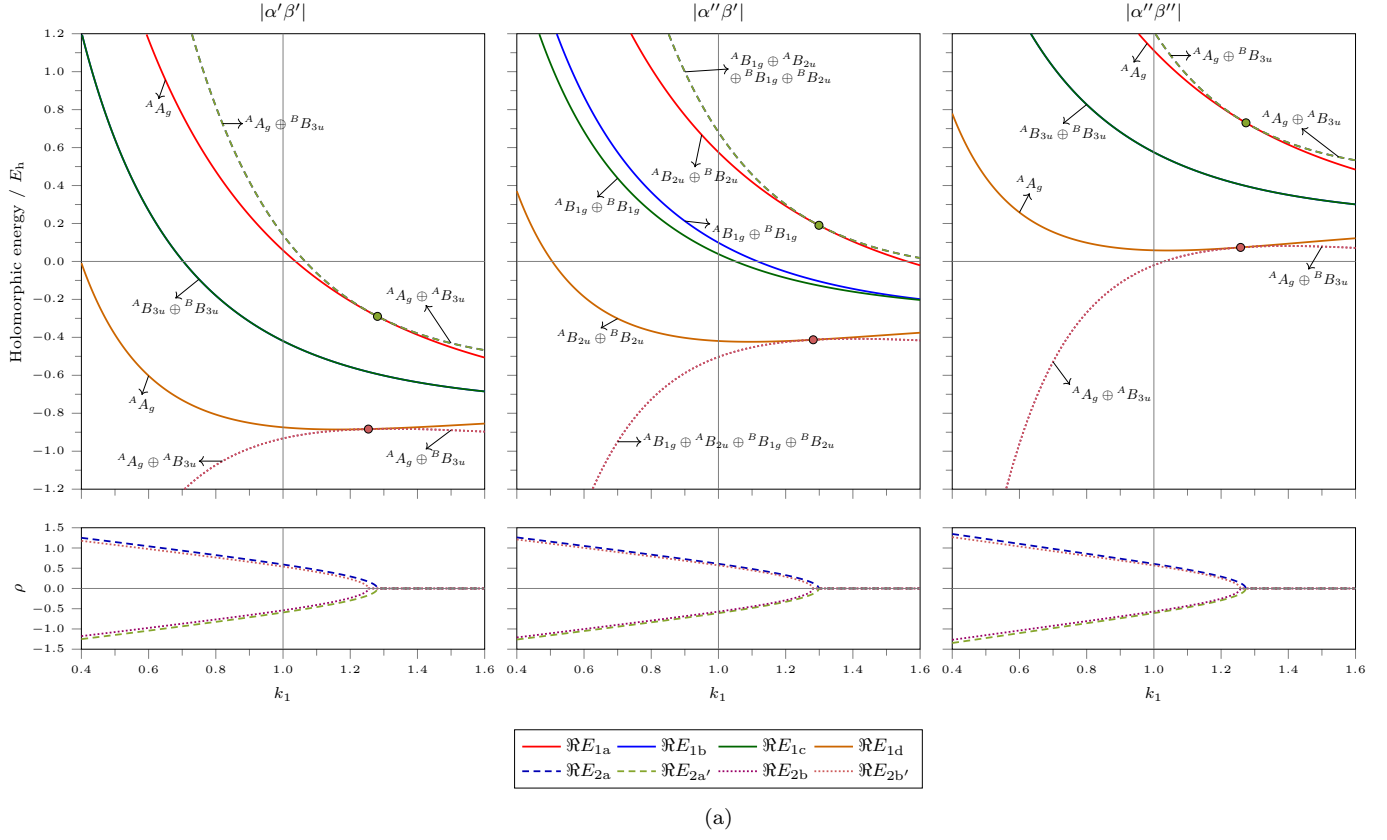


FIG. 6. Solutions under special  $\hat{\sigma}^{xz}$ -symmetry-conserved extrinsic constraints. (a) Holomorphic energy,  $\mathcal{T} \otimes \mathcal{D}_{2h}$  symmetry, and reality indicators along molecular symmetry pathway A at  $a = 1.058\,350\text{ \AA}$ . (b) Reality indicators of solutions 2a (top) and 2b (bottom) along pathway A at different scale lengths  $a$ . The vertical line at  $k_1 = 1$  indicates  $\mathcal{D}_{4h}$  symmetry, and the dashed horizontal line indicates  $a = 1.058\,350\text{ \AA}$ .

terms of the former. However, by tracking these solutions along pathway B, the missing coalescence with the 1c solution which accounts for the remaining two symmetry terms can now be observed (Figure 7a).

### C. Symmetry-Broken Extrinsic Constraints

The symmetry-conserved extrinsic constraints examined in detail so far have been deliberately chosen such that the analytic solutions we obtain do correspond to true stationary points of the SCF energy landscape. In fact, by considering the spin-orbital-dependent terms of the Fock operator  $\hat{f}$  in Equation 5 in conjunction with the extrinsic constraints in Table II, we see that, by imposing symmetry conservation, *i.e.*, setting  $x, y = \pm 1$ , the constraining symmetry operations leave  $\hat{f}$  invariant under their actions. The spin-orbitals that conserve these symmetries are thus allowed to be eigenfunctions of  $\hat{f}$  without any contradiction. In other words, the symmetry-conserved constraints are compatible with, and hence encompass, SCF stationary points.

The analysis so far makes it clear that both intrinsic and extrinsic constraints must cooperate to strongly force reality on the transiently real solutions. Essentially, intrinsic constraints determine the global structure of the SCF energy landscape alongside its regimes of both strong and weak reality requirements. Extrinsic constraints then enable us to choose and explore stationary points within certain local regions of this landscape, some of which happen to admit strong reality requirements. It is therefore expected that there exist pathways in the SCF energy landscape that connect regions of extrinsic constraints together and that reveal some local structures of the regimes of reality requirements between stationary points in this landscape. We shall henceforth refer to these pathways as ‘‘SCF pathways’’ to distinguish them from the molecular symmetry pathways A and B that we have been considering. These SCF pathways shall involve the variations of the  $x$  and  $y$  constraining parameters over the domain  $\mathcal{D}$  that are defined for each constraining space  $[\hat{R}]'_{xy}$  in Table II.

We note that, as we move away from the corners of  $\mathcal{D}$  in any constraining space  $[\hat{R}]'_{xy}$ , the spin-orbitals  $\chi_i$ , and hence the overall determinant  $\Psi^{\text{HF}}$ , are constrained to break symmetry under  $\hat{R}$ . This also forces the Fock operator  $\hat{f}$  to break symmetry, and consequently, there is no guarantee that  $\chi_i$  would be an eigenfunction of  $\hat{f}$  because  $\chi_i$  and  $\hat{f}$  cannot be expected to transform compatibly under  $\hat{R}$ . An optimization procedure under these symmetry-broken constraints thus yields solutions that are not expected to be stationary points of the SCF energy landscape in general. In fact, as the four corners of  $\mathcal{D}$  must correspond to true SCF stationary points, stepping away from them into  $\mathcal{D}$  in *any* direction must mean traversing along non-stationary paths.

In Figure 8, we plot the values of the reality indica-

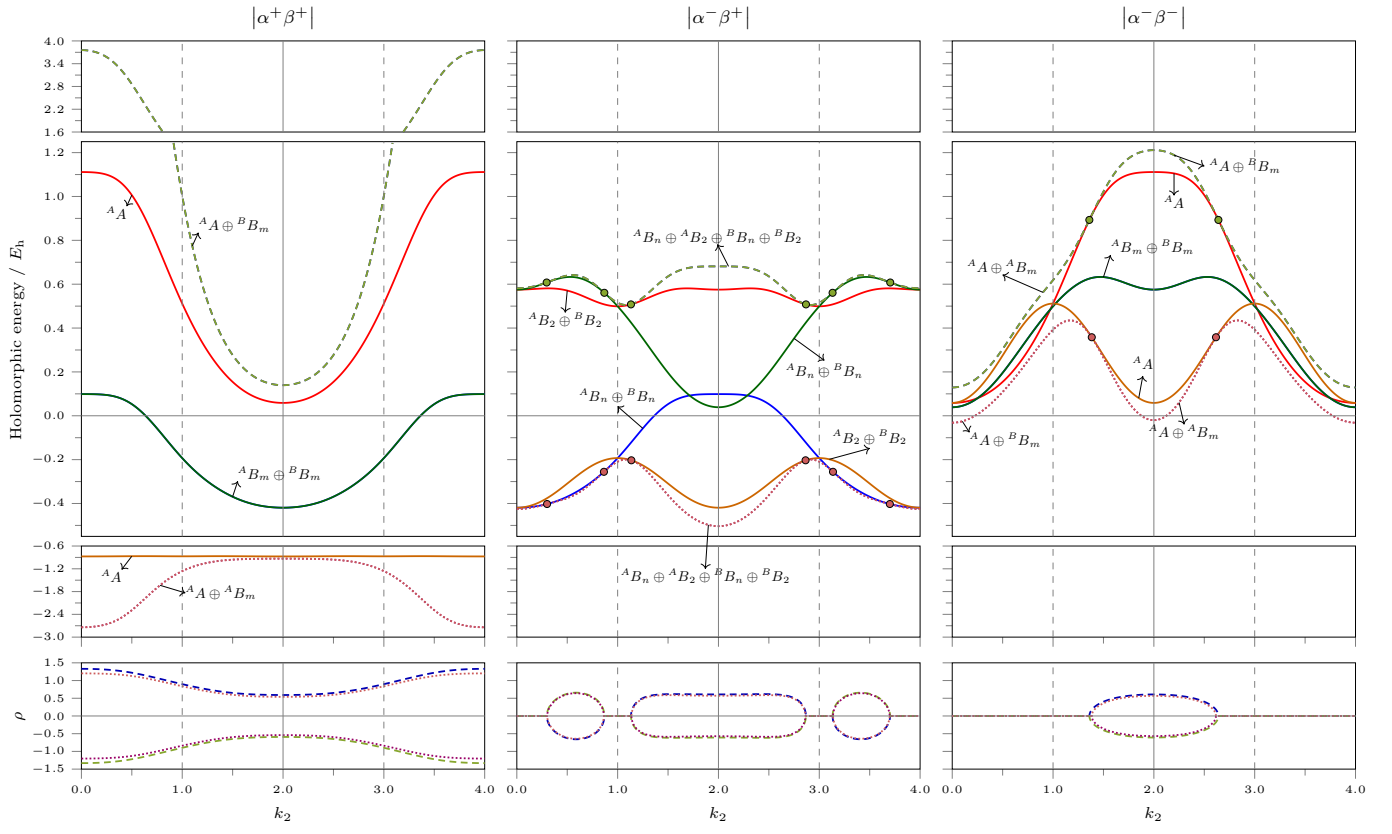
tor  $\rho$  over the domain  $\mathcal{D}$  at various symmetry factors  $k_i$  while fixing the scale length  $a = 1.058\,350\text{ \AA}$ . Every horizontal slice in this plot therefore corresponds to a two-dimensional cross-section of the SCF landscape cornered by the  $\hat{R}$ -symmetry-conserved extrinsic constraints within the  $[\hat{R}]'_{xy}$  symmetry-broken constraining space. We identify the vertical edges at  $(x, y) = (\pm 1, \pm 1)$  with the  $\rho$ - $k_i$  indicator plots for the various  $\hat{R}$ -symmetry-conserved extrinsic constraints in Figures 4, 6a, and 7a.

We observe that the points of strong reality requirements for  $|\alpha^u\beta^g|$  (and  $|\alpha^g\beta^u|$  by time-reversal symmetry) and  $|\alpha^u\beta^u|$  at  $\mathcal{D}_{4h}$  along pathway A ( $k_1 = 1$ ) and for  $|\alpha^-\beta^+|$  (and  $|\alpha^+\beta^-|$  by time-reversal symmetry) and  $|\alpha^-\beta^-|$  at  $\mathcal{T}_d$  along pathway B ( $k_2 = 1$ ) are actually embedded within local ‘‘seas’’ of reality over  $\mathcal{D}$ . In addition, there exist continuously real paths in  $\mathcal{D}$  that connect points of strong reality requirements. The cross-sections at  $k_i = 1$  for the  $[\hat{i}]'_{xy}$  and  $[\hat{C}_2^\clubsuit]'_{xy}$  constraining spaces plotted as insets in Figure 8 show these features clearly. In fact, for these two constraining spaces, there are two special paths in  $\mathcal{D}$ , one along the  $x = -1$  edge and the other along the  $y = -1$  edge, that admit strong reality requirements as verifiable by considering the relevant forms of the electron-integral coefficients shown in Section S-I of the Supplementary Material in a similar fashion to that described in Section V B 1.

These special paths reveal that the strong reality requirements observed so far are really the consequence of either  $x$  or  $y$  being equal to  $-1$ , but not necessarily both. In other words, as long as one of the two spin-orbitals undergoes a phase reversal under  $\hat{i}$  at  $\mathcal{D}_{4h}$  or  $\hat{C}_2^\clubsuit$  at  $\mathcal{T}_d$ , then strong reality requirements are in force. In addition, since phase reversals introduce nodes into the spin-orbitals and raise their energy, the transiently real solutions that benefit from strong reality requirements are most likely *not* the ground solutions in the holomorphic formalism. This can be seen most clearly in Figure 4: the  $|\alpha^u\beta^g|$  and  $|\alpha^u\beta^u|$  extrinsic constraints admit transiently real solutions in the vicinity of  $\mathcal{D}_{4h}$  that are real and fairly high in energy, whereas the  $|\alpha^g\beta^g|$  extrinsic constraint admits a pair of much lower-lying transiently real solutions that remain non-real throughout the depicted  $k_1$  range. A similar observation can be made for the  $\hat{C}_2^\clubsuit$ -symmetry-conserved transiently real solutions at  $\mathcal{T}_d$  in Figure 7a.

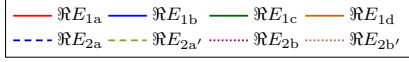
## VIII. DISCUSSION

In this article, we discuss the various forms of constraints impossible on the HF theory and then present an analytic investigation of the SCF solutions for a model two-electron  $[\text{H}_4]^{2+}$  system at different molecular geometries. Through this, we gain insight into the roles of symmetry constraints on the reality of holomorphic HF solutions. In particular, we discover that intrinsic and extrinsic constraints cooperate intimately to determine local properties of the SCF landscape and impose real-

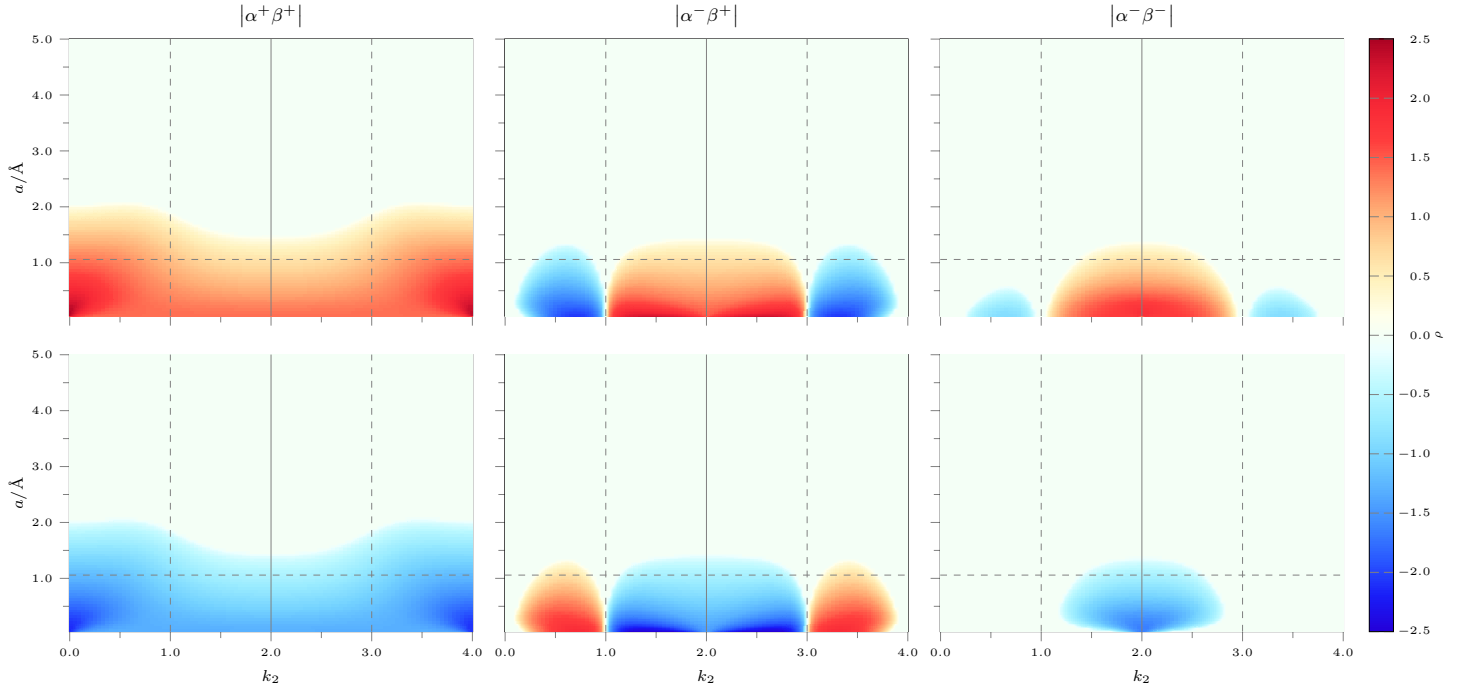


$$k_2 \in [0, 1] \cup [3, 4]: m=1, n=3$$

$$k_2 \in (1, 3) : m=3, n=1$$



(a)



(b)

FIG. 7. Solutions under special  $\hat{C}_3$ -symmetry-conserved extrinsic constraints. (a) Holomorphic energy,  $\mathcal{T} \otimes \mathcal{D}_2$  symmetry, and reality indicators along molecular symmetry pathway B at  $a = 1.058\,350\text{\AA}$ . (b) Reality indicators of solutions 2a (top) and 2b (bottom) along pathway B at different scale lengths  $a$ . The dashed vertical lines indicate  $\mathcal{T}_d$  symmetry, the solid vertical line indicates the twisted  $\mathcal{D}_{4h}$  configuration (see Figure 2), and the dashed horizontal line indicates  $a = 1.058\,350\text{\AA}$ .



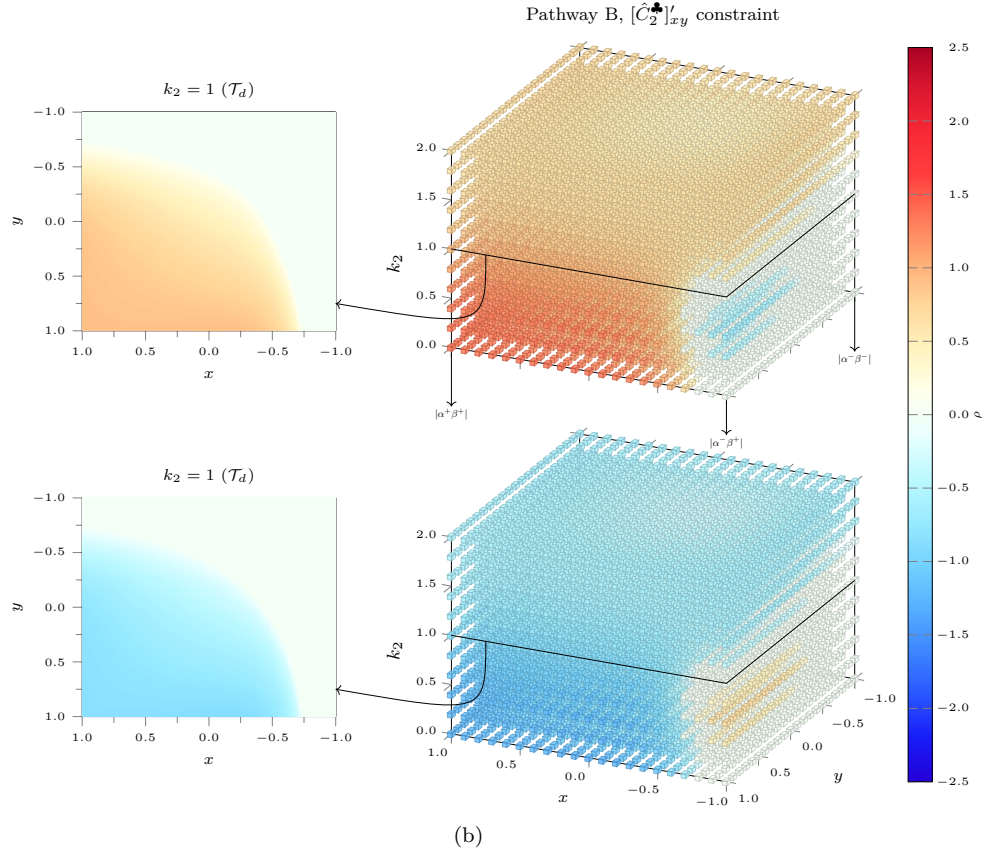
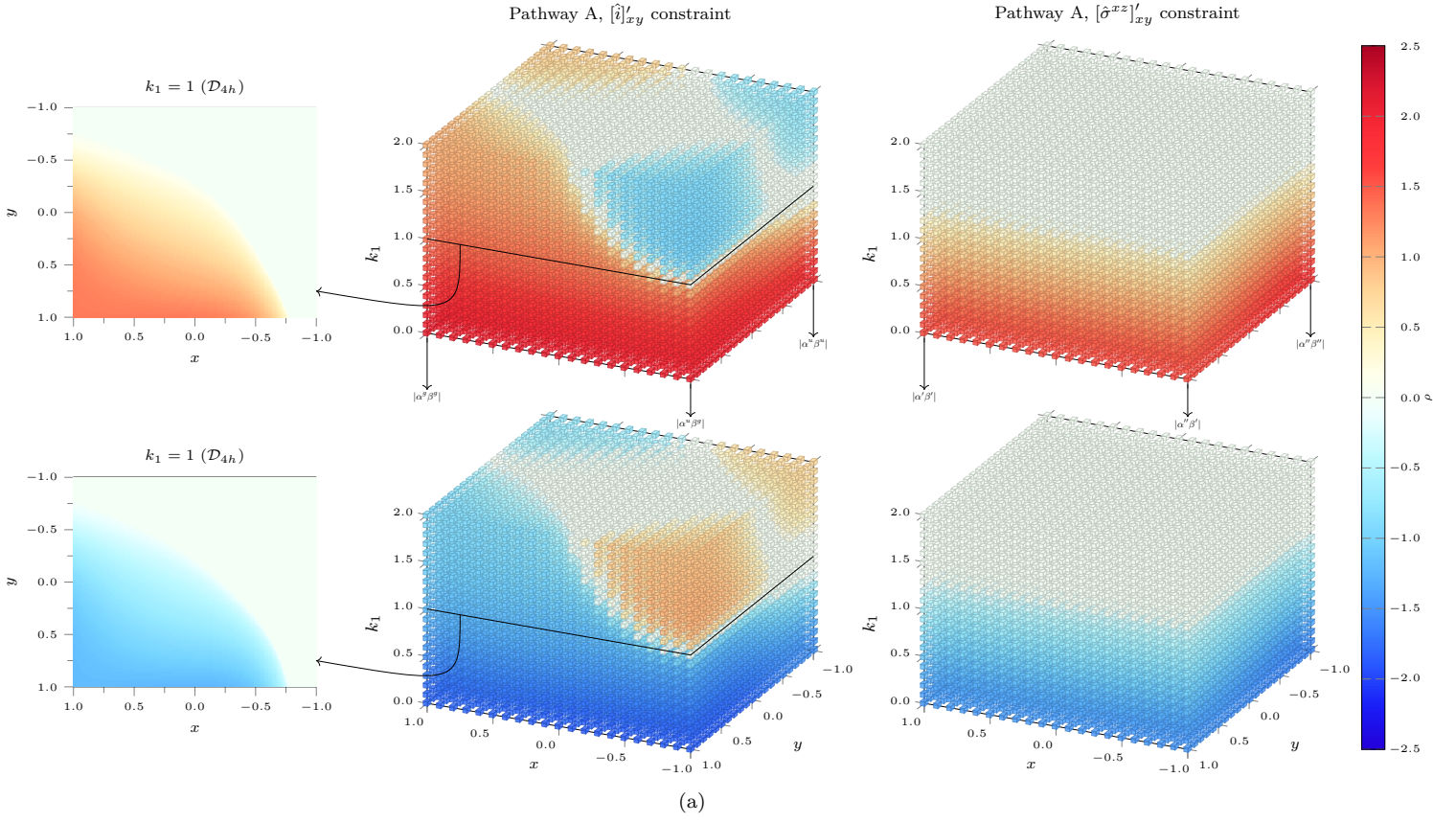


FIG. 8. Reality indicators of solutions 2a and 2b in the constraining spaces  $[\hat{R}]'$ , where  $\hat{R} \in \{\hat{i}, \hat{\sigma}^{xz}, \hat{C}_2^*\}$ , at a fixed scale length  $a = 1.058350 \text{ \AA}$  and different symmetry factors  $k_i$ . In each plot, the top panel is for solution 2a and the bottom one for solution 2b. The domain  $\mathcal{D}$  of the parameters  $(x, y)$  within each constraining space connects the symmetry-conserved extrinsic constraints located at the corners of  $\mathcal{D}$ .



ity requirements on holomorphic HF solutions. An SCF search based on conventional HF performed within these symmetry constraints must be able to locate these solutions in the real domains of the MO coefficients. We also show that these constraints dictate the existence and locations of coalescence boundaries, therefore making them a fundamental feature of the SCF landscape. Hence, any disappearance of SCF solutions in conventional HF must be interpreted as an essential consequence of the HF equations that is governed in part by symmetry.

The reality requirements analyzed thus far arise from the intrinsic and extrinsic constraints specifically chosen partly to target the numerically obtained solutions shown at the beginning in Figure 1, and partly to result in the system  $P(\boldsymbol{\theta}; \mathbf{B}) = 0$  (Equation 21) for which it is possible to obtain closed-form analytic solutions. This thus restricts the investigation to a very small system in the minimal basis set. Unfortunately, a rigorous generalization to larger systems in larger basis sets based on the results presented so far is not yet possible due to the complicated algebraic structure of the general HF equations. Nonetheless, we believe that the qualitative features that have been brought to our attention by the analytic solutions, namely the distinction between persistently real and transiently real solutions and the strong and weak reality requirements in relation to the symmetry of the system and of the solutions, also exist in larger systems, based on the ubiquity of the coalescence and disappearance of certain SCF solutions away from high-symmetry geometries in other larger systems that we have observed numerically as described in Section I.

Finally, it is conceivable that there are other symmetries that the electron integrals can exhibit that give rise to other types of constraints, and these might very well provide more structure to the observed weak reality requirements of the investigated solutions. These symmetries are considered to be “hidden” because so far they have not shown any obvious relationships to the molecular and wavefunction symmetries we examine, as evident by the rather arbitrary nature of the coalescence boundaries enclosing regimes of weak reality requirements. One example of such symmetries involves the effective nuclear charge felt by the valence electrons which controls the extent to which the one-electron integrals contribute to the algebraic coefficients. It is therefore imperative that an investigation into other factors that can affect electron integrals be carried out so that a more general understanding of how symmetry beyond spatial governs the reality of SCF solutions can be obtained. This will be the focus of a future study.

We conclude the article with a remark that the analytic model used in this work for  $[\text{H}_4]^{2+}$  and the associated constraints can be extended to other valence-isoelectronic systems, such as  $\text{H}_4$  with a frozen core, or the  $\pi$ -framework of the  $2\pi$ -aromatic  $[\text{C}_4\text{H}_4]^{2+}$ . For example, a possible isomorphism for the  $\text{H}_4$  case is one in which we choose the two lowest-lying spin-orbitals from certain SCF solutions of  $\text{H}_4$  to form a totally symmetric

frozen core which allows us to determine the effective nuclear charges experienced by the remaining two electrons in the higher-lying spin-orbitals. The effective nuclear charges then let us map the actual  $\text{H}_4$  SCF solutions to those in  $[\text{H}_4]^{2+}$  obtained with the one-electron integrals appropriately modified to take into account the effective nuclear charges. We believe that this will provide a way to map a subset of SCF solutions in  $\text{H}_4$  to those that we have discussed in detail for  $[\text{H}_4]^{2+}$ .

The isomorphism proposed above reveals that the effective nuclear charges felt by the valence electrons now become an important factor in the weak reality requirements of the solutions, for they control the extent to which the one-electron integrals contribute to the algebraic coefficients that influence whether the transiently real solutions are real or non-real. This will form part of a future investigation in which we hope to understand the roles of other factors and hidden symmetries in governing the reality of solutions.

## SUPPLEMENTARY MATERIAL

See Supplementary Material for the detailed functional forms of the electron integral coefficients  $S$  and  $A$  in terms of the one- and two-electron integrals, the video entitled `spatialsymreality.orbitalplots.mp4` showing the forms of the MOs for the analytic holomorphic solutions of  $[\text{H}_4]^{2+}$  in STO-3G and animating their variations as the geometry of the cation changes, and the derivation of the weak reality requirements and the equations describing the coalescence boundaries.

## ACKNOWLEDGMENTS

B.C.H. is grateful for the financial support from Cambridge Commonwealth, European & International Trust and Peterhouse during the duration of this work throughout the COVID-19 national lockdowns in England. A.J.W.T. thanks the Royal Society for a University Research Fellowship (UF110161). Both authors thank the anonymous reviewers who provided many critical and constructive comments that helped refine the discussions in this article.

## Appendix A: Non-Vanishing Electron Integrals

### 1. General Formulation

Given a set of real AO basis functions  $\{\varphi_i\}$  localized on nuclei that are invariant under a certain point group  $\mathcal{G}$ , the numbers of non-vanishing independent components of the one-electron integral matrix,  $\langle \varphi_{\mu'} | \hat{O} | \varphi_{\mu} \rangle$ , two-electron integral tensor,  $\langle \varphi_{\mu'} \varphi_{\nu'} | \varphi_{\mu} \varphi_{\nu} \rangle$ , and antisymmetrized two-electron integral tensor,  $\langle \varphi_{\mu'} \varphi_{\nu'} || \varphi_{\mu} \varphi_{\nu} \rangle$  depend on the constraints imposed by both the permutation

symmetries of the integrals and the point-group symmetries under  $\mathcal{G}$ .

Let  $S = \{\alpha^k \mid k = 1, 2, \dots, n\}$  be a set of *function labels* where each function label  $\alpha^k$  has associated with it an index  $i_{\alpha^k}$  to specify a function  $\alpha_{i_{\alpha^k}}^k$ . For example, if  $\alpha^k$  is the label  $2p$ , then the index  $i_{\alpha^k}$  can take on one of  $x, y, z$ , so that  $\alpha_{i_{\alpha^k}}^k$  is one of the three  $2p$  hydrogenic orbitals. Then, consider  $n$  sets of functions  $F^k = \{\alpha_{i_{\alpha^k}}^k \mid i_{\alpha^k} = 1, 2, \dots\}$  where  $k = 1, 2, \dots, n$ . A general element in an  $n$ -ary Cartesian product over the  $F^k$  is an  $n$ -tuple that we denote as

$$\begin{aligned} \Omega^{(n)} &= \underbrace{(\alpha_{i_{\alpha^1}}^1, \alpha_{i_{\alpha^2}}^2, \dots, \alpha_{i_{\alpha^n}}^n)}_{n\text{-tuple}} \\ &\equiv \left(\alpha_{i_{\alpha^k}}^k\right)_{k=1}^n \in F^1 \times F^2 \times \dots \times F^n. \end{aligned}$$

The notation  $(\cdot)_{k=1}^n$  means an  $n$ -tuple whose elements are labeled by the index  $k$ . All of the (real) AO electron integrals of interest to us can be considered generically as a multilinear map

$$\begin{aligned} M : F^1 \times F^2 \times \dots \times F^n &\rightarrow \mathbb{R} \\ \Omega^{(n)} &\mapsto M[\Omega^{(n)}] \end{aligned}$$

that is linear in each of its arguments. The permutation symmetries of the electron integrals then imply that  $M$  has some permutation invariance

$$M[\Omega^{(n)}] = M[\Omega_{\sigma}^{(n)}], \quad (\text{A1})$$

where

$$\begin{aligned} \Omega_{\sigma}^{(n)} &= \hat{P}_{\sigma} \Omega^{(n)} \\ &= \hat{P}_{\sigma} \left(\alpha_{i_{\alpha^k}}^k\right)_{k=1}^n = \left(\sigma \alpha_{i_{\alpha^k}}^k\right)_{k=1}^n \end{aligned} \quad (\text{A2})$$

is the  $n$ -tuple that has been acted on by  $\hat{P}_{\sigma} \in \text{Sym}(S)$  which permutes the function labels, sending  $\alpha^k$  to  $\sigma \alpha^k$ .

We now consider the effects of point-group symmetry on a general permutation sum over a subgroup  $T$  of  $\text{Sym}(S)$  for a particular index combination  $\{i_{\alpha}\}$  of the multi-linear map  $M$ :

$$A_{\{i_{\alpha}\}} = \sum_{\sigma \in T} \lambda_{\sigma} M[\Omega_{\sigma}^{(n)}] = \sum_{\sigma \in T} \lambda_{\sigma} \hat{P}_{\sigma} M[\Omega^{(n)}], \quad (\text{A3})$$

where  $\lambda_{\sigma}$  is the signature associated with the permutation  $\hat{P}_{\sigma}$  and determined by the physics of the problem that gives rise to  $A_{\{i_{\alpha}\}}$ . We require that the set  $\{\lambda_{\sigma} \mid \hat{P}_{\sigma} \in T\}$  forms the basis for one of the one-dimensional irreducible representations of  $T$  so that

$$\hat{P}_{\sigma} \hat{P}_{\sigma'} = \hat{P}_{\sigma''} \Leftrightarrow \lambda_{\sigma} \lambda_{\sigma'} = \lambda_{\sigma''}, \quad (\text{A4})$$

where group multiplication under  $\text{Sym}(S)$  is denoted by juxtaposition. Let  $\hat{R}$  be a symmetry element in the group

$\mathcal{G}$  with a representation matrix  $D^k(\hat{R})$  in the basis of  $F^k = \{\alpha_{i_{\alpha^k}}^k\}$ :

$$\hat{R} \alpha_{i_{\alpha^k}}^k = \sum_{i'_{\alpha^k}} \alpha_{i'_{\alpha^k}}^k D_{i'_{\alpha^k} i_{\alpha^k}}^k(\hat{R}). \quad (\text{A5})$$

The effect of  $\hat{R}$  on a general term  $M[\Omega_{\sigma}^{(n)}]$  in  $A_{\{i_{\alpha}\}}$  is given by

$$\hat{R} M[\Omega_{\sigma}^{(n)}] \quad (\text{A6a})$$

$$= \hat{R} M \left( \sigma \alpha_{i_{\alpha^k}}^k \right)_{k=1}^n \quad (\text{A6b})$$

$$= M \left( \hat{R} \sigma \alpha_{i_{\alpha^k}}^k \right)_{k=1}^n \quad (\text{A6c})$$

$$= M \left( \sum_{i'_{\sigma \alpha^k}} \sigma \alpha_{i'_{\sigma \alpha^k}}^k D_{i'_{\sigma \alpha^k} i_{\alpha^k}}^k(\hat{R}) \right)_{k=1}^n \quad (\text{A6d})$$

$$= \sum_{\{i'_{\sigma \alpha}\}} M \left( \sigma \alpha_{i'_{\sigma \alpha^k}}^k \right)_{k=1}^n \prod_{k=1}^n D_{i'_{\sigma \alpha^k} i_{\alpha^k}}^k(\hat{R}) \quad (\text{A6e})$$

$$= \sum_{\{i'_{\alpha}\}} M \left( \alpha_{i'_{\alpha^k}}^k \right)_{k=1}^n \prod_{k=1}^n D_{i'_{\sigma \alpha^k} i_{\alpha^k}}^k(\hat{R}), \quad (\text{A6f})$$

where we use the definition in Equation A2 to write Equation A6b. Next, we utilise the fact that  $\hat{R}$  acts on each function in the argument of the linear map  $M$  separately to move  $\hat{R}$  inside the tuple in Equation A6c. The definition of the representation matrices for  $\hat{R}$  in Equation A5 is then invoked to expand each term in the tuple to give Equation A6d. The linearity of  $M$  on each of its arguments allows the individual sums in the tuple to be pulled outside as multiple sums over all function indices in Equation A6e,  $\sum_{\{i'_{\sigma \alpha}\}} \equiv \sum_{i'_{\sigma \alpha^1}} \dots \sum_{i'_{\sigma \alpha^n}}$ . Finally, the permutation invariance of  $M$  (Equation A1) and the closure of  $S$  under  $\hat{P}_{\sigma}$  yield Equation A6f. The overall effect of  $\hat{R}$  on  $A_{\{i_{\alpha}\}}$  is thus

$$\hat{R} A_{\{i_{\alpha}\}} = \sum_{\{i'_{\alpha}\}} M \left( \alpha_{i'_{\alpha^k}}^k \right)_{k=1}^n \sum_{\sigma} \lambda_{\sigma} \prod_{k=1}^n D_{i'_{\sigma \alpha^k} i_{\alpha^k}}^k(\hat{R}). \quad (\text{A7})$$

We note that the sum  $A_{\{i_{\alpha}\}}$  is invariant up to a phase factor under the permutation subgroup  $T$  since

$$\begin{aligned} \forall \hat{P}_{\sigma'} \in T, \quad \hat{P}_{\sigma'} A_{\{i_{\alpha}\}} &= \sum_{\sigma \in T} \lambda_{\sigma} \hat{P}_{\sigma'} \hat{P}_{\sigma} M[\Omega^{(n)}] \\ &= \sum_{\sigma'' \in T} \lambda_{\sigma'}^{-1} \lambda_{\sigma''} \hat{P}_{\sigma''} M[\Omega^{(n)}] \\ &= \lambda_{\sigma'}^{-1} A_{\{i_{\alpha}\}}, \end{aligned}$$

where we have invoked the closure of  $T$  under group multiplication and the requirement for signature multiplication (Equation A4) to “absorb” one of the permutation operators into the other for the second equality. This

allows us to write

$$\begin{aligned}\hat{R}A_{\{i_\alpha\}} &= \hat{R} \left( \frac{1}{|T|} \sum_{\sigma' \in T} \lambda_{\sigma'} \hat{P}_{\sigma'} A_{\{i_\alpha\}} \right) \\ &= \frac{1}{|T|} \sum_{\sigma' \in T} \lambda_{\sigma'} \hat{P}_{\sigma'} \hat{R}A_{\{i_\alpha\}}.\end{aligned}$$

Substitution of the result in Equation A7 for the  $\hat{R}A_{\{i_\alpha\}}$  term under the summation gives

$$\begin{aligned}\hat{R}A_{\{i_\alpha\}} &= \sum_{\{i'_\alpha\}} \left[ \sum_{\sigma' \in T} \lambda_{\sigma'} \hat{P}_{\sigma'} M \left( \alpha_{i'_\alpha}^k \right)_{k=1}^n \right] \\ &\quad \times \left[ \frac{1}{|T|} \sum_{\sigma \in T} \lambda_\sigma \prod_{k=1}^n D_{\sigma \alpha^k i_\alpha^k}^k(\hat{R}) \right] \\ &= \sum_{\{i'_\alpha\}} A_{\{i'_\alpha\}} D_{\{i'_\alpha\}, \{i_\alpha\}}^{A_{\{i_\alpha\}}}(\hat{R}).\end{aligned}$$

We thus obtain an expression for the representation matrix of the permutation sum  $A_{\{i_\alpha\}}$  under  $\hat{R}$ :

$$D_{\{i'_\alpha\}, \{i_\alpha\}}^{A_{\{i_\alpha\}}}(\hat{R}) = \frac{1}{|T|} \sum_{\sigma \in T} \lambda_\sigma \prod_{k=1}^n D_{\sigma \alpha^k i_\alpha^k}^k(\hat{R}). \quad (\text{A8})$$

which gives a practical way to determine how  $\hat{R}$  affects the multilinear map  $M[\Omega^{(n)}]$  subject to the permutation invariance A1. For  $A_{\{i_\alpha\}}$  to be non-vanishing,  $D^{A_{\{i_\alpha\}}}(\hat{R})$  must contain totally symmetric components.

## 2. Applications to Particular Electron Integrals

*a. One-Electron Integrals.* The map of interest for (real) one-electron integrals is  $M = \langle \cdot | \hat{O} | \cdot \rangle$ , where  $\hat{O}$  is a one-electron Hermitian operator. We consider a set  $S$  of two function labels,  $S = \{\xi, \eta\}$ , which gives rise to two sets of real functions  $F^\xi = \{\xi_{i_\xi}\}$  and  $F^\eta = \{\eta_{i_\eta}\}$  that we insist form *identical* bases for a representation  $\Gamma_{\mathcal{G}}$  of the group  $\mathcal{G}$ . The Hermiticity of  $\hat{O}$  and the reality of the functions in  $F$  imply that the invariant permutation sum we need to consider is

$$A_{\{i_\xi i_\eta\}} = \langle \xi_{i_\xi} | \hat{O} | \eta_{i_\eta} \rangle + \langle \eta_{i_\eta} | \hat{O} | \xi_{i_\xi} \rangle,$$

which defines a permutation subgroup  $T = \{\hat{e}, (\xi\eta)\}$  where both elements have a signature of +1. From Equation A8, the representation matrix for any element  $R \in \mathcal{G}$  is

$$\begin{aligned}D_{i'_\xi i'_\eta, i_\xi i_\eta}^{A_{\{i_\xi i_\eta\}}}(\hat{R}) &= \\ &= \frac{1}{2} \left\{ D_{i'_\xi i'_\eta}^{\Gamma_{\mathcal{G}}}(\hat{R}) D_{i'_\eta i'_\xi}^{\Gamma_{\mathcal{G}}}(\hat{R}) + D_{i'_\eta i'_\xi}^{\Gamma_{\mathcal{G}}}(\hat{R}) D_{i'_\xi i'_\eta}^{\Gamma_{\mathcal{G}}}(\hat{R}) \right\}.\end{aligned}$$

Setting  $i'_\xi = i_\xi$  and  $i'_\eta = i_\eta$  and summing over, we get

$$\chi^{A_{\{i_\xi i_\eta\}}}(\hat{R}) = \frac{1}{2} \left\{ \left[ \chi^{\Gamma_{\mathcal{G}}}(\hat{R}) \right]^2 + \chi^{\Gamma_{\mathcal{G}}}(\hat{R}^2) \right\},$$

which is the character of  $\hat{R}$  in the familiar symmetrized square of  $\Gamma_{\mathcal{G}}$ .<sup>42,46</sup> Applying the reduction formula for the totally symmetric irreducible representation of  $\mathcal{G}$  then gives the number of totally symmetric components contained in the representation spanned by  $A_{\{i_\xi i_\eta\}}$ , and thus the number of non-vanishing components:

$$\begin{aligned}n_1(\Gamma_{\mathcal{G}}, \mathcal{G}) &= \frac{1}{|\mathcal{G}|} \sum_{\hat{R} \in \mathcal{G}} \frac{1}{2} \left\{ \left[ \chi^{\Gamma_{\mathcal{G}}}(\hat{R}) \right]^2 + \chi^{\Gamma_{\mathcal{G}}}(\hat{R}^2) \right\}. \quad (\text{A9})\end{aligned}$$

*b. Two-Electron Integrals.* The map of interest for (real) two-electron integrals is now  $M = \langle \cdot \cdot | \cdot \cdot \rangle$  with the function labels  $S = \{\alpha, \beta, \gamma, \delta\}$  giving rise to four sets of functions  $F^\alpha = \{\alpha_{i_\alpha}\}$ ,  $F^\beta = \{\beta_{i_\beta}\}$ ,  $F^\gamma = \{\gamma_{i_\gamma}\}$ , and  $F^\delta = \{\delta_{i_\delta}\}$  forming *identical* bases for a representation  $\Gamma_{\mathcal{G}}$  in  $\mathcal{G}$ . The relevant invariant permutation sum  $A_{\{i_\alpha i_\beta i_\gamma i_\delta\}}$  can be constructed from the permutation subgroup

$$\begin{aligned}T = \{ &\hat{e}, \\ &(\alpha\gamma)(\beta\delta), (\alpha\beta)(\gamma\delta), (\alpha\delta)(\beta\gamma), \\ &(\alpha\gamma), (\beta\delta), \\ &(\alpha\beta\gamma\delta), (\alpha\delta\gamma\beta)\}\end{aligned}$$

where all eight elements have a signature of +1. Following the same approach as above, we obtain the character formula for  $\hat{R} \in \mathcal{G}$ ,

$$\begin{aligned}\chi^{A_{\{i_\alpha i_\beta i_\gamma i_\delta\}}}(\hat{R}) &= \\ &= \frac{1}{8} \left\{ \left[ \chi^{\Gamma_{\mathcal{G}}}(\hat{R}) \right]^4 + 3 \left[ \chi^{\Gamma_{\mathcal{G}}}(\hat{R}^2) \right]^2 \right. \\ &\quad \left. + 2 \chi^{\Gamma_{\mathcal{G}}}(\hat{R}^2) \left[ \chi^{\Gamma_{\mathcal{G}}}(\hat{R}) \right]^2 + 2 \chi^{\Gamma_{\mathcal{G}}}(\hat{R}^4) \right\}.\end{aligned}$$

An application of the reduction formula for the totally symmetric irreducible representation of  $\mathcal{G}$  thus yields

$$\begin{aligned}n_2(\Gamma_{\mathcal{G}}, \mathcal{G}) &= \frac{1}{|\mathcal{G}|} \sum_{\hat{R} \in \mathcal{G}} \frac{1}{8} \left\{ \left[ \chi^{\Gamma_{\mathcal{G}}}(\hat{R}) \right]^4 + 3 \left[ \chi^{\Gamma_{\mathcal{G}}}(\hat{R}^2) \right]^2 \right. \\ &\quad \left. + 2 \chi^{\Gamma_{\mathcal{G}}}(\hat{R}^2) \left[ \chi^{\Gamma_{\mathcal{G}}}(\hat{R}) \right]^2 + 2 \chi^{\Gamma_{\mathcal{G}}}(\hat{R}^4) \right\}. \quad (\text{A10})\end{aligned}$$

*c. Anti-Symmetrized Two-Electron Integrals.* The map of interest is now  $M = \langle \cdot \cdot | \cdot \cdot \rangle$ . Since  $\langle \alpha\beta | \gamma\delta \rangle = \langle \alpha\beta | \gamma\delta \rangle - \langle \alpha\beta | \delta\gamma \rangle$ , the relevant permutation subgroup is now

$$\begin{aligned}T = \{ &\hat{e}, \\ &(\alpha\beta)(\gamma\delta), (\alpha\gamma)(\beta\delta), (\alpha\delta)(\beta\gamma), \\ &(\alpha\beta), (\gamma\delta), \\ &(\alpha\delta\beta\gamma), (\alpha\gamma\beta\delta)\},\end{aligned}$$

TABLE IX. Character table for the time-reversal group.

$\mathcal{T}$	$\hat{E}$	$\hat{\Theta}$
$A$	1	1
$B$	1	-1

but the signatures of the last four elements are  $-1$ . This thus leads to the character formula

$$\chi^{A\{\alpha^i\beta^i\gamma^i\delta^i\}}(\hat{R}) = \frac{1}{8} \left\{ \left[ \chi^{\Gamma_{\mathcal{G}}}(\hat{R}) \right]^4 + 3 \left[ \chi^{\Gamma_{\mathcal{G}}}(\hat{R}^2) \right]^2 - 2 \chi^{\Gamma_{\mathcal{G}}}(\hat{R}^2) \left[ \chi(\hat{R}) \right]^2 - 2 \chi^{\Gamma_{\mathcal{G}}}(\hat{R}^4) \right\}.$$

### Appendix B: The Time-Reversal Group

Let  $\mathcal{T}$  be the abstract cyclic group of order 2:  $\mathcal{T} = \{e, t \mid t^2 = e\}$ , and let  $\rho$  be a linear-antilinear representation<sup>47</sup> (also known as corepresentation<sup>42</sup>) of  $\mathcal{T}$  on a complex Hilbert space  $\mathcal{H}$  so that the familiar identity operator (which is linear) and the time-reversal operator (which is antilinear) on this space can be identified as

$$\hat{E} \equiv \rho_e, \quad \hat{\Theta} \equiv \rho_t,$$

respectively. Due to the homomorphism of  $\rho$ , we can speak of  $\mathcal{T}$  as the concrete group  $\{\hat{E}, \hat{\Theta}\}$  instead of the abstract cyclic group of order 2. The characters for  $\mathcal{T}$  for its two corepresentations  $A$  and  $B$  are given in Table IX. These corepresentations are constructed based on the procedure described by Wigner<sup>42</sup> and then later summarized by Cracknell.<sup>48</sup>

### Appendix C: Variation of Representations

In this Appendix, we state and prove a proposition that allows us to relate the symmetry of a wavefunction (or a set of symmetry-related degenerate wavefunctions) at a coalescence point with that in the vicinity. This relation implies that coalescing wavefunctions must contain common (co)representations. For example, a set of degenerate wavefunctions  $\{\Psi_i\}$  spanning a (co)representation  $\Gamma_1 \oplus \Gamma_2 \oplus \Gamma_3 \oplus \Gamma_4$  can coalesce with another set of degenerate wavefunctions  $\{\Psi'_j\}$  spanning a (co)representation  $\Gamma_2 \oplus \Gamma_3 \oplus \Gamma_5$  ( $\Gamma_i$  being irreducible representations of a certain group), where at the coalescence point, wavefunctions from both sets become identical and span either  $\Gamma_2$ ,  $\Gamma_3$ , or  $\Gamma_2 \oplus \Gamma_3$ . As a consequence, in the cases discussed in this article where the symmetry of persistently real solutions does not change upon coalescence with transiently real solutions, the transiently real solutions must then contain the (co)representations of the persistently real solutions with which they come into coalescence.

Let  $f$  and  $g$  be two *linearly independent* wavefunctions in a certain Hilbert space  $\mathcal{H}$ . We shall be interested in the linear or antilinear actions of a symmetry group  $\mathcal{G}$  on the above wavefunctions. Let us consider the identity-containing subsets  $\mathcal{G}_f \subseteq \mathcal{G}$  and  $\mathcal{G}_g \subseteq \mathcal{G}$  such that each of the sets

$$\mathcal{G}_f \cdot f = \{\hat{R}_i f \mid \hat{R}_i \in \mathcal{G}_f\}, \quad \mathcal{G}_g \cdot g = \{\hat{R}_j g \mid \hat{R}_j \in \mathcal{G}_g\}$$

contains all possible linearly independent elements so that for any  $\hat{R}_m \in \mathcal{G}$ , we can always write

$$\hat{R}_m f = \sum_{\hat{R}_i \in \mathcal{G}_f} \lambda_{im}^f \hat{R}_i f, \quad \hat{R}_m g = \sum_{\hat{R}_j \in \mathcal{G}_g} \lambda_{jm}^g \hat{R}_j g \quad (\text{C1})$$

for some  $\lambda_{im}^f, \lambda_{jm}^g \in \mathbb{C}$ . We further require that the elements in the two sets  $\mathcal{G}_f \cdot f$  and  $\mathcal{G}_g \cdot g$  are linearly independent of one another. These two sets thus form bases for two linear subspaces of  $\mathcal{H}$  which we denote  $\Gamma_f$  and  $\Gamma_g$ , respectively. Clearly,  $\Gamma_f$  and  $\Gamma_g$  are guaranteed by construction to be invariant under the linear actions of  $\mathcal{G}$  and are therefore also representation spaces of  $\mathcal{G}$ . For brevity, in this Appendix, we shall refer to both linear representations and linear-antilinear corepresentations<sup>42,47</sup> simply as representations.

Let us now consider a wavefunction  $\psi$  in the same Hilbert space  $\mathcal{H}$  given by

$$\psi = f + g \quad (\text{C2})$$

and the corresponding subset  $\mathcal{G}_\psi \subseteq \mathcal{G}$  for the linearly independent set

$$\mathcal{G}_\psi \cdot \psi = \{\hat{R}_k \psi \mid \hat{R}_k \in \mathcal{G}_\psi\}$$

that forms a basis for the representation space  $\Gamma_\psi$ . We now state and prove a key proposition.

**Proposition 1.** *Take  $\Gamma_f$  and  $\Gamma_g$  to be irreducible representations of  $\mathcal{G}$ . If  $\Gamma_f$  and  $\Gamma_g$  are not equivalent to each other, or if they are equivalent but their representation matrices in the bases  $\mathcal{G}_f \cdot f$  and  $\mathcal{G}_g \cdot g$  are not identical, then  $\Gamma_\psi$  is equivalent to  $\Gamma_f \oplus \Gamma_g$ , which we denote  $\Gamma_\psi \sim \Gamma_f \oplus \Gamma_g$ . On the other hand, if  $\Gamma_f$  and  $\Gamma_g$  are equivalent and have identical representation matrices, then  $\Gamma_\psi \sim \Gamma_f \sim \Gamma_g$ .*

*Proof.* For notational convenience, we gather the linearly independent elements of  $\mathcal{G}_f \cdot f$ ,  $\mathcal{G}_g \cdot g$ , and  $\mathcal{G}_\psi \cdot \psi$  into the corresponding column vectors  $\mathbf{f}$ ,  $\mathbf{g}$ , and  $\boldsymbol{\psi}$ :

$$\begin{aligned} f_i &= \hat{R}_i f, & \hat{R}_i &\in \mathcal{G}_f, \\ g_j &= \hat{R}_j g, & \hat{R}_j &\in \mathcal{G}_g, \\ \psi_k &= \hat{R}_k \psi, & \hat{R}_k &\in \mathcal{G}_\psi. \end{aligned}$$

Let  $\hat{R}$  be an element in  $\mathcal{G}$ . The representation matrices

of  $\hat{R}$  in the spaces  $\Gamma_f$ ,  $\Gamma_g$ , and  $\Gamma_\psi$  are given by

$$\hat{R}f_i = \sum_{i'=1}^{|\mathcal{G}_f|} f_{i'} D_{i'i}^{\Gamma_f}(\hat{R}) \quad \Leftrightarrow \quad \hat{R}\mathbf{f}^\top = \mathbf{f}^\top \mathbf{D}^{\Gamma_f}(\hat{R}), \quad (\text{C3a})$$

$$\hat{R}g_j = \sum_{j'=1}^{|\mathcal{G}_g|} g_{j'} D_{j'j}^{\Gamma_g}(\hat{R}) \quad \Leftrightarrow \quad \hat{R}\mathbf{g}^\top = \mathbf{g}^\top \mathbf{D}^{\Gamma_g}(\hat{R}), \quad (\text{C3b})$$

$$\hat{R}\psi_k = \sum_{k'=1}^{|\mathcal{G}_\psi|} \psi_{k'} D_{k'k}^{\Gamma_\psi}(\hat{R}) \quad \Leftrightarrow \quad \hat{R}\boldsymbol{\psi}^\top = \boldsymbol{\psi}^\top \mathbf{D}^{\Gamma_\psi}(\hat{R}). \quad (\text{C3c})$$

To prove the proposition, we seek a relation between these representation matrices. From the definition of  $\psi$  in (C2) and the expansions in (C1), we can write

$$\begin{aligned} \psi_k &= \hat{R}_k f + \hat{R}_k g \\ &= \sum_{i=1}^{|\mathcal{G}_f|} f_i \lambda_{ik}^f + \sum_{j=1}^{|\mathcal{G}_g|} g_j \lambda_{jk}^g, \end{aligned} \quad (\text{C4a})$$

or more compactly,

$$\boldsymbol{\psi}^\top = (\mathbf{f}^\top \quad \mathbf{g}^\top) \begin{pmatrix} \boldsymbol{\lambda}^f \\ \boldsymbol{\lambda}^g \end{pmatrix} = (\mathbf{f}^\top \quad \mathbf{g}^\top) \boldsymbol{\lambda}^\psi, \quad (\text{C4b})$$

where the second equality defines the matrix  $\boldsymbol{\lambda}^\psi$  with dimensions  $(|\mathcal{G}_f| + |\mathcal{G}_g|) \times |\mathcal{G}_\psi|$ . The linear independence of  $\psi_k$  implies that the columns of  $\boldsymbol{\lambda}^\psi$  are linearly independent. In addition, the linear independence of  $\{f_i\}$  and  $\{g_j\}$  requires that  $|\mathcal{G}_\psi|$ , the number of columns in  $\boldsymbol{\lambda}^\psi$ , must satisfy

$$\max(|\mathcal{G}_f|, |\mathcal{G}_g|) \leq |\mathcal{G}_\psi| \leq |\mathcal{G}_f| + |\mathcal{G}_g|.$$

Combining (C3c) and (C4b), we get

$$\hat{R}\boldsymbol{\psi}^\top = (\mathbf{f}^\top \quad \mathbf{g}^\top) \boldsymbol{\lambda}^\psi \mathbf{D}^{\Gamma_\psi}(\hat{R}), \quad (\text{C5a})$$

for any  $\hat{R} \in \mathcal{G}$ . But from (C3a) and (C3b), we can also write

$$\begin{aligned} \hat{R}\boldsymbol{\psi}^\top &= (\hat{R}\mathbf{f}^\top \quad \hat{R}\mathbf{g}^\top) \boldsymbol{\lambda}^\psi \\ &= (\mathbf{f}^\top \quad \mathbf{g}^\top) \begin{pmatrix} \mathbf{D}^{\Gamma_f}(\hat{R}) & \mathbf{0} \\ \mathbf{0} & \mathbf{D}^{\Gamma_g}(\hat{R}) \end{pmatrix} \boldsymbol{\lambda}^\psi. \end{aligned} \quad (\text{C5b})$$

Comparing (C5a) with (C5b) and making use of the linear independence of the functions in  $\mathbf{f}$  and  $\mathbf{g}$ , we deduce that

$$\boldsymbol{\lambda}^\psi \mathbf{D}^{\Gamma_\psi}(\hat{R}) = \begin{pmatrix} \mathbf{D}^{\Gamma_f}(\hat{R}) & \mathbf{0} \\ \mathbf{0} & \mathbf{D}^{\Gamma_g}(\hat{R}) \end{pmatrix} \boldsymbol{\lambda}^\psi. \quad (\text{C6})$$

To proceed, we now need to condition  $\boldsymbol{\lambda}^\psi$ . Without loss of generality, let us choose  $\hat{R}_1$  to be the identity of

$\mathcal{G}$ . The definition of  $\psi$  in (C2) and the fact that  $\hat{R}_1$  is also a member of  $\mathcal{G}_f$ ,  $\mathcal{G}_g$ , and  $\mathcal{G}_\psi$  by construction imply that

$$\lambda_{i1}^f = \delta_{i1}, \quad \lambda_{j1}^g = \delta_{j1}.$$

Then, writing  $\hat{R}_k = \hat{R}_k \hat{R}_1$  for any  $\hat{R}_k \in \mathcal{G}_\psi$  and applying the expansion in (C4a), we get

$$\begin{aligned} \psi_k &= \hat{R}_k \hat{R}_1 f + \hat{R}_k \hat{R}_1 g \\ &= \hat{R}_k \sum_{i=1}^{|\mathcal{G}_f|} f_i \lambda_{i1}^f + \hat{R}_k \sum_{j=1}^{|\mathcal{G}_g|} g_j \lambda_{j1}^g \\ &= \sum_{i=1}^{|\mathcal{G}_f|} \hat{R}_k f_i \delta_{i1} + \sum_{j=1}^{|\mathcal{G}_g|} \hat{R}_k g_j \delta_{j1}, \end{aligned}$$

where in the last equality we have used the fact that  $\hat{R}_k$  is linear or antilinear and that the Kronecker deltas are real. Using the definition of the representation matrices in (C3) for  $\hat{R} = \hat{R}_k$ , we obtain

$$\begin{aligned} \psi_k &= \sum_{i,i'=1}^{|\mathcal{G}_f|} f_{i'} D_{i'i}^{\Gamma_f}(\hat{R}_k) \delta_{i1} + \sum_{j,j'=1}^{|\mathcal{G}_g|} g_{j'} D_{j'j}^{\Gamma_g}(\hat{R}_k) \delta_{j1} \\ &= \sum_{i=1}^{|\mathcal{G}_f|} f_i D_{i1}^{\Gamma_f}(\hat{R}_k) + \sum_{j=1}^{|\mathcal{G}_g|} g_j D_{j1}^{\Gamma_g}(\hat{R}_k), \end{aligned} \quad (\text{C7})$$

where we have relabeled the dummy indices  $i'$  to  $i$  and  $j'$  to  $j$  in the second equality. Comparing (C7) to (C4a), we deduce that

$$\lambda_{ik}^f = D_{i1}^{\Gamma_f}(\hat{R}_k), \quad \lambda_{jk}^g = D_{j1}^{\Gamma_g}(\hat{R}_k),$$

which says that the  $k^{\text{th}}$  columns of  $\boldsymbol{\lambda}^f$  and  $\boldsymbol{\lambda}^g$  are given by the first columns of the representation matrices for  $\hat{R}_k$  in the bases  $\mathcal{G}_f \cdot f$  and  $\mathcal{G}_g \cdot g$ , respectively.

If  $\Gamma_f$  and  $\Gamma_g$  have non-identical representation matrices, then there must exist at least one  $\hat{R}_k$  such that  $\mathbf{D}^{\Gamma_f}(\hat{R}_k) \neq \mathbf{D}^{\Gamma_g}(\hat{R}_k)$ . Consequently,  $\boldsymbol{\lambda}^f \neq \boldsymbol{\lambda}^g$  and there is thus no constraint between  $\boldsymbol{\lambda}^f$  and  $\boldsymbol{\lambda}^g$ . Therefore, we are guaranteed to be able to find  $\mathcal{G}_\psi$  such that  $|\mathcal{G}_\psi| = |\mathcal{G}_f| + |\mathcal{G}_g|$  and  $\boldsymbol{\lambda}^\psi$  is a square invertible matrix. From (C6), we obtain

$$\mathbf{D}^{\Gamma_\psi}(\hat{R}) = (\boldsymbol{\lambda}^\psi)^{-1} \begin{pmatrix} \mathbf{D}^{\Gamma_f}(\hat{R}) & \mathbf{0} \\ \mathbf{0} & \mathbf{D}^{\Gamma_g}(\hat{R}) \end{pmatrix} \boldsymbol{\lambda}^\psi,$$

and subsequently,

$$\text{tr } \mathbf{D}^{\Gamma_\psi}(\hat{R}) = \text{tr } \mathbf{D}^{\Gamma_f}(\hat{R}) + \text{tr } \mathbf{D}^{\Gamma_g}(\hat{R}),$$

or equivalently,

$$\chi^{\Gamma_\psi}(\hat{R}) = \chi^{\Gamma_f}(\hat{R}) + \chi^{\Gamma_g}(\hat{R}).$$

The above equation holds for all  $\hat{R} \in \mathcal{G}$ , from which it must follow that  $\Gamma_\psi \sim \Gamma_f \oplus \Gamma_g$ .



On the other hand, if  $\Gamma_f$  and  $\Gamma_g$  have identical representation matrices in the sense that  $\mathbf{D}^{\Gamma_f}(\hat{R}_k) = \mathbf{D}^{\Gamma_g}(\hat{R}_k) \equiv \mathbf{D}^\Gamma(\hat{R}_k)$  for all  $\hat{R}_k \in \mathcal{G}_\psi$ , then  $\boldsymbol{\lambda}^f = \boldsymbol{\lambda}^g$  and it follows that the linear independence of the columns of  $\boldsymbol{\lambda}^\psi$  is constrained by the linear independence of the columns of  $\boldsymbol{\lambda}^f$  or  $\boldsymbol{\lambda}^g$ . Hence,  $|\mathcal{G}_\psi| = |\mathcal{G}_f| = |\mathcal{G}_g|$  so that  $\boldsymbol{\lambda}^\psi$  is rectangular and non-invertible. However, the identity between  $\boldsymbol{\lambda}^f$  and  $\boldsymbol{\lambda}^g$  enables us to write  $\boldsymbol{\psi}^\top$  in (C4b) as

$$\boldsymbol{\psi}^\top = (\mathbf{f}^\top + \mathbf{g}^\top) \bar{\boldsymbol{\lambda}}^\psi$$

where  $\bar{\boldsymbol{\lambda}}^\psi = \boldsymbol{\lambda}^f = \boldsymbol{\lambda}^g$  is now a square invertible matrix. This gives two equations analogous to (C5):

$$\begin{aligned} \hat{R}\boldsymbol{\psi}^\top &= (\mathbf{f}^\top + \mathbf{g}^\top) \bar{\boldsymbol{\lambda}}^\psi \mathbf{D}^{\Gamma_\psi}(\hat{R}), \\ \hat{R}\boldsymbol{\psi}^\top &= (\mathbf{f}^\top + \mathbf{g}^\top) \mathbf{D}^\Gamma(\hat{R}) \bar{\boldsymbol{\lambda}}^\psi, \end{aligned}$$

the comparison of which results in

$$\mathbf{D}^{\Gamma_\psi}(\hat{R}) = (\bar{\boldsymbol{\lambda}}^\psi)^{-1} \mathbf{D}^\Gamma(\hat{R}) \bar{\boldsymbol{\lambda}}^\psi,$$

so that

$$\chi^{\Gamma_\psi}(\hat{R}) = \chi^\Gamma(\hat{R}) = \chi^{\Gamma_f}(\hat{R}) = \chi^{\Gamma_g}(\hat{R})$$

for all  $\hat{R} \in \mathcal{G}$ . Hence,  $\Gamma_\psi \sim \Gamma_f \sim \Gamma_g$ .  $\square$

*Remark.* If either one or both of  $\Gamma_f$  and  $\Gamma_g$  are reducible, they can be decomposed into irreducible components to which Proposition 1 can be applied. It is then trivial to see that, in all cases,  $\Gamma_\psi$  must contain two possibly non-disjoint subrepresentations, one of which is equivalent to  $\Gamma_f$  and the other to  $\Gamma_g$ .

Let us now consider a certain wavefunction  $\Psi_0$  in a Hilbert space  $\mathcal{H}$  and another wavefunction  $\Psi_1$  in its immediate neighborhood such that there exists  $\delta\Psi$  that is linearly independent of  $\Psi_0$  and that allows us to write

$$\Psi_1 = c_0\Psi_0 + c_\delta\delta\Psi$$

where the coefficients  $c_0$  and  $c_\delta$  ensure that  $\Psi_1$  is normalized. If  $\Gamma_1$  and  $\Gamma_0$  are the representations spanned by all symmetry-equivalent partners of  $\Psi_1$  and  $\Psi_0$  respectively, then, from the above proposition and the remark that follows,  $\Gamma_1$  must contain a subrepresentation that is equivalent to  $\Gamma_0$ , *i.e.*,  $\Gamma_1 \supseteq \Gamma'_0 \sim \Gamma_0$ . Consequently, as  $\Psi_0$  varies smoothly along any pathway, if its representation changes, then it is either restricted to one of its subrepresentations or included as a subrepresentation of a larger representation.

<sup>1</sup>R. Mjolsness and H. Ruppel, “Multiple Solutions of Hartree–Fock Equations,” *J. Comput. Phys.* **3**, 259–272 (1968).

<sup>2</sup>R. E. Stanton, “Multiple Solutions to the Hartree–Fock Problem. I. General Treatment of Two-Electron Closed-Shell Systems,” *J. Chem. Phys.* **48**, 257–262 (1968).

<sup>3</sup>H. F. King and R. E. Stanton, “Multiple Solutions to the Hartree–Fock Problem. II. Molecular Wavefunctions in the Limit of Infinite Internuclear Separation,” *J. Chem. Phys.* **50**, 3789–3797 (1969).

<sup>4</sup>P. Redondo, J. R. Flores, and J. Largo-Cabrerizo, “Multiple Solutions of Unrestricted Hartree–Fock Equations: The [SNH]<sup>+</sup> Radical as an Example,” *J. Comput. Chem.* **10**, 295–301 (1989).

<sup>5</sup>P. Pulay and R. F. Liu, “Methods for Finding Unrestricted Hartree–Fock Solutions and Multiple Solutions,” *J. Phys. Chem.* **94**, 5548–5551 (1990).

<sup>6</sup>A. J. W. Thom and M. Head-Gordon, “Hartree–Fock Solutions as a Quasidiabatic Basis for Non-Orthogonal Configuration Interaction,” *J. Chem. Phys.* **131**, 124113 (2009).

<sup>7</sup>E. J. Sundstrom and M. Head-Gordon, “Non-Orthogonal Configuration Interaction for the Calculation of Multi-Electron Excited States,” *J. Chem. Phys.* **140**, 114103 (2014).

<sup>8</sup>N. J. Mayhall, P. R. Horn, E. J. Sundstrom, and M. Head-Gordon, “Spin–Flip Non-Orthogonal Configuration Interaction: a Variational and Almost Black-Box Method for Describing Strongly Correlated Molecules,” *Phys. Chem. Chem. Phys.* **16** (2014), 10.1039/C4CP02818J.

<sup>9</sup>K. T. Jensen, R. L. Benson, S. Cardamone, and A. J. W. Thom, “Modeling Electron Transfers Using Quasidiabatic Hartree–Fock States,” *J. Chem. Theory Comput.* **14**, 4629–4639 (2018).

<sup>10</sup>B. C. Huynh and A. J. W. Thom, “Symmetry in Multiple Self-Consistent-Field Solutions of Transition-Metal Complexes,” *J. Chem. Theory Comput.* **16**, 904–930 (2020).

<sup>11</sup>A. J. W. Thom and M. Head-Gordon, “Locating Multiple Self-Consistent Field Solutions: An Approach Inspired by Metadynamics,” *Phys. Rev. Lett.* **101**, 193001 (2008).

<sup>12</sup>C. Coulson and I. Fischer, “XXXIV. Notes on the molecular orbital treatment of the hydrogen molecule,” *London, Edinburgh, Dublin Philos. Mag. J. Sci.* **40**, 386–393 (1949).

<sup>13</sup>H. G. A. Burton and A. J. W. Thom, “Holomorphic Hartree–Fock Theory: An Inherently Multireference Approach,” *J. Chem. Theory Comput.* **12**, 167–173 (2016).

<sup>14</sup>H. G. Hiscock and A. J. W. Thom, “Holomorphic Hartree–Fock Theory and Configuration Interaction,” *J. Chem. Theory Comput.* **10**, 4795–4800 (2014).

<sup>15</sup>P. Mori-Sánchez and A. J. Cohen, “Qualitative Breakdown of the Unrestricted Hartree–Fock Energy,” *J. Chem. Phys.* **141**, 164124–44110 (2014).

<sup>16</sup>H. Fukutome, “The Unrestricted Hartree-Fock Theory of Chemical Reactions. II,” *Prog. Theor. Phys.* **49**, 22–36 (1973).

<sup>17</sup>H. G. A. Burton, M. Gross, and A. J. W. Thom, “Holomorphic Hartree–Fock Theory: The Nature of Two-Electron Problems,” *J. Chem. Theory Comput.* **14**, 607–618 (2018).

<sup>18</sup>E. Epifanovsky, A. T. B. Gilbert, X. Feng, J. Lee, Y. Mao, N. Mardirossian, P. Pokhilko, A. F. White, M. P. Coons, A. L. Dempwolff, Z. Gan, D. Hait, P. R. Horn, L. D. Jacobson, I. Kaliman, J. Kussmann, A. W. Lange, K. U. Lao, D. S. Levine, J. Liu, S. C. McKenzie, A. F. Morrison, K. D. Nanda, F. Plasser, D. R. Rehn, M. L. Vidal, Z.-Q. You, Y. Zhu, B. Alam, B. J. Albrecht, A. Aldossary, E. Alguire, J. H. Andersen, V. Athavale, D. Barton, K. Begam, A. Behn, N. Bellonzi, Y. A. Bernard, E. J. Berquist, H. G. A. Burton, A. Carreras, K. Carter-Fenk, R. Chakraborty, A. D. Chien, K. D. Closser, V. Cofer-Shabica, S. Dasgupta, M. de Wergifosse, J. Deng, M. Diederhofen, H. Do, S. Ehlert, P.-T. Fang, S. Fatehi, Q. Feng, T. Friedhoff, J. Gayvert, Q. Ge, G. Gidofalvi, M. Goldey, J. Gomes, C. E. González-Espinoza, S. Gulania, A. O. Gunina, M. W. D. Hanson-Heine, P. H. P. Harbach, A. Hauser, M. F. Herbst, M. Hernández Vera, M. Hodecker, Z. C. Holden, S. Houck, X. Huang, K. Hui, B. C. Huynh, M. Ivanov, Á. Jász, H. Ji, H. Jiang, B. Kaduk, S. Kähler, K. Khistyayev, J. Kim, G. Kis, P. Klunzinger, Z. Koczor-Benda, J. H. Koh, D. Kosenkov, L. Koulias, T. Kowalczyk, C. M. Krauter, K. Kue, A. Kunitsa, T. Kus, I. Ladjánszki, A. Landau, K. V. Lawler, D. Lefrançois, S. Lehtola, R. R. Li, Y.-P. Li, J. Liang, M. Liebenthal, H.-H. Lin, Y.-S. Lin, F. Liu, K.-Y. Liu, M. Loipersberger, A. Luenser, A. Manjanath, P. Manohar, E. Mansoor, S. F. Manzer, S.-P. Mao, A. V. Marenich, T. Markovich, S. Mason, S. A. Maurer, P. F. McLaughlin, M. F. S. J. Menger, J.-M. Mewes, S. A. Mewes, P. Morgante, J. W. Mullinax, K. J. Oosterbaan,

- G. Paran, A. C. Paul, S. K. Paul, F. Pavošević, Z. Pei, S. Prager, E. I. Proynov, Á. Rák, E. Ramos-Cordoba, B. Rana, A. E. Rask, A. Rettig, R. M. Richard, F. Rob, E. Rossomme, T. Scheele, M. Scheurer, M. Schneider, N. Sergueev, S. M. Sharada, W. Skomorowski, D. W. Small, C. J. Stein, Y.-C. Su, E. J. Sundstrom, Z. Tao, J. Thirman, G. J. Tornai, T. Tsuchimochi, N. M. Tubman, S. P. Veccham, O. Vydrov, J. Wenzel, J. Witte, A. Yamada, K. Yao, S. Yeganeh, S. R. Yost, A. Zech, I. Y. Zhang, X. Zhang, Y. Zhang, D. Zuev, A. Aspuru-Guzik, A. T. Bell, N. A. Besley, K. B. Bravaya, B. R. Brooks, D. Casanova, J.-D. Chai, S. Coriani, C. J. Cramer, G. Cserey, A. E. DePrince, R. A. DiStasio, A. Dreuw, B. D. Dunietz, T. R. Furlani, W. A. Goddard, S. Hammes-Schiffer, T. Head-Gordon, W. J. Hehre, C.-P. Hsu, T.-C. Jagau, Y. Jung, A. Klamt, J. Kong, D. S. Lambrecht, W. Liang, N. J. Mayhall, C. W. McCurdy, J. B. Neaton, C. Ochsenfeld, J. A. Parkhill, R. Peverati, V. A. Ras-solov, Y. Shao, L. V. Slipchenko, T. Stauch, R. P. Steele, J. E. Subotnik, A. J. W. Thom, A. Tkatchenko, D. G. Truhlar, T. Van Voorhis, T. A. Wesolowski, K. B. Whaley, H. L. Woodcock, P. M. Zimmerman, S. Faraji, P. M. W. Gill, M. Head-Gordon, J. M. Herbert, and A. I. Krylov, "Software for the frontiers of quantum chemistry: An overview of developments in the Q-Chem 5 package," *J. Chem. Phys.* **155**, 084801 (2021).
- <sup>19</sup>F. Bihan and F. Sottile, "Fewnomial Bounds for Completely Mixed Polynomial Systems," *Adv. Geom.* **11**, 541–556 (2011).
- <sup>20</sup>F. Sottile, *Real Solutions to Equations from Geometry* (American Mathematical Society, 2011).
- <sup>21</sup>M. Head-Gordon, P. E. Maslen, and C. A. White, "A Tensor Formulation of Many-Electron Theory in a Non-Orthogonal Single-Particle Basis," *J. Chem. Phys.* **108**, 616–625 (1998).
- <sup>22</sup>U. V. Riss, "Extension of the Hilbert Space by  $J$ -Unitary Transformations," *Helv. Phys. Acta* **71**, 288–313 (1998).
- <sup>23</sup>S. R. Garcia, "The Eigenstructure of Complex Symmetric Operators," in *Recent Adv. Matrix Oper. Theory*, Vol. 179, edited by J. A. Ball, Y. Eidelman, J. W. Helton, V. Olshevsky, and J. Rovnyak (Birkhäuser, Basel, Switzerland, 2007).
- <sup>24</sup>H. Fukutome, "Unrestricted Hartree–Fock Theory and Its Applications to Molecules and Chemical Reactions," *Int. J. Quantum Chem.* **20**, 955–1065 (1981).
- <sup>25</sup>J. L. Stuber and J. Paldus, "Symmetry Breaking in the Independent Particle Model," in *Fundam. World Quantum Chem. A Tribut. to Mem. Per-Olov Löwdin, Vol. 1*, edited by E. Brändas and E. S. Kryachko (Kluwer Academic Publishers, 2003) pp. 67–139.
- <sup>26</sup>D. J. Thouless, *The Quantum Mechanics of Many-Body Systems: Second Edition* (Dover Publications, Inc., 2014).
- <sup>27</sup>J. Čížek and J. Paldus, "Stability Conditions for the Solutions of the Hartree–Fock Equations for Atomic and Molecular Systems. Application to the Pi-Electron Model of Cyclic Polyenes," *J. Chem. Phys.* **47**, 3976–3985 (1967).
- <sup>28</sup>R. Seeger and J. A. Pople, "Self-Consistent Molecular Orbital Methods. XVIII. Constraints and Stability in Hartree–Fock Theory," *J. Chem. Phys.* **66**, 3045–3050 (1977).
- <sup>29</sup>J. Paldus and J. Čížek, "Hartree–Fock Stability and Symmetry Breaking: Oxygen Doubly Negative Ion," *Can. J. Chem.* **63**, 1803–1811 (1985).
- <sup>30</sup>J. J. Goings, F. Ding, M. J. Frisch, and X. Li, "Stability of the Complex Generalized Hartree–Fock Equations," *J. Chem. Phys.* **142**, 154109 (2015).
- <sup>31</sup>I. Mayer, "The Spin-Projected Extended Hartree–Fock Method," in *Adv. Quantum Chem.*, Vol. 12 (Academic Press, 1980) pp. 189–262.
- <sup>32</sup>G. E. Scuseria, C. A. Jiménez-Hoyos, T. M. Henderson, K. Samanta, and J. K. Ellis, "Projected Quasiparticle Theory for Molecular Electronic Structure," *J. Chem. Phys.* **135** (2011), 10.1063/1.3643338.
- <sup>33</sup>C. A. Jiménez-Hoyos, T. M. Henderson, T. Tsuchimochi, and G. E. Scuseria, "Projected Hartree–Fock Theory," *J. Chem. Phys.* **136**, 164109 (2012).
- <sup>34</sup>H.-Z. Ye and T. Van Voorhis, "Half-Projected  $\sigma$  Self-Consistent Field For Electronic Excited States," *J. Chem. Theory Comput.* **15**, 2954–2965 (2019).
- <sup>35</sup>D. W. Small, E. J. Sundstrom, and M. Head-Gordon, "A Simple Way to Test for Collinearity in Spin-Symmetry-Broken Wave Functions: General Theory and Application to Generalized Hartree–Fock," *J. Chem. Phys.* **142**, 94112 (2015).
- <sup>36</sup>L. M. Thompson, "Global Elucidation of Broken Symmetry Solutions to the Independent Particle Model Through a Lie Algebraic Approach," *J. Chem. Phys.* **149**, 194106 (2018).
- <sup>37</sup>B. Fine and G. Rosenberger, *The Fundamental Theorem of Algebra* (Springer New York, 1997).
- <sup>38</sup>C. B. Garcia and T. Y. Li, "On the Number of Solutions to Polynomial Systems of Equations," *SIAM J. Numer. Anal.* **17**, 540–546 (1980).
- <sup>39</sup>K.-T. Chen, "On the Bézout Theorem," *Am. J. Math.* **106**, 725 (1984).
- <sup>40</sup>J. Schmid, "On the Affine Bézout Inequality," *Manuscripta Math.* **88**, 225–232 (1995).
- <sup>41</sup>W. R. Inc., "Mathematica, Version 12.1," Champaign, IL, 2020.
- <sup>42</sup>E. Wigner, *Group Theory and Its Application to the Quantum Mechanics of Atomic Spectra* (Academic Press, London, 1959) p. 386.
- <sup>43</sup>A. P. Cracknell, "Corepresentations of Magnetic Point Groups," *Prog. Theor. Phys.* **35**, 196–213 (1966).
- <sup>44</sup>J. D. Newmarch and R. M. Golding, "The Character Table for the Corepresentations of Magnetic Groups," *J. Math. Phys.* **23**, 695–704 (1982).
- <sup>45</sup>C. J. Bradley and B. L. Davies, "Magnetic Groups and Their Corepresentations," *Rev. Mod. Phys.* **40**, 359–379 (1968).
- <sup>46</sup>J. S. Griffith, *The Theory of Transition-Metal Ions* (Cambridge University Press, Cambridge, United Kingdom, 2009).
- <sup>47</sup>C. Garola and L. Solombrino, "Irreducible Linear–Antilinear Representations and Internal Symmetries," *J. Math. Phys.* **22**, 1350–1358 (1981).
- <sup>48</sup>A. P. Cracknell, "Corepresentations of Magnetic Cubic Space Groups," *Prog. Theor. Phys.* **33**, 812–827 (1965).

# On Symmetry and the Reality of Holomorphic Hartree–Fock Wavefunctions Supplementary Material

Bang C. Huynh\*

*School of Chemistry, University of Nottingham, University Park, Nottingham NG7 2RD, United Kingdom and*

*Yusuf Hamied Department of Chemistry, Lensfield Road, Cambridge CB2 1EW, United Kingdom*

Alex J. W. Thom

*Yusuf Hamied Department of Chemistry, Lensfield Road, Cambridge CB2 1EW, United Kingdom*

(Dated: March 3, 2022)

## CONTENTS

S-I. Electron Integral Coefficients	S2
A. Overlap Integrals	S2
B. One-Electron Integrals	S2
C. Two-Electron Integrals	S3
S-II. Molecular Orbitals and Symmetry of Solutions	S5
S-III. Weak Reality Requirements and Coalescence Boundary Locations	S6

---

\* [bang.huynh@nottingham.ac.uk](mailto:bang.huynh@nottingham.ac.uk)

## S-I. ELECTRON INTEGRAL COEFFICIENTS

### A. Overlap Integrals

TABLE S-I. Functional forms of the overlap integral coefficients  $S_1^\pm$  and  $S_2^\pm$  in terms of the overlap integrals. Refer to Figure 2 in the main text for the labels of the hydrogen atoms, which are also the labels for the  $1s$  atomic orbitals (AOs) in STO-3G used in the integral notations. For example,  $\langle\mu|\nu\rangle$  means  $\langle\varphi_\mu|\varphi_\nu\rangle$ , where  $\varphi_\mu$  is the sole  $1s$  AO localised on hydrogen  $\mu$ .

Pathway	Constraining space	Overlap integral coefficients
A	$\Psi\{\hat{s}_z, 0\}[\hat{i}]'$	$S_1^- = \frac{1}{2}(x^2 + 1) \langle 1 1\rangle + x \langle 1 3\rangle$ $S_2^- = \frac{1}{2}(x^2 + 1) \langle 1 2\rangle + x \langle 1 4\rangle$ $S_1^+ = \frac{1}{2}(y^2 + 1) \langle 1 1\rangle + y \langle 1 3\rangle$ $S_2^+ = \frac{1}{2}(y^2 + 1) \langle 1 2\rangle + y \langle 1 4\rangle$
	$\Psi\{\hat{s}_z, 0\}[\hat{\sigma}^{xz}]'$	$S_1^- = \frac{1}{2}(x^2 + 1) \langle 1 1\rangle + x \langle 1 4\rangle$ $S_2^- = \frac{1}{2}(x^2 + 1) \langle 1 2\rangle + x \langle 1 3\rangle$ $S_1^+ = \frac{1}{2}(y^2 + 1) \langle 1 1\rangle + y \langle 1 4\rangle$ $S_2^+ = \frac{1}{2}(y^2 + 1) \langle 1 2\rangle + y \langle 1 3\rangle$
B	$\Psi\{\hat{s}_z, 0\}[\hat{C}_2^\clubsuit]'$	$S_1^- = \frac{1}{2}(x^2 + 1) \langle 1 1\rangle + x \langle 1 3\rangle$ $S_2^- = \frac{1}{2}(x^2 + 1) \langle 1 2\rangle + x \langle 1 4\rangle$ $S_1^+ = \frac{1}{2}(y^2 + 1) \langle 1 1\rangle + y \langle 1 3\rangle$ $S_2^+ = \frac{1}{2}(y^2 + 1) \langle 1 2\rangle + y \langle 1 4\rangle$

### B. One-Electron Integrals

TABLE S-II. Functional forms of the one-electron integral coefficients  $A_1^\pm$  and  $A_2^\pm$  in terms of the one-electron integrals. Refer to Figure 2 in the main text for the labels of the hydrogen atoms, which are also the labels for the  $1s$  AOs in STO-3G used in the integral notations. For example,  $\langle\mu|\hat{h}|\nu\rangle$  means  $\langle\varphi_\mu|\hat{h}|\varphi_\nu\rangle$ , where  $\varphi_\mu$  is the sole  $1s$  AO localised on hydrogen  $\mu$ .

Pathway	Constraining space	One-electron integral coefficients
A	$\Psi\{\hat{s}_z, 0\}[\hat{i}]'$	$A_1^- = (x^2 + 1) \langle 1 \hat{h} 1\rangle + 2x \langle 1 \hat{h} 3\rangle$ $A_2^- = (x^2 + 1) \langle 1 \hat{h} 2\rangle + 2x \langle 1 \hat{h} 4\rangle$ $A_1^+ = (y^2 + 1) \langle 1 \hat{h} 1\rangle + 2y \langle 1 \hat{h} 3\rangle$ $A_2^+ = (y^2 + 1) \langle 1 \hat{h} 2\rangle + 2y \langle 1 \hat{h} 4\rangle$
	$\Psi\{\hat{s}_z, 0\}[\hat{\sigma}^{xz}]'$	$A_1^- = (x^2 + 1) \langle 1 \hat{h} 1\rangle + 2x \langle 1 \hat{h} 4\rangle$ $A_2^- = (x^2 + 1) \langle 1 \hat{h} 2\rangle + 2x \langle 1 \hat{h} 3\rangle$ $A_1^+ = (y^2 + 1) \langle 1 \hat{h} 1\rangle + 2y \langle 1 \hat{h} 4\rangle$ $A_2^+ = (y^2 + 1) \langle 1 \hat{h} 2\rangle + 2y \langle 1 \hat{h} 3\rangle$
B	$\Psi\{\hat{s}_z, 0\}[\hat{C}_2^\clubsuit]'$	$A_1^- = (x^2 + 1) \langle 1 \hat{h} 1\rangle + 2x \langle 1 \hat{h} 3\rangle$ $A_2^- = (x^2 + 1) \langle 1 \hat{h} 2\rangle + 2x \langle 1 \hat{h} 4\rangle$ $A_1^+ = (y^2 + 1) \langle 1 \hat{h} 1\rangle + 2y \langle 1 \hat{h} 3\rangle$ $A_2^+ = (y^2 + 1) \langle 1 \hat{h} 2\rangle + 2y \langle 1 \hat{h} 4\rangle$

### C. Two-Electron Integrals



TABLE S-III. Functional forms of the two-electron integral coefficients  $A_3$ ,  $A_4^\pm$ ,  $A_5$ , and  $A_6$  in terms of the two-electron integrals. Refer to Figure 2 in the main text for the labels of the hydrogen atoms, which are also the labels for the 1s AOs in STO-3G used in the integral notations. For example,  $\langle \mu\nu|\mu'\nu' \rangle$  means  $\langle \varphi_\mu \varphi_\nu | \varphi_{\mu'} \varphi_{\nu'} \rangle$ , where  $\varphi_\mu$  is the sole 1s AO localised on hydrogen  $\mu$ . Physicists' notation is used throughout.

Path.	Constraining space	Two-electron integral coefficients
A	$\Psi\{\hat{s}_z, 0\}[\hat{i}]'_{xy}$	$A_3 = (x^2 y^2 + 1) \langle 11 11 \rangle + 2(x+y)(xy+1) \langle 11 13 \rangle + 4xy \langle 11 33 \rangle + (x^2 + y^2) \langle 13 13 \rangle$
		$A_4^+ = (x^2 y^2 + 1) \langle 11 12 \rangle + (x^2 + 1)y \langle 11 14 \rangle + (y^2 + 1)x^2 \langle 11 23 \rangle + 4xy \langle 11 34 \rangle + (x^2 + 1)y \langle 12 13 \rangle + (x^2 + y^2) \langle 13 14 \rangle$
		$A_4^- = (x^2 y^2 + 1) \langle 11 12 \rangle + (y^2 + 1)x \langle 11 14 \rangle + (x^2 + 1)y^2 \langle 11 23 \rangle + 4xy \langle 11 34 \rangle + (y^2 + 1)x \langle 12 13 \rangle + (x^2 + y^2) \langle 13 14 \rangle$
		$A_5 = (x^2 y^2 + 1) \langle 12 12 \rangle + 2(x+y)(xy+1) \langle 12 14 \rangle + 4xy \langle 12 34 \rangle + (x^2 + y^2) \langle 14 14 \rangle$
		$A_6 = (x^2 y^2 + 1) \langle 11 22 \rangle + 2(x+y)(xy+1) \langle 11 24 \rangle + 2xy \langle 11 44 \rangle + 2xy \langle 12 43 \rangle + (x^2 + y^2) \langle 13 24 \rangle$
	$\Psi\{\hat{s}_z, 0\}[\hat{\sigma}^{xz}]'_{xy}$	$A_3 = (x^2 y^2 + 1) \langle 11 11 \rangle + 2(x+y)(xy+1) \langle 11 14 \rangle + 4xy \langle 11 33 \rangle + (x^2 + y^2) \langle 14 14 \rangle$
		$A_4^+ = (x^2 y^2 + 1) \langle 11 12 \rangle + (x^2 + 1)y \langle 11 13 \rangle + (y^2 + 1)x^2 \langle 11 24 \rangle + 4xy \langle 11 34 \rangle + (x^2 + 1)y \langle 12 14 \rangle + (x^2 + y^2) \langle 13 14 \rangle$
		$A_4^- = (x^2 y^2 + 1) \langle 11 12 \rangle + (y^2 + 1)x \langle 11 13 \rangle + (x^2 + 1)y^2 \langle 11 24 \rangle + 4xy \langle 11 34 \rangle + (y^2 + 1)x \langle 12 14 \rangle + (x^2 + y^2) \langle 13 14 \rangle$
		$A_5 = (x^2 y^2 + 1) \langle 12 12 \rangle + 2(x+y)(xy+1) \langle 12 13 \rangle + 4xy \langle 12 43 \rangle + (x^2 + y^2) \langle 13 13 \rangle$
		$A_6 = (x^2 y^2 + 1) \langle 11 22 \rangle + 2(x+y)(xy+1) \langle 11 23 \rangle + 2xy \langle 11 33 \rangle + 2xy \langle 12 34 \rangle + (x^2 + y^2) \langle 13 24 \rangle$
B	$\Psi\{\hat{s}_z, 0\}[\hat{C}_2^\bullet]'_{xy}$	$A_3 = (x^2 y^2 + 1) \langle 11 11 \rangle + 2(x+y)(xy+1) \langle 11 13 \rangle + 4xy \langle 11 33 \rangle + (x^2 + y^2) \langle 13 13 \rangle$
		$A_4^+ = (x^2 y^2 + 1) \langle 11 12 \rangle + (x^2 + 1)y \langle 11 14 \rangle + (y^2 + 1)x^2 \langle 11 23 \rangle + 4xy \langle 11 34 \rangle + (x^2 + 1)y \langle 12 13 \rangle + (x^2 + y^2) \langle 13 14 \rangle$
		$A_4^- = (x^2 y^2 + 1) \langle 11 12 \rangle + (y^2 + 1)x \langle 11 14 \rangle + (x^2 + 1)y^2 \langle 11 23 \rangle + 4xy \langle 11 34 \rangle + (y^2 + 1)x \langle 12 13 \rangle + (x^2 + y^2) \langle 13 14 \rangle$
		$A_5 = (x^2 y^2 + 1) \langle 12 12 \rangle + 2(x+y)(xy+1) \langle 12 14 \rangle + 4xy \langle 12 34 \rangle + (x^2 + y^2) \langle 14 14 \rangle$
		$A_6 = (x^2 y^2 + 1) \langle 11 22 \rangle + 2(x+y)(xy+1) \langle 11 24 \rangle + 2xy \langle 11 44 \rangle + 2xy \langle 12 43 \rangle + (x^2 + y^2) \langle 13 24 \rangle$

## S-II. MOLECULAR ORBITALS AND SYMMETRY OF SOLUTIONS

The evolutions of the molecular orbitals (MOs) for the eight solutions under the extrinsic constraints along the two molecular symmetry pathways considered are animated in the chapters of the included `mp4` video titled `spatialsymreality.orbitalplots.mp4`. Table S-IV relates the chapter names to the special extrinsic constraints discussed in the main article. Each MO is a linear combination of four  $1s$  AOs localized on the four hydrogen atoms. In these animations, the magnitudes of the linear combination coefficients are proportional to the radii of the circles used to represent the  $1s$  AOs. The phases of these coefficients are depicted by the color hues in the HSV model, and also by the angular position of a black dot on the circumferences of the AO circles. When the coefficient is entirely real, the circumference is bolded, and when the coefficient is entirely imaginary, the circumference is dotted.

TABLE S-IV. Video chapters of the animations for the MO evolution of the analytic solutions obtained under the symmetry-conserved extrinsic constraints considered in this work. These chapters have been encoded individually by `ffmpeg` in the `H.264` standard using the `x264` encoder with the `yuv420p` pixel format, and then merged together as part of a single video file entitled `spatialsymreality.orbitalplots.mp4`. This video can be opened with any common video viewer, but for the best viewing experience, the open-source VLC Media Player should be used which allows for the easy navigation between video chapters and which preserves the potentially different aspect ratios of the different chapters. During playback, the embedded subtitles can be turned on or off to show or hide the chapter names. See Table VII in the main article for an explanation of how to interpret the areas and colors of the orbital plots.

Pathway	Extrinsic constraint	Video chapter name	Start time
A	$ \alpha^g \beta^g $	<code>chapter1.D2h.rectangle.i.gg.orbitalplots</code>	00:00:00.000
	$ \alpha^u \beta^g $	<code>chapter2.D2h.rectangle.i.ug.orbitalplots</code>	00:00:18.101
	$ \alpha^u \beta^u $	<code>chapter3.D2h.rectangle.i.uu.orbitalplots</code>	00:00:36.201
	$ \alpha' \beta' $	<code>chapter4.D2h.rectangle.sigma.dashdash.orbitalplots</code>	00:00:54.301
	$ \alpha'' \beta' $	<code>chapter5.D2h.rectangle.sigma.ddashdash.orbitalplots</code>	00:01:12.401
	$ \alpha'' \beta'' $	<code>chapter6.D2h.rectangle.sigma.ddashddash.orbitalplots</code>	00:01:30.501
B	$ \alpha^+ \beta^+ $	<code>chapter7.D2.C2z-like.pp.orbitalplots</code>	00:01:48.601
	$ \alpha^- \beta^+ $	<code>chapter8.D2.C2z-like.mp.orbitalplots</code>	00:02:08.701
	$ \alpha^- \beta^- $	<code>chapter9.D2.C2z-like.mm.orbitalplots</code>	00:02:28.801

### S-III. WEAK REALITY REQUIREMENTS AND COALESCENCE BOUNDARY LOCATIONS

Under the condition that  $\Delta$  is non-negative, which holds for all cases investigated in this work, the radical forms of  $u_\sigma$  and  $v_\sigma$  (Table IV in the main text) imply that they are either entirely real or entirely imaginary. This considerably simplifies the expression for the reality indicator  $\rho \equiv \rho_\alpha$  (Equation 26 in the main text). For real self-consistent-field (SCF) solutions, we require that  $\rho = 0$ , or equivalently,  $e^{-\rho} = 1$ , which we shall use from here on to simplify the notations. There are four cases to consider.

**Case 1:**  $u_\alpha$  and  $v_\alpha$  are both real. Straightforwardly, we can write  $\Re u_\alpha = u_\alpha$  and  $\Re v_\alpha = v_\alpha$  while  $\Im u_\alpha = 0$  and  $\Im v_\alpha = 0$ . Furthermore, from Table IV in the main text, we identify  $u_\alpha$  with  $u^{-\mp}$  and  $v_\alpha$  with  $v^{-\pm}$  and the reality indicator simplifies to

$$e^{-\rho} = u_\alpha^2 + v_\alpha^2 = (u^{-\mp})^2 + (v^{-\pm})^2 = \frac{D_1^{-+} \mp D_2^- \sqrt{\Delta}}{D_1^{-+} + D_1^{-+}} + \frac{D_1^{--} \pm D_2^- \sqrt{\Delta}}{D_1^{--} + D_1^{-+}} = 1,$$

where we have substituted the expressions for  $u^{-\mp}$  and  $v^{-\pm}$  from Table IV in the main text for the third equality. This identity holds whatever the values of the electron integral coefficients, thus requiring the SCF solutions to be identically real.

**Case 2:**  $u_\alpha$  is real,  $v_\alpha$  is imaginary. This implies that  $\Re u_\alpha = u_\alpha$  and  $\Im v_\alpha = -iv_\alpha$  while  $\Im u_\alpha = 0$  and  $\Re v_\alpha = 0$ , and subsequently,  $e^{-\rho} = (u_\alpha \pm iv_\alpha)^2$ . We note that, for the red  $\pm$ , the top sign corresponds to the unprimed variant of the transiently real solutions, and the bottom sign the primed variant. We then have

$$\begin{aligned} e^{-\rho} &= (u^{-\mp})^2 - (v^{-\pm})^2 \pm 2iu^{-\mp}v^{-\pm} \\ &= \frac{D_1^{-+} \mp D_2^- \sqrt{\Delta}}{D_1^{-+} + D_1^{-+}} - \frac{D_1^{--} \pm D_2^- \sqrt{\Delta}}{D_1^{--} + D_1^{-+}} \pm 2i \frac{\sqrt{D_1^{-+} \mp D_2^- \sqrt{\Delta}} \sqrt{D_1^{--} \pm D_2^- \sqrt{\Delta}}}{\sqrt{D_1^{--} + D_1^{-+}} \sqrt{D_1^{--} + D_1^{-+}}} \\ &= \frac{D_1^{-+} - D_1^{--} \mp 2D_2^- \sqrt{\Delta} \pm 2i \sqrt{(D_1^{-+} \mp D_2^- \sqrt{\Delta})(D_1^{--} \pm D_2^- \sqrt{\Delta})}}{D_1^{--} + D_1^{-+}}. \end{aligned}$$

For SCF solution reality, we require

$$D_1^{-+} - D_1^{--} \mp 2D_2^- \sqrt{\Delta} \pm 2i \sqrt{(D_1^{-+} \mp D_2^- \sqrt{\Delta})(D_1^{--} \pm D_2^- \sqrt{\Delta})} = D_1^{--} + D_1^{-+}$$

with  $D_1^{--} + D_1^{-+} \neq 0$ , or equivalently,

$$\pm i \sqrt{(D_1^{-+} \mp D_2^- \sqrt{\Delta})(D_1^{--} \pm D_2^- \sqrt{\Delta})} = D_1^{--} \pm D_2^- \sqrt{\Delta}. \quad (\text{S1})$$

Squaring both sides and factorising out common terms, we obtain

$$D_1^{--} \pm D_2^- \sqrt{\Delta} = 0$$

which satisfies both  $\pm$  variations of Equation S1 and when substituted into the expressions for  $u^{-\mp}$  and  $v^{-\pm}$  yields

$$u^{-\mp} = +1 \quad \text{and} \quad v^{-\pm} = 0 \quad (\text{S2})$$

for both unprimed and primed variants.

**Case 3:**  $u_\alpha$  is imaginary,  $v_\alpha$  is real. Here, we have  $e^{-\rho} = (-iu_\alpha \pm v_\alpha)^2$ . Following the same approach as in Case 2, we get

$$\pm i \sqrt{(D_1^{-+} \mp D_2^- \sqrt{\Delta})(D_1^{--} \pm D_2^- \sqrt{\Delta})} = -(D_1^{-+} \mp D_2^- \sqrt{\Delta}),$$

with  $D_1^{--} + D_1^{-+} \neq 0$ , which implies that

$$u^{-\mp} = 0 \quad \text{and} \quad v^{-\pm} = +1 \quad (\text{S3})$$

for both unprimed and primed variants.

**Case 4:**  $u_\alpha$  and  $v_\alpha$  are both imaginary. The reality indicator now becomes

$$e^{-\rho} = (-iu^{-\mp})^2 + (-iv^{-\pm})^2 = -\frac{D_1^{-+} \mp D_2^- \sqrt{\Delta}}{D_1^{-+} + D_1^{-+}} - \frac{D_1^{--} \pm D_2^- \sqrt{\Delta}}{D_1^{--} + D_1^{-+}} = -1,$$

which is forbidden for real  $\rho$ . This case is therefore impossible. In other words, we cannot have

$$\frac{D_1^{-+} \mp D_2^- \sqrt{\Delta}}{D_1^{-+} + D_1^{-+}} < 0 \quad \text{and} \quad \frac{D_1^{--} \pm D_2^- \sqrt{\Delta}}{D_1^{--} + D_1^{-+}} < 0$$

simultaneously for real  $D$  and non-negative  $\Delta$ .

Combining the results from the four cases, we deduce that, for the transiently real solutions to be real,  $u_\alpha$  and  $v_\alpha$  must both be real, and if one of them is +1 then the other must vanish. This is achieved when

$$\frac{D_1^{-+} \mp D_2^- \sqrt{\Delta}}{D_1^{-+} + D_1^{-+}} \geq 0 \quad \text{and} \quad \frac{D_1^{--} \pm D_2^- \sqrt{\Delta}}{D_1^{--} + D_1^{-+}} \geq 0 \quad (\text{S4})$$

These are in fact the conditions given by Equation 27 in the main text.

In addition, the real–non-real transition takes place when either  $u_\alpha$  or  $v_\alpha$  switches from being entirely real to being entirely imaginary. If the  $D$  and  $\Delta$  coefficients vary smoothly such that  $u_\alpha$  and  $v_\alpha$  also vary smoothly, then this switch can only occur at

$$u_\alpha = 0 \quad \text{or} \quad v_\alpha = 0,$$

which is equivalent to

$$D_1^{-+} \mp D_2^- \sqrt{\Delta} = 0 \quad \text{or} \quad D_1^{--} \pm D_2^- \sqrt{\Delta} = 0.$$

This gives implicit equations for the locations of the coalescence boundaries as stated in Equation 28 in the main text.